Electricity generation by living plants in a plant microbial fuel cell

Ruud Timmers

Thesis committee

Thesis supervisor

Prof.dr.ir. C.J.N. Buisman
Professor of Biological Recovery and Reuse Technology
Wageningen University

Thesis co-supervisor
Dr.ir. H.V.M. Hamelers
Assistant professor at the sub-department of Environmental Technology

Dr. ir. D.P.B.T.B. Strik
Post-doc at the sub-department of Environmental Technology

Other members
Prof.dr. ir. A.J.M. Stams, Wageningen University
Prof.dr. L.E.M. Vet, The Netherlands Institute of Ecology (NIOO-KNAW),
Wageningen / Wageningen University
dr.ir. M. Saakes, Wetsus, Centre of Excellence for Sustainable Water, Leeuwarden
dr.ir. A.J. Kuhn, Forschungszentrum Jülich GmbH, Germany

This research was conducted under the auspices of the Graduate School SENSE
(Socio-Economic and Natural Sciences of the Environment).

Electricity generation by living plants in a plant microbial fuel cell

Ruud Timmers

Thesis
submitted in fulfillment of the requirements for the degree of doctor
at Wageningen University
by the authority of the Rector Magnificus
Prof.dr. M.J. Kropff,
in the presence of the
Thesis Committee appointed by the Academic Board
to be defended in public
on Tuesday 15 May 2012
at 16:00 in the Aula

Ruud Timmers
Electricity generation by living plants in a plant microbial fuel cell
220 pages.

Thesis, Wageningen University, Wageningen, NL (2012)
With references, with summaries in Dutch and English
ISBN: 978-94-6191-282-4

Summary

Microbial solar cells: applying photo synthetic and electrochemically active organisms

Society is facing local and global challenges to secure needs of people. One of those needs is the increasing demand of energy. Currently most energy is generated by conversion of fossil fuels. The major drawback of using fossil fuels is pollution of the environment by emission of carbon dioxide, nitrogen oxides, sulfur dioxide, volatile organic compounds, heavy metals, and fine particles. Furthermore fossil fuels are not renewable in a time scale in the order of decades. The microbial solar cell (MSC) is a new collective name of biotechnological systems that integrate photosynthetic and electrochemically active organisms to generate electricity in a clean and renewable manner. Among the MSCs, the plant microbial fuel cell (PMFC) that employs higher plants, is the most promising MSCs. In PMFCs, plant roots provide substrate for electrochemically active bacteria in the anode by the loss of organic compounds. In natural environments plant roots loose organic compound by diffusion through the cell membrane, or release organic compounds in order to acquire necessary nutrient. In both cases these organic compounds are an energy source for micro-organisms. In the PMFC these lost or released organic compounds are partly utilized by electrochemically active bacteria. During the oxidation of these organic compounds s electrochemically active bacteria transfer electrons to the anode electrode and produce protons and carbon dioxide. The electrons flow via a power harvester to the cathode compartment where the electrons are consumed by typically oxygen reduction. The aim of this thesis was to characterize the PMFC biologically and electrochemically and to improve the design towards higher applicable power outputs. The approach of this thesis was to understand processes in the PMFC which limit electrical power generation and use these findings to improve electrical power generation and the applicability of the PMFC design.

Part 1: Characterisation of the PMFC

Chapter two describes a rhizosphere anode model which focused on the interaction between root, microorganisms and electrical power generation. The model describes the effect of oxygen loss by living plant roots on the availability of low molecular weight organic compounds lost by living plant roots (exudates) for electrical power generation. The model predicted that all exudates were consumed by biological oxygen reduction. Nevertheless electricity was generated; therefore, it is likely that electrical power was generated of dead root derived organic material via hydrolysis and fermentation. This is supported by the fact that results showed an increase in electrical power generation during dark periods. This indicated that production of organic compounds by plants (that is photosynthesis) was not required for electricity generation in the PMFC. In the next chapter the competition between microbial communities was investigated in order to increase the knowledge on the coulombic efficiency of the PMFC. To do so the microbial communities present in the *Glyceria maxima* PMFC were analyzed. Based on the microbial community analysis, this chapter proposes substrate and electron pathways in the PMFC. The results show that denitrifying bacteria are present and consume low molecular weight organic compounds and therefore lower the coulombic efficiency of the PMFC. The absence of acetate utilising methanogens indicated that methanogens play a minor role in the low coulombic efficiency of the PMFC.

The PMFC is electrochemically characterized in chapter four to understand the processes that result in the internal resistance of the PMFC. The PMFC is characterized by the current interrupt method and polarization curves. The characterization showed that the internal resistance of the PMFC increased during current generation. The major components of the internal resistance were the anode resistance and membrane resistance. The increase in anode resistance was likely the result of an increase of the proton concentration in the electrochemically active biofilm which was due to limited proton transport from the anode to the cathode. The membrane resistance was the results of cation transport from the anode to the

cathode, required to maintain electroneutrality. The resistance to this transport and thus the membrane resistance increased due to an increase of cations in the cathode compartment and resulted in diffusion opposite to the required transport direction.

Part 2: Improvement of PMFC design

The concept of the bicathode PMFC, presented in chapter five, was designed to decrease the membrane resistance and by this the internal resistance and thus increase the electrical power output. During this experiment the PMFC was equipped with 2 cathode compartments of which only one at the time was used to generate electrical power. Objective of this experiment was to decrease the membrane resistance by switching between the 2 cathode compartments. As a consequence accumulation of cations in the cathode compartments decreased which reduces membrane resistance. Switching between cathode 1 and cathode 2 resulted in decrease of membrane as well as anode resistance, and thus increase in electrical power output of the PMFC.

The sixth chapter presents the tubular PMFC design which lowers the amount of anode electrode material needed. This design can be integrated in agricultural food production and wetlands without the need to excavate the topsoil of the fields. In this experiment a tubular microfiltration membrane around which a graphite felt is wrapped to function as anode electrode. The results show that the power density (power output per membrane surface) of the tubular PMFC was comparable to previous PMFC designs. In this context, the amount of anode electrode material and thus volume of the PMFC can be reduced without decreasing the electrical power output.

The seventh chapter of this thesis investigated the applicability of PMFC in salt marches by using a salt marsh species plant (*Spartina anglica*) in a PMFC. Application of a salt march species is advantageous because it allows a higher ionic strength of the electrolyte which could reduce the internal resistance and thus increase power output. Furthermore, this application of PMFC technology avoids competition with agricultural food production for arable land. The results show that long term electricity generation with *S.*

maxima is possible and with a higher average power output than achieved with *G. maxima*.

Concluding remarks

The final chapter of the thesis addresses the main limitations in PMFC performance and evaluated the prospects and application described in the introduction according to current knowledge of PMFC performance. The major challenge of the PMFC technology is to decrease the high internal resistance in an energy efficient way.

In current state of the development of the PMFC it is difficult to calculate the exact costs of a full scale application of the PMFC technology. However the full scale application that is envisioned has low operational costs because no chemicals and or pumping are required. Therefore it is possible to make a cost estimation based on based on the material use and an estimation of the implementation costs. Based on these estimations the costs range between 127 and 897 € per square meter of planted surface.

However, because no catalysts other than electrochemically active bacteria are used the costs of the PMFC are probably in the lower range of the price range (127 € m^{-2}, thus 26 € m^{-2} $year^{-1}$). The costs of electricity generation by renewable technologies are in the range of 0.064 through 0.23 € kWh^{-1}. Assumed the maximum theoretical power output is achieved the cost of electricity generation by the PMFC is 0.15 € kWh^{-1} which is in the range of the competing renewable technologies. However, at the maximum achieved power output (126 GJ ha^{-1} $year^{-1}$ (chapter 4)) the cost of electricity generation by the PMFC is 1.21 € kWh^{-1}. Therefore, at currently achieved power outputs, the PMFC technology does not seem to be economically feasible to produce renewable electricity.

The main opportunity for the PMFC technology is to create an added value by providing a self sustaining energy source in remote areas. In remote areas there is a need for stand alone renewable electricity generation, which usually consists of solar panels and / or wind turbines in combination with a power storage system. The costs electricity generations of these stand alone systems vary from 1.1 to 1.5 € kWh^{-1} (1.44 to 1.95 $ kWh^{-1}). At this cost range the PMFC could be a competitive alternative to these stand

alone systems for electricity generation in remote areas. The cost estimation of the PMFC does not include a power storage system, however as the PMFC generates electricity day and night a power storage system is not required (provided the PMFC generates electricity in every season)

In remote areas low power input applications such as sensors and led light are generally powered by batteries. Batteries have two disadvantages; they contain toxic compounds and only provide electrical power for a limited time. The electrical power price generated by batteries is in the range of 6.5 through 660 € kWh^{-1}, depending on the type of battery. The cost of electrical power generated by the PMFC is equivalent to 9.5 € kWh^{-1}, based on the highest reported average power output per square meter of membrane (0.05 W m^{-2} 16 GJ ha^{-1} $year^{-1}$ chapter 4) and the lowest costs. This shows that the PMFC is already competitive with batteries regarding the price of a kWh. Besides offering a good price the additional added value of the PMFC technology would be the indefinite generation of electrical power and the absence of toxic compounds. Taking into consideration all mentioned drawbacks of batteries, it can be suggested that application of the PMFC technology as a power source for low power input application in remote areas is just around the corner.

Samenvatting

Levende planten produceren elektriciteit in een plant mikrobiële brandstofcel

Een van de grote uitdagingen voor de hedendaagse samenleving is om in haar behoeften te voorzien zonder de leefomgeving onherstelbaar te beschadigen. Een van die behoeften is energie. Wereldwijd neemt de vraag naar energie toe en de verwachting is dat deze vraag blijft toenemen. Op dit moment wordt de meeste energie geproduceerd door omzetting van fossiele brandstoffen. Een groot nadeel hiervan is dat de omzetting van fossiele brandstoffen leidt tot verontreiniging van het milieu door emissie van stikstof oxiden, zwaveldioxide, vluchtige organische koolwaterstoffen, zware metalen, en fijnstof. Een niet gering bijkomend probleem is natuurlijk het gegeven dat fossiele brandstoffen niet hernieuwbaar zijn op korte termijn. De mikrobiële zonnecel is een biotechnologie die photosynthetiserende organismen integreert met elektrochemisch aktieve organismen, met als doel zowel schone als hernieuwbare productie van electriciteit. Van de mikrobiële zonnecellen is de plant mikrobiële brandstofcel (PMBC) de meest belovende technologie. In de PMBC, voorzien hogere planten elektrochemisch aktieve organismen van voeding door het verlies van organische stof via de wortels. De verloren organische stof wordt in de anode van de PMBC geoxideerd door de elektrochemisch aktieve bacteriën. De elektochemisch aktieve bacteriën doneren hierbij elektronen aan de electrode in het anode compartiment en produceren hierbij protonen en koolstofdioxide. De elektronen stromen vervolgens via een externe weerstand naar de kathode waar ze opgenomen worden door een reductieproces, in het ideale geval zuurstof reductie. Het doel van dit proefschrift was de (beschrijving) karakterisering van de PMBC, zowel biologisch als electrochemisch, om vervolgens het ontwerp te verbeteren met als doel het verhogen van de stroomproductie. Om dit te bereiken concentreert het eerste deel van het proefschrift zich op de processen die de stroom- productie limiteren. In het tweede deel van dit proefschrift wordt vervolgens het ontwerp verbeterd met als doel verhoging van de stroomproductie.

Deel 1: Characterizatie van de PMBC

Hoofstuk 2 concentreert zich op de interaktie tussen wortels en mikroorganismen en hoe dit stroomproductie beïnvloed. In het hoofdstuk wordt een model ontwikkeld dat het effect van het verlies van zuurstof door wortels op de beschikbaarheid van organische stof met een lage molekuul massa (exudaten) voor stroomproductie. Het model voorspelt dat alle exudaten worden geconsumeerd door biologische zuurstof reductie. En dat stroom daarom waarschijnlijk wordt geproduceert via de hydrolyse van organische materiaal afkomstig van wortels. Bovendien, de resultaten laten een verhoging van de stroomprodutie zien tijdens donker perioden waaruit blijkt dat er geen direct verbandt tussen fotosyntheze en stroomproductie is. In het volgende hoofdstuk wordt de competitie tussen mikroorganismen onderzocht met als doel inzicht te krijgen in de coulomische efficientie van de PMBC. De verschillende groepen mikroogenismen die aanwezig zijn in de *Glyceria maxima* PMBC zijn in geanalyzeerd. Met behulp van deze resultaten worden de routes voor oxidatie van organische stof en het verlies van electronen voorgesteld. Uit de resultaten blijkt dat de meeste organische stof wordt geoxideerd door denitrificerende bacteriën en dat de dentrificerende bacteriën de lage coulombische efficientie veroorzaken. Verder blijkt dat acetaat consumeerende methanogenen vrijwel geheel afwezig zijn en dat deze dus een verwaarloosbare rol spelen in de coulombische efficientie van de PMBC.

De electrochemische karakterizatie vindt plaats in hoofdstuk vier met als doel inzicht te krijgen in de interne weerstand van de PMBC. De electrochemische karaktrizatie vindt plaats door middel van de ´current interrupt´ methode en door polarizatie curves. De interne weerstand van de PMBC blijkt toe te nemen gedurende stroom productie en bestaat voornamelijk uit de anode weerstand en de membraan weerstand. De anode weerstand en de membraan weerstand zijn het gevolg van massa transport verschijnselen in achtereenvolgens de electrochemisch actieve biofilm en bulk anoliet.

Deel 2: Verbetering van het PMBC ontwerp

In hoofstuk 5 wordt het bicathode ontwerp gepresenteerd, met als doel de interne weerstand te verlagen. Het ontwerp bestaat uit een anode en twee cathodes waarvan slecht een cathode gebruikt wordt voor stroomproductie. Gedurende het experiment wordt gewisseld tussen beide cathodes waardoor de membraan weerstand velaagd door een vermindering van accumulatie van kationen in het desbetreffende cathode compartiment. Uit de resultaten blijkt dat zowel de membraan weerstand als de anode weerstand verminderen na wisseling van cathode compartiment. De vermindering van de interne weerstand resulteerde in een verhoging van de stroomproductie.

In het zesde hoofdstuk wordt de buis PMBC geïntroduceerd. Dit ontwerp toont aan dat vermindering van anode electrode materiaal mogelijk is zonder een aanzienlijk verlies van stroomproductie. Een bijkomend voordeel is dat de buis PMBC kan worden toegepast worden in agrarische voedselproductie en moerasland zonder de bodem te verwijderen.

Het zevende hoofdstuk van dit proefschrift onderzoekt de mogelijkheid om de PMBC toe te passen in kustgebieden met een hoog zoutgehalte door een plant (*Spartina anglica)* te gebruiken die in getijde gebieden kan groeien. Het voordeel van toepassingen in gebieden met een hoog zoutgehalte is dat dit een hogere ion concentratie in de anoliet toestaat wat kan leiden tot een lagere membraan weerstand.

De resultaten tonen aan dat gemiddelde stroomproductie met *S. anglica* PMBC gedurende een periode vergelijkbaar met een groei seizoen hoger is dan met een *G. maxima* PMBC.

Conclusie

In het laatste hoofdstuk van dit proefschrift worden de limitaties van de PMBC aangegeven. Verder wordt kort ingegaan op de perspectieve voor de PMBC technologie als een hernieuwbare en schone technologie voor het opwekken van electriciteit. De grootste limitatie van de PMBC technolgie is de hoge interne weerstand van de ontworpene systemen. De uitdaging is om deze hoge interne weerstand te velagen op een energy efficiente

manier. Zonder deze verlaging is het niet mogelijk om van PMBC een economisch attractieve technologie te maken voor de productie van stroom op groote schaal. De PMBC vereist een anaerobe omgeving terwijl de meeste planten een aerobe omgeving nodig hebben om optimaal te kunnen groeien. Dit maakt een succesvolle integratie van deze technologie in agrarische voedselproductie is twijfelachtig.

Voor de toekomst van de PMBC is het van vitaal belang om een extra toegevoegde waarde te creëren om te kunnen concureren op de energie markt. De grootste kans om deze extra toegevoegde waarde te creëren is: toepassing van de PMBC technologie in afgelegen gebieden voor applicaties die een lage stroom input vereisen (zoals sensoren, led verlichting, het opladen van mobiele telefoons of labtops). In afgelegen gebieden worden deze applicaties meestal van energie voorzien door batterijen. De toepassing van batterijen heeft twee belangrijke nadelen: batterijen bevatten toxische stoffen, en de periode van energie voorziening is gelimiteerd (batterijen raken op). De prijs van energy opgewekt door batterijen is afhankelijk van het type batterij en varieert tussen 125 en 1100 € kWh^{-1}. De prijs van energie opgewekt door de PMBC, gebaseerd op de gemeten maximale productie, varieert tussen 53 en 180 € kWh^{-1} afhankelijk van het ontwerp en is dus lager. Naast dat de prijs competatief is heeft de PMBC het voordeel dat de energy opwekking oneindig is en in principe geen gebruik maakt van toxische stoffen. Rekeninghoudend met de nadelen van batterijen kan gesteld worden dat toepassing van de PMBC voor applicaties, in afgelegen gebieden, die een lage stroom input vereisen haalbaar is.

In afgelegen gebieden worden sensoren in het algemeen voorzien van stroom door baterijen. Baterijen hebben twee nadelen, ten eerste bevatten ze giftige stoffen, en ten tweede ze hebben een beperkte levensduur. Afhankelijk van het type batterij de kosten varieren tussen 6.5 en 660 € kWh^{-1}. Gebaseerd op de minimale kosten voor de PMBC en de maximaal gemeten gemiddelde opbrengst, de prijs is 9.5 € kWh^{-1}. Dit toont aan dat de PMBC al concurrerend kan zijn met batterijen als energie voorziening voor sensoren in afgelegen gebieden. Naast de competatieve prijs, heeft de PMBC het voordeel dat de periode van stroomproductie niet is gelimiteerd en er inprincipe geen giftige stoffen worden gebruikt. Rekeninghoudend

met de nadelen van batterijen lijkt de PMBC als energiebron voor sensoren in afgelegen gebieden tot de mogelijkheden behoord.

Table of Contents

1 Microbial solar cells: applying photosynthetic and electrochemically active organisms

This introduction is based on the review: Microbial solar cells: applying photosynthetic and electrochemically active organisms

1 Microbial solar cells: applying photosynthetic and electrochemically active organisms

1.1 Introduction

Society is facing local and global challenges to secure needs of people (Imhoff et al., 2004; Solomon, 2007). More specifically, one of those needs is energy, which should be available in the form of electricity and fuels. The need for energy is increasing and is expected to keep on increasing in the coming decades. Currently most energy (68%) is generated by conversion of fossil fuels into electricity or fuels. The major drawback of using fossil fuels is that conversion of fossil fuels into electricity or fuels is polluting the environment by emission of carbon dioxide, nitrogen oxides, sulfur dioxide, volatile organic compounds, heavy metals, and fine particles. These emissions result in all kind of environmental problems such as climate change , acid rain (Larssen et al., 2006) and public health issues. Furthermore, they can be considered to be not renewable (they are renewable but only on a time scale of millions of years), which inevitable result in depletion of this resource. To overcome these drawbacks, the ideal energy form of the future should be derived from a renewable source and converted into electricity or fuel via a clean technology.

Wind and solar energy are an interesting alternative as future energy source because they are both inexhaustible. At the same time, however, environmental impact of both wind turbines (avian mortality, visual impacts, noise, electromagnetic interference) and solar panels (visual impacts, loss of green space and biodiversity, increasing dark surface, use of polluting metals) is negative and quite controversial (Campoccia et al., 2009; Kazmerski, 2006).

The microbial solar cell (MSC) is a new collective name of biotechnological systems that integrate photosynthetic and electrochemically active organisms to generate *in situ* “green” electricity or chemical compounds, such as hydrogen, methane, ethanol and hydrogen peroxide (Hamelers et al., 2010; Rozendal et al., 2006; Steinbusch et al., 2010). The MSC is a recent development that builds on the discovery of electrochemically active bacteria (Potter, 1911) and subsequent development of microbial fuel cells (MFCs) (Getter et al., 2009; Kim et al., 1999; Niachou et al., 2001; Pham et al., 2009; Rozendal et al., 2008). MFC technology converts organic matter in electricity. Within the MFC, electrochemically active bacteria at the anode

oxidize organic compounds and deliver electrons to the anode. These electrons flow through a power harvester to the cathode, where electrons are delivered to reduce oxygen (Rabaey & Verstraete, 2005). The use of electrochemically active bacteria to convert organic matter into energy makes the MFC a clean conversion technology. It is a clean conversion technology because only carbon dioxide is emitted. Because this carbon dioxide was recently converted it does not contribute to the increase of the carbon dioxide concentration like conversion of fossil fuels in energy. The integration of the MFC technology with photosynthetic organism makes the MSC technology renewable. This is because the organic matter that is converted into energy was recently generated by photosynthesis.

1.2 Principles of microbial fuel cells

The MFC is a technology that uses electrochemically active bacteria as a catalyst to oxidize organic and inorganic matter to generate current. The microbial fuel cell consists of an anode compartment where the electrons are released by electrochemically active bacteria and transferred to the electrode. The electron transferred to the electrode in the anode flow via an electrical circuit with a power harvester towards the cathode compartment where the electrons are consumed by a reduction process. The anode and cathode compartment are mostly separated by a membrane to separate the oxidation and reduction process.

The cell potential (driving force for current generation) is the difference between cathode and anode potential. The maximum potential difference between cathode and anode potential is determined by difference between Nernst potential of cathode and anode. The Nernst potential is determined by the reduction and oxidation process.

Ideally, the reduction process in the cathode is, oxygen reduction in water,

$$O_2 + 4H^+ + 4e^- \rightarrow H_2O \qquad 1$$

of which the Nernst potential can be determined as

$$E_{cath} = E^0_{cath} - \frac{RT}{nF}\ln\left(\frac{1}{pO_2\left[H^+\right]^4}\right). \qquad 2$$

In the above equation, E_{cath} is the cathode Nernst potential (V), E_{cath}^{0} is the standard cathode potential (V), R is the universal gas constant (J mol^{-1} K^{-1}), T is the temperature (K), n is the number of electrons in the reaction (-), F is Faraday´s constant (C mol^{-1}), pO_2 is the partial oxygen pressure (P), and $\left[H^+\right]$ is the proton concentration (mol L^{-1}).

Likewise, the oxidation process in most MFCs is acetate oxidation

$$CH_3COO^- + 4H_2O \rightarrow 2HCO_3^- + 9H^+ + 8e^- \qquad 3$$

of which the Nernst potential can be determined as

$$E_{an} = E_{an}^{0} - \frac{RT}{nF}\ln\left(\frac{\left[CH_3COO^-\right]}{\left[H^+\right]^9\left[HCO_3^-\right]^2}\right). \qquad 4$$

In the above equation, E_{an} is the anode Nernst potential (V), E_{an}^{0} is the standard anode potential (V), R is the universal gas constant (J mol^{-1} K^{-1}), T is the temperature (K), n is the number of electrons in the reaction (-), F is Faraday´s constant (C mol^{-1}), $\left[CH_3COO^-\right]$ is the acetate concentration (mol L^{-1}), $\left[H^+\right]$ is the proton concentration (mol L^{-1}), and $\left[HCO_3^-\right]$ is the bicarbonate concentration (mol L^{-1}).

Finally, the maximum cell potential is defined as the difference between the cathode Nernst potential and the anode Nernst potential $\left(E_{cell}^{\max} = E_{cath} - E_{an}\right)$. The maximum cell potential is reached when no internal potential losses occur and is approached by the open circuit potential (when no current is generated) (Logan et al., 2006). The difference between open circuit potential and the Nernst potential is the result of thermodynamic losses due to anabolic process in the electrochemically active bacteria, and the chemical reduction of alternative electron acceptors resulting in a mixed potential (Harnisch & Schröder, 2010) Therefore, the open circuit cathode and open circuit anode potential approach the theoretical cathode and anode potential. It is worth to mention that the Nernst potential, and thus the open circuit cathode and anode potential, depend on the specific oxidation/reduction that takes. For

example if the cathode potential will be considerably lower if oxygen is not reduced to water but to peroxide.

1.2.1 Internal resistance

The theoretical maximum cell potential is higher than the measured cell potential. This is due to the internal resistance of the MFC. The internal resistance can be determined by a polarization curve which represents the cell potential as a linear function of the current $\left(E_{cell} = E_{OC} - R_{\text{int}} I\right)$ (Figure 1.1). The internal resistance of the MFC is then a linear function of the maximum theoretical cell potential approximated to the open cell potential, the current and the internal resistance (Logan et al., 2006).

$$R_{\text{int}} = \frac{E_{OCP} - E_{cell}}{I} \qquad 5$$

In the above equation, R_{int} is the internal resistance (Ω), E_{OCP} is the open cell potential (V), E_{cell} is the measured cell potential (V), and I is the current density (A).

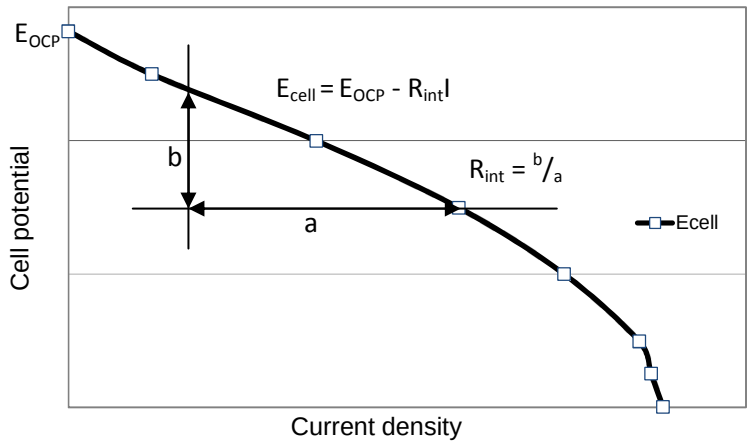

Figure 1.1: *A typical polarization curve for a Microbial Fuel Cell. The open circuit potential (E_{OC}) is the maximum cell potential, found when no current flows. Cell potential decreases with increasing current as a result of increasing potential losses.*

The internal resistance consists of resistances due to the cathode overpotential, anode overpotential, and current dependent potential losses

such as ionic losses and transport losses (Logan et al., 2006) which are measured as the membrane potential (Harnisch et al., 2009) (Bard & Faulkner, 1980). Therefore, combining this with equation (1), E_{cell} (cell potential) can be calculated as:

$$E_{cell} = E_{OCP} - \eta_{cath} - \eta_{an} - i(R_M) \quad 6$$

where η_{cath} is the cathode overpotential (V), η_{an} is the anode overpotential (V), and R_M is membrane resistance ($\Omega\ m^2$). According to Sleutels (2009a), cathode and anode overpotential can be calculated as:

$$\eta_{cath} = E_{cath} - E_{cath,measured} \quad 7$$

$$\eta_{an} = E_{an,measured} - E_{an} \quad 8$$

where $E_{cath,measured}$ is the measured cathode potential (V) and $E_{an,measured}$ is the measured anode potential (V). The cathode and anode overpotential are due to activation of the electrode and concentration difference between the electrode and the bulk solution (Larminie & Dicks) (Figure 1.2)

The membrane potential is the sum of the ionic potential losses and transport potential losses and according to Sleutels (2009a) it can be calculated as

$$E_M = E_{cath,measured} - E_{an,measured} - E_{cell} \quad 9$$

In the above equation, E_M is the membrane potential loss (V), and E_{cell} is the measured cell potential (V). According to Sleutels (2009a) the membrane potential loss can also be calculated as

$$E_M = E_{ionic} - E_T \quad 10$$

where the ionic losses $(E_{ionic}\ (V))$ are a function of current $(I\ (A))$, conductivity of the electrolyte solution $(\sigma\ (S\ m))$, and the average distance $(d\ (m))$ between the anode and the cathode. And can be calculated as

$$E_{ionic} = I\frac{d}{\sigma} \qquad 11$$

Ionic losses can be determined with the current interruption technique, in which the current is interrupted and thus the ionic potential loss immediately disappears.

In this manner, transport losses (E_T) can be calculated by subtracting membrane potential and ionic potential loss.

$$E_T = E_M - E_{ionic} \qquad 12$$

The transport losses in the MFC are due to the resistance to mass transfer through the membrane and the stagnant boundary layer adjacent to the membrane. Mass transfer through the membrane of the MFC is required to maintain electroneutrality in the MFC. In the absence of convection mass transfer is determined by diffusion (driven by the concentration gradient $\left(\frac{dC}{dx}\right)$) and migration (driven by a potential gradient $\left(\frac{d\varphi}{dx}\right)$) and can be described by the Nernst-Planck flux equation.

$$J_T = J_D + J_M = -D\frac{dC}{dx} - \frac{zF}{RT}DC(x)\frac{d\varphi}{dx} \qquad 13$$

Where J_T is total transport of a specific ion (mol $m^{-2}s^{-1}$), J_D is diffusive transport (mol $m^{-2}s^{-1}$) driven by the concentration gradient, J_M migratory transport (mol $m^{-2}s^{-1}$) driven by a potential gradient, D is the diffusion constant ($m^2\ s^{-1}$), $\frac{dC}{dx}$ is the concentration gradient (mol m^{-4}), z is the charge number (-), F is the Faraday constant 46485 (C mol^{-1}), R is the gas constant 8.314 (J $mol^{-1}\ K^{-1}$), T is the temperature (K), $C(x)$ concentration

at distance x from the membrane (mol m^{-3}), $\frac{d\varphi}{dx}$ is the potential gradient (V m^{-1}). The transport potential loss due to the potential gradient needed as a driving force for migration.

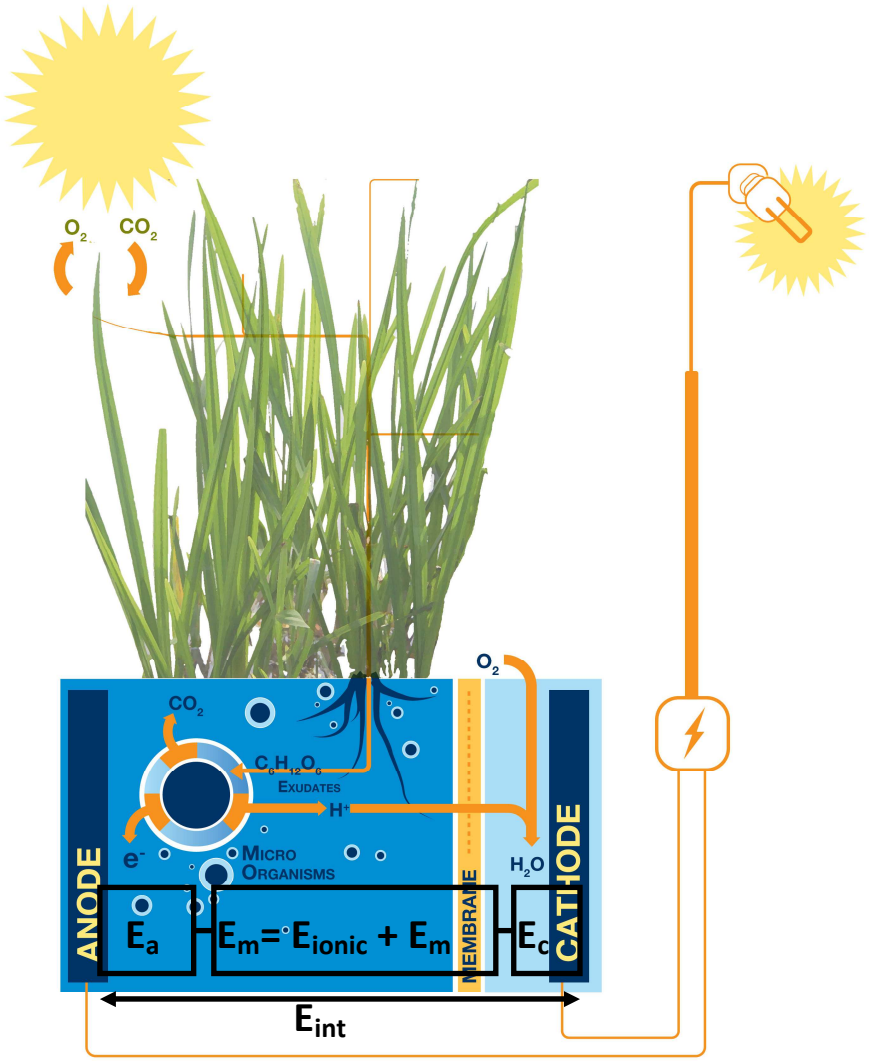

Figure 1.2: *Schematic overview of the partial potential losses in the plant microbial fuel cell. The internal potential loss (E_{int}) of the PMFC can be represented as a series of the anode (E_a), membrane (E_m), and cathode potential loss (E_c) in an equivalent circuit. The membrane potential loss consists of the ionic potential losses (E_{ionic}) and the transport potential losses (E_T)*

1.2.2 Coulombic efficiency of the MFC

The energy efficiency of the MFC is determined by the voltage efficiency (internal resistance) and the coulombic efficiency. Coulombic efficiency of the MFC is defined as the ratio between the number of electrons measured as current divided by the number of electrons present on the substrate (Logan et al., 2006). The coulombic efficiency is affected by the presence of alternative electron acceptors such as: O_2, NO_3^-, Mn(IV) oxides, Fe(III) oxides, SO_4^{2-}, and CO_2 in the anode compartment. These alternative electron acceptors can be reduced either chemically or biologically. In either case the coulombic efficiency is negatively affected, because electrons that are present in the substrate are not measured as current. During chemical reduction of alternative electron acceptors, the reduction process takes place at the electrode surface and consumed electrons that are already transferred to the anode electrode by electrochemically bacteria. During biological reduction of alternative electron acceptors substrate is consumed by bacteria that do not use the anode electrode as terminal electron acceptor. This competition for substrate reduces the amount of substrate available for current generation and thus coulombic efficiency. In natural fresh water sediments, terminal electron acceptors are used in the following order of preference: O_2, NO_3^-, Mn(IV) oxides, Fe(III) oxides, SO_4^{2-}, and CO_2 (Stumm & Morgan, 1996). Likewise, some electrochemically active bacteria, such as *G. sulfurreducens* and *G. metallireducens*, reduce Fe(III) oxides in natural sediments (Holmes et al.). This means that electrochemically active bacteria are likely outcompeted in the presence of oxygen and nitrate.

Besides the presence of alternative electron acceptors the coulombic efficiency is affected by the substrate conversion pathway or in other words the suitability of the substrate for electrochemically active bacteria. The degradation of complex organic compounds in MFCs follow pathways similar to anaerobic digestion, such as the hydrolysis and fermentation. The energy losses during hydrolysis and fermentation decrease the maximum coulombic efficiency of the MFC (Velasquez-Orta et al., 2011) and thus possibly reduces the coulombic efficiency.

1.3 Principles of microbial solar cells

The basic principles of MSCs, as illustrated in Figure 1.2, are: (i) photosynthesis; (ii) transport of organic matter to the anode compartment; (iii) anodic oxidation of organic matter by electrochemically active bacteria; and (iv) cathodic reduction of generally oxygen. The MSCs are characterized according to the way solar energy is captured and the mode of organic matter transfer: the higher plant with rhizodeposition (PMFC); the phototrophic biofilm with diffusion; and the photobioreactor or coastal marine ecosystem, which use pumps for translocation. The in-depth bio-electrochemical principles of all systems are yet to be fully revealed (Hamelers et al., 2010; Herrero & Flores, 2008; Logan & Regan, 2006; Lovley, 2008; Lynch, 1990; Richmond, 2004; Rozendal et al., 2008; Strik et al., 2008a; Taiz & Zeiger, 2006; Zou et al., 2009). Table 1 gives an overview of recent developments on MSC performance and efficiency.

1.3.1 Plant microbial fuel cell

MSCs with living higher plants are called plant microbial fuel cells (PMFCs) (Strik et al., 2008a). In PMFCs, the plant's roots fuel the electrochemically active bacteria at the anode by excreting rhizodeposits (De Schamphelaire et al., 2010; De Schamphelaire et al., 2008b; Helder et al., 2010; Kaku et al., 2008; Strik et al., 2008a; Takanezawa et al., 2010; Timmers et al., 2010). Rhizodeposition of plant roots is the loss of organic compounds into soil, including sugars, organic acids, polymeric carbohydrates, enzymes and dead-cell material. There is a wide range of processes by which rhizodeposition can take place, such as: root cap and border cell loss, death and lysis of root cell, flow of organic carbon to root-associated symbionts, gaseous losses, leakage of solutes from living cells (exudation), and insoluble polymer excretion (mucilage). It is extremely different to experimentally quantify and make a differentiation between these processes, furthermore it is highly likely that all these processes occur simultaneously in a root system (Jones et al., 2009). Rhizodeposition accounts for approximately 20–40% of the plant's photosynthetic productivity, and these compounds can be degraded by a mixture of microorganisms (Lynch, 1990).

Table 1.1: Performance and power conversion efficiency of Microbial Solar Cells. Performance is determined by the operating time (OT), average power density over this OT (PDavg), and the maximum power density (PDmax). The power conversion efficiency (PCE) is defined as as average energy output (W m^{-2}) divided by light energy input (W m^{-2})

Category MSC	**Photosynthetic organism(s)**	**ED**	**OT (d)**	**PDavg[a] (mWm^{-2})**	**PDmax[a] (mWm^{-2})**	**PCE (%)**	**EA (catalyst)**	**Ref**
Plant	*Glyceria maxima*	RD	67	4	67	0.01	O_2	1
Plant	*Oryza sativa ssp. indica*	RD	134	21	33	0.004	$Fe(CN)6^{3-}$.	2, 3
Plant	*Spartina anglica*	RD	78	22	79	0.01	O_2	4
Plant	*Spartina anglica*	RD	33	50	100	0.01	$Fe(CN)6^{3-}$.	4
Plant	*Arundinella donax*	RD	112	10	22	0.001	O_2/ $Fe(CN)6^{3-}$.	5
Plant	*Spartina anglica*	RD	154	21	222	0.001	O_2/ $Fe(CN)6^{3-}$	5
Plant	*Oryza sativa ssp. indica*	RD, potting soil	175	26	-	-	O_2/$Fe(CN)6^{3}$ (B)	2, 3
Plant	*Oryza sativa L.cv.Sasanishiki*	RD, rice paddy soil	120	-	6	-	O_2	6
Plant	*Oryza sativa L cv.Satojiman*	RD, rice paddy soil	-	-	14	-	O_2 (Pt)	7
Phototrophic biofilm	Filamentous *Cyanophyta Chlorophyta*	MPM	8	-	5.9	-	O_2 (Pt)	8
Phototrophic biofilm	Filamentous *Cyanophyta Chlorophyta*	MPM	20	-	0.2	-	O_2 (Pt)	9
Phototrophic biofilm	*Cyanophyta Chlorophyta*	MPM	22	2	41	0.001	O_2/$Fe(CN)6^{3}$ (B)	10
Phototrophic biofilm	*Chlorophyta*	MPM	9	0.3	84	-	O_2 (Pt)	11
Phototrophic biofilm	*Cyanophyta Chlorophyta*	MPM	5	-	0.001	-	O_2	12
Phototrophic biofilm	*Cyanophyta Chlorophyta*	MPM, sediment	> 20	-	1.4	-	O_2	12
Phototrophic biofilm	*Chlorophyta*	MPM, sediment	> 7	7	14	-	O_2	13
Phototrophic biofilm	*Synechaocystis PCC-6803*	MPM (*Synechaocystis)*	18	-	0.5	-	O_2 (Pt)	9

Photobio-reactor	*Chlorella*	MPM (*Chlorella)*	161	14	110	0.04	$Fe(CN)6^3$	14
Photobio-reactor Digester	*Chlorella*	Effluent of digested algae	58	0.1	1	-	O_2	15
Photobio-reactor[b]	*Chlorella vulgaris*	*Chlorella vulgaris* composite	5	-	980 [c]	-	O_2 (Pt)	16
Coastal marine ecosystem	Phytoplankton	MPM(phyto- &zoo-plankton)	50	-	17 [c]	-	-	17
Coastal marine ecosystem**	*Ulva lactuca*	*Ulva lactuca* composite	7	-	760 [c]	-	O_2 (Pt)	16

RD = rhizodeposition
B = bacteria
MPM = metabolites of photosynthetic microoganisms
[a]Geometric photosynthetic surface area (m^2).
[b]Electron donor was produced external.
[c]Geometric anode electrode surface area (m^2).

1. Strik et al., 2008a
2. De Schamphelaire et al., 2010
3. De Schamphelaire et al., 2008b
4. Timmers et al., 2010
5. Helder et al., 2010
6. Kaku et al., 2008
7. Takanezawa et al., 2010
8. Zou et al., 2010
9. Strik et al., 2008a
10. De Schamphelaire et al., 2010
11. De Schamphelaire et al., 2008b
12. Timmers et al., 2010
13. Helder et al., 2010
14. Kaku et al., 2008
15. Takanezawa et al., 2010
16. Zou et al., 2010

Typical substrates for EAB include LMW organic compounds such as organic acids, amino acids, and sugars (Hamelers et al., 2009). Exudation of LMW compounds is a continuous process that is driven by passive diffusion (driven by the concentration gradient) and migration (driven by the potential gradient) (Jones, 1998; Pinton & Varanini, 2007).

When the plant is growing with its roots in the MFC, electricity is continuously generated *in situ*. The first published PMFC study estimated that 21 GJ ha^{-1} $year^{-1}$ (67 mW m^{-2}) net power generation is theoretically possible under Western European (i.e. Netherlands, Belgium, France) climate conditions (Strik et al., 2008a). This net yield is similar to that of biomass electricity production systems, including harvest, storage, and

conversion of energy crops which achieve net power generation of 2.8 to 70 GJ ha^{-1} $year^{-1}$ (based on: biogas production of 160-400 GJ CH_4 ha^{-1} $year^{-1}$ (Pabón Pereire, 2009); gas combustion efficiency of 25% (Weiland, 2010); and energy input of 30% (Berglund & Börjesson, 2006)) and biomass combustion which achieves net power generation of 27 to 91 GJ ha^{-1} $year^{-1}$ (based on: biomass productivity of 8–12 ton dry weight/ha/year; heating value of 18-20 GJ/ton; biomass combustion efficiency of 20-40% and energy input of 5% (Turkenburg W.C., 2001)).

It is important to realize that the PMFC technology does not compete for biomass with other biomass electricity production systems because the energy source rhizodeposition. Rhizodeposition is lost during plant growth and is therefore not available for other biomass electricity production systems. Moreover because it uses rhizodeposits *in situ* the PMFC technology can possibly be integrated with biomass production for other biomass electricity production systems. Furthermore the PMFC generates electricity from below ground plant biomass which is generally not used for biomass electricity production systems as the majority systems use above ground plant biomass (Pabón Pereire, 2009) (Gerbens-Leenes et al., 2009).

The theoretical power output of 21 GJ ha^{-1} $year^{-1}$ for the PMFC is a relatively conservative estimation considering that a multidisciplinary European research consortium (www.plantpower.eu) estimated that the power output of the PMFC could reach 1,000 GJ ha^{-1} $year^{-1}$ (3.2 W m^{-2} or 28 kWh m^{-2} $year^{-1}$). This value is based on the highest data reported for the conceptual process steps. With average solar radiation of 150 MW km^{-2} in Western Europe (Fontoynont et al., 1998), increased photosynthetic efficiency of 5% (Taiz & Zeiger, 2006), a majority (70%) of photosynthates transported to the soil (Whipps & Lynch, 1985) and possible 60% energy recovery of these photosynthates by the MFC (Gorby et al., 2006), power output of 3.2 W m^{-2} would be possible. For application in natural conditions, it is expected that 50% of this output (1.6 W m^{-2}) could be harvested. Of course, it is recognized that these values all depend on the system constituents, the environmental conditions and the time course of the experiment. Nevertheless, this example shows that there is room for optimization to achieve higher power output. The primary challenge is to

further understand the principal processes of PMFCs to subsequently design and operate PMFCs with higher power outputs.

Three PMFC studies have integrated the anode in the sediment in which plants were growing (De Schamphelaire et al., 2008b; Kaku et al., 2008; Takanezawa et al., 2010). In these studies, rhizodeposits from plants and organic matter from the sediment were available for generating a current. It was found that introduction of growing rice plants in a MFC resulted in a sevenfold increase power output as compared to the sediment MFC (De Schamphelaire et al., 2008b). Also, outdoor experiments have been performed in a rice paddy field (Kaku et al., 2008; Takanezawa et al., 2010). However, in these cases, power output was not higher than reported for sediment MFC without plants (Holmes et al., 2004; Kaku et al., 2008). The difference in power output between the rice paddy experiments and the sediment MFC experiment may be due to a variety of factors, including: the presence of rice plants, the sediment composition, the microbial species and the fuel cell design (De Schamphelaire et al., 2008a).

The average power density (PD) over the operation time (OT) of 33 days of the PMFC with the plant *Spartina anglica* was 0.05 W m^{-2}. Of all reviewed varieties of MSCs, the *Spartina anglica* PMFC study achieved the highest long-term current and power density (Timmers et al., 2010).

Microbial communities at the anode PMFCs have been analyzed to elucidate principles and performance of PMFCs. It was shown that the most common bacteria were from the families *Desulfobulbus* or *Geobacteraceae* (De Schamphelaire et al., 2010) or were closely related to *Natronocella, Beijerinckiaceae, Rhizobiales* and *Rhodobacter* (Kaku et al., 2008). Some species, like *Geobacter sulfurreducens*, are electrochemically active (Bond & Lovley, 2003). However, it has not been shown whether electrochemical active species are indeed present and active in a PMFC.

1.3.2 MSCs with phototrophic biofilms

Solar energy is converted in electricity by growing a phototrophic biofilm on the anode of the fuel cell (Table 1) (He et al., 2009; Malik et al., 2009; Nishio et al., 2010; Strik et al., 2010; Zou et al., 2010; Zou et al., 2009). MSCs with phototrophic biofilms have a self-organizing biofilm containing *Chlorophyta*

and/or *Cyanophyta* and can operate for periods of more than 20 days (He et al., 2009). All studies to date have used mixed microbe populations, which likely includes electrochemically active bacteria. An exception is one study in which a pure culture of *Synechocystis PCC-6803* was applied to generate an electrical current (Zou et al., 2009). This cyanobacterium is able to form electrically conductive nanowires when cultivated under carbon dioxide limitation and excess light. *Synechocystis,* therefore, can be responsible for electron transfer from the microorganism to the anode (Gorby et al., 2006; Zou et al., 2009).

Some of the MSCs include sediment, which provides additional organic matter. One of these studies estimated that the 2.5-cm-thick marine sediment applied, contained enough organic matter to operate the system for 22 years (Malik et al., 2009). To date, the theoretical output for a MSC with a phototrophic biofilm has not been estimated. Based on the primary carbon production of benthic biofilms of 250 g m^{-2} $year^{-1}$ in the Netherlands, a MFC energy recovery of 60% and glucose as the carbon composite (Brotas & Catarino, 1995; Sleutels et al., 2009b), the estimated maximum power output is 0.06 W m^{-2} (He et al., 2009; Malik et al., 2009). This value is of the same order of magnitude as the PMFCs (Strik et al., 2008a). The maximum measured average PD of MSCs with phototrophic biofilms was 0.007 W m^{-2}, which is sevenfold lower than best PMFC (Table 1) (Malik et al., 2009; Timmers et al., 2010).

1.3.3 MSCs with photobioreactors

MSCs can use photobioreactors to harvest solar energy via photosynthetic microorganisms such as algae (De Schamphelaire & Verstraete, 2009; Strik et al., 2008b; Velasquez-Orta et al., 2009; Zou et al., 2009). Figure 1.3 shows an example of a MSC with a photobioreactor and an anaerobic digester. The digester treats photosynthetic metabolites and microorganisms before supplying them to the MFC (De Schamphelaire & Verstraete, 2009). Photobioreactors with algae can achieve PAR (photosynthetic active radiation; spectral range of solar radiation from 400 to 700 nm which can be used by micro algae for photosynthesis) photosynthetic efficiencies of 15%, defined as the energy content of the produced algae divided by the energy content of the PAR irradiation (Janssen et al., 2003). For MFC energy

recovery of 29%, a power production of 2806 mW m^{-2} is theoretically possible under Western European climate conditions (Strik et al., 2008b; Ter Heijne et al., 2006).

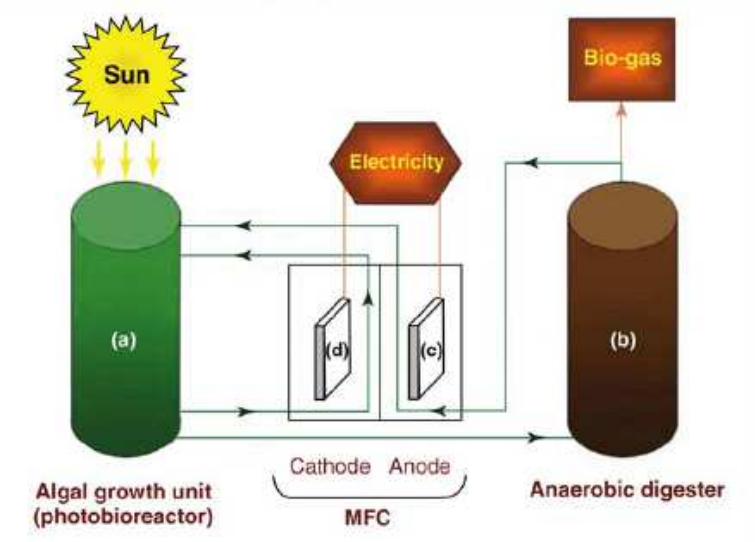

Figure 1.3: *Schematic overview of a closed loop concept of a MSC with photobioreactor and digester (Reprint with permission of John Wiley and Sons) (De Schamphelaire & Verstraete, 2009); (i) photosynthesis by micro algae takes place in the photobioreactor (a) (ii) biogas is produced from organic matter which is transported from the photobioreactor to the digester (b); (iii) in the anode of the MFC the remaining organic matter, which is transported from the digester to the anode, is oxidized by electrochemically active bacteria; (v) in the cathode of the MFC oxygen, which is transported from the photobioreactor to the cathode, is reduced to water.*

The best results have been achieved with *Chlorella* in a photobioreactor, where a photosynthetic efficiency of 6.3% (PAR-based) was reached. This system most effectively converted light energy into electricity of all reviewed MSCs (Table 1). The power conversion efficiency (PCE) defined as average energy output (W m^{-2}) divided by light energy input (W m^{-2}), was 0.04 %. This resulted in 0.014 W m^{-2} average power production, which was only 0.5% of the theoretical maximum (Strik et al., 2008b). It is important to note that, for the production of photosynthetic metabolites in photobioreactors, energy is needed for mixing and removing oxygen up to

values of 10 W m^{-2} (Strik et al., 2008b). Thus, with the current state-of-the-art, MSCs with photobioreactors will have no net electricity production.

1.3.4 MSCs with coastal marine ecosystem

MSCs can be integrated into the coastal marine ecosystem (Girguis et al., 2010). This ecosystem uses solar energy and produces phytoplankton like macro-algae and zooplankton that float in the ocean. If these substrates are harvested, electricity can be generated by a MFC (Girguis et al., 2010; Reimers et al., 2007; Velasquez-Orta et al., 2009). For real life implementation, it was envisioned that pumps could be used to feed raw seawater to a 40-km-long, tubular MFC to generate electricity (Girguis et al., 2010). It has been estimated that MSCs at coastal zones, which account for 10% of the ocean, can generate electrical power of 2.4 to 16 TWh $year^{-1}$ which is, or when divided by the surface area, 0.01-0.05 mW m^{-2} (Girguis et al., 2010; Martin et al., 1987). This PD is more than three orders of a magnitude less than MSCs that use higher plants or phototrophic biofilms. Furthermore, for current state-of-the-art, estimates that the energy input is 18 times more than the electricity output (Girguis et al., 2010).

1.4 Trade-off between PMFC, wind turbines, and solar panels

Focussed on energy production, the use of PMFCs or phototrophic biofilms may be an alternative for photovoltaic solar panels or wind turbines to create energy-producing landscapes. As opposed to other alternative renewable electricity sources, PMFCs offer the opportunity to increase both the aesthetic value and the biodiversity of such landscapes. However, photovoltaic solar panels and wind turbines can achieve higher power yields per square meter; thus, a cost-benefit analysis is required when considering implementation of a renewable electricity technology (Goldemberg et al., 2004).

When applied in a natural environment, PMFC power yield is estimated at a maximum of 1.6 MW km^{-2}. Whereas wind turbines could generate 5-7.7 MW km^{-2} on a typical wind farm in Europe (McGowan & Connors, 2000); solar panels could generate 4.5-7.5 MW km^{-2} under Western European

conditions (solar radiation: 150W m^{-2} PCE: 15-25%; tilted position of solar panel thus uses 2.5 m^2 land per m^2 solar panel) (Kazmerski, 2006). In summary, power output of wind farms and solar farms will be 3-5-fold higher than that of PMFCs. With an increasing need for electricity and in light of the European political goal of generating 20% of its energy-need in 2020 from renewable sources, pressure on high-energy-yield per surface area is increasing (Campoccia et al., 2009). At the same time, however, environmental impact of both wind turbines (avian mortality, visual impacts, noise, electromagnetic interference) and solar panels (visual impacts, loss of green space and biodiversity, increasing dark surface, use of polluting metals) is large and is a source of societal debate (Campoccia et al., 2009; Kazmerski, 2006). PMFCs can offer an opportunity for electricity generation while sustaining the natural environment at locations where wind turbines or solar panels are not desirable. Future integration of PMFCs into closed systems can provide 24 hour per day electricity generation, without the use of scarce materials and with nutrient preservation.

1.5 Prospects and future applications

The most promising MSCs employing higher plants i.e. the PMFC. The basic principle of PMFC is demonstrated; now it is time to improve the systems for 'real life' applications. Compared to conventional solar cells, PMFC have some attractive properties that warrant further development and will influence future applications of this technology:

PMFCs can be easily incorporated into landscapes or into urban areas where it "greens" the city. For example, PMFCs can be combined with green roofs to create electricity-producing green roofs powering up to a third of a modern household (Strik et al., 2010).

Both the photosynthetic and electrochemical reactions are carried out by a continuously growing population of microorganisms. This makes the system capable of self-repair, conferring a longer lifetime and low maintenance.

Another advantage of using of reproducing organisms is that there is no need for special catalysts, like Cd, that are either costly or toxic (Kazmerski, 2006). Thus the PMFC can be applied in natural surroundings with no risk of pollution.

PMFCs have organic material as intermediate energy carriers between the photosynthetic and the electrochemical portions of the cell. This organic material accumulates in the MSC, therefore allowing electricity generation in the dark (Strik et al., 2010; Strik et al., 2008a; Strik et al., 2008b).

Closed PMFC systems can preserve nutrients for the organisms, which enable long-term, low-maintenance power production.

Integrated PMFCs can add value to other applications, such as greenhouses with food or flower production, or rice paddy fields with rice production, or biomass production for bio-energy production (De Schamphelaire et al., 2008b; Kaku et al., 2008). Additionally, wastewater and surface water treatment can be integrated into PMFCs to supply extra organic matter for energy production (Hamelers et al., 2010; Strik et al., 2008a). Currently, there are promising possibilities for application of PMFC according to the best long-term power output of 0.05 W m^{-2} (Table 1). Meteorological sensors for temperature, pressure and humidity installed on a buoy which requiring 24 mW were powered by a sediment MFC (Tender et al., 2008). Therefore it is expected that these sensors and other low power requiring applications like LED lights can be powered by PMFC.

1.6 Outline of this thesis

The aim of this thesis was to characterize the PMFC biologically as well as electrochemically to be able to improve the design to increase the electrical power generation. To achieve this, the main focus of this thesis was to understand processes in the PMFC which limit electrical power generation and to use these findings to improve electrical power generation and the applicability of the PMFC design.

All chapters, except chapter seven, concern fresh water PMFCs in which *Glyceria maxima* was used as model plant to provide the electrochemically active bacteria with substrate. *G. maxima* was used as model plant because it grows in wet areas such as riverbanks and ponds and is highly productive (Tanner, 1996). The high productivity of *G. maxima* is likely advantageous for the PMFC technology because the high productivity of the plant likely results in a high productivity of substrate for the electrochemically active bacteria and thus a high energy output of the PMFC.

The second chapter describes a rhizosphere anode model which focused on the interaction between root, microorganisms and electrical power generation. The model describes the effect of oxygen loss of plant roots on the availability of low molecular weight organic compounds lost by plant roots (exudates) for electrical power generation. In the model it is assumed that all oxygen lost by plant roots is consumed by biological oxygen reduction. Based on theoretical framework for competition between aerobic bacteria, denitrifying bacteria, sulfate reducing bacteria, electrochemically active bacteria and methanogens.

The model predicted that all exudates were consumed by biological oxygen reduction. And that therefore it is likely that was electrical power was generated via hydrolysis of root derived organic material. Furthermore the results showed an increase in electrical power generation during dark periods which indicated that power generation in the PMFC was not directly related to photosynthesis.

In the next chapter the theoretical framework for competition between microbial communities is tested in order to improve the coulombic efficiency of the PMFC. To do so the microbial communities present in the *Glyceria maxima* PMFC were analyzed. The microbial communities were analyzed by PCR 454 sequencing, fluorescent in situ hybridisation in combination with confocal laser scanning microscopy. Additionally, based on the results of the analysis of the microbial community this chapter proposes substrate and electron pathways in the PMFC. The results show that denitrifying bacteria are present which consume low molecular weight organic compounds and therefore lower the coulombic efficiency of the PMFC. Furthermore, the absence of acetate utilising methanogens indicated that methanogens play a minor role in the low coulombic efficiency of the PMFC.

The PMFC is electrochemically characterized in chapter four to understand the processes that result in the high internal resistance of the PMFC. The PMFC is characterized by the current interrupt method and polarization curves. The internal resistance of the PMFC increased during current generation which explained the consistent hysteresis seen in the polarization curves. The major components of the internal resistance were

the anode resistance and membrane resistance which are due to mass transfer in the electrochemically active biofilm and mass transfer in the bulk anolyte, respectively.

The results of the electrochemical characterization in chapter four were used to design a bicathode PMFC to decrease the internal resistance and thus increase the electrical power output. The concept of the bicathode PMFC is presented in chapter five. During this experiment the PMFC was equipped with 2 cathode compartments of which only one at the time was used to generate electrical power. The objective of this experiment was to decrease the membrane resistance by switching between the 2 cathode compartments. As a consequence the accumulation of cations in the cathode compartments decreased which reduces the membrane resistance. Switching between cathode 1 and cathode 2 resulted in decrease of the membrane as well as the anode resistance, and thus an increase in the electrical power output of the PMFC.

The sixth chapter presents the tubular PMFC design which lowers the amount of anode electrode material needed, can be integrated in agricultural food production, and wet lands without the need to excavate the topsoil of the fields. In this experiment a tubular microfiltration membrane around which graphite felt is wrapped to function as anode electrode. Graphite felt was placed inside the tubular microfiltration membrane to function as cathode electrode. The use of a tubular shaped PMFC which allows integration of the PMFC technology into agricultural food production and wetlands by horizontal drilling. Horizontal drilling is a technique to apply pipe lines without the need to dig a ditch. The results show that the power density (power output per membrane surface) of the tubular PMFC was comparable to previous PMFC designs. Furthermore is showed that the amount of anode electrode material can be reduced without significantly decreasing the electrical power output.

The seventh chapter of this thesis investigated the applicability of PMFC in salt marches by using a salt marsh species (*Spartina maxima*) in a PMFC. Application of a salt march species has the advantage that the ionic strength of the electrolyte can be higher which reduces the ionic potential

loss. Furthermore application of PMFC technology in salt marshes avoids competition with agricultural food production for arable land.

The final chapter of the thesis addresses the main limitations in PMFC performance and re-evaluated the prospects and application described in the introduction according to current knowledge of the main limitation in PMFC performance.

References

Bard, A.J., Faulkner, L.R. 1980. *Electrochemical methods: fundamentals and applications*. Wiley, New York.

Berglund, M., Börjesson, P. 2006. Assessment of energy performance in the life-cycle of biogas production. *Biomass and Bioenergy*, **30**(3), 254-266.

Bond, D.R., Lovley, D.R. 2003. Electricity production by *Geobacter sulfurreducens* attached to electrodes. *Applied and Environmental Microbiology*, **69**(3), 1548-1555.

Brotas, V., Catarino, F. 1995. Microphytobenthos primary production of Tagus estuary intertidal flats (Portugal). *Netherlands Journal of Aquatic Ecology*, **29**(3-4), 333-339.

Campoccia, A., Dusonchet, L., Telaretti, E., Zizzo, G. 2009. Comparative analysis of different supporting measures for the production of electrical energy by solar PV and Wind systems: Four representative European cases. *Solar Energy*, **83**(3), 287-297.

De Schamphelaire, L., Cabezas, A., Marzorati, M., Friedrich, M.W., Boon, N., Verstraete, W. 2010. Microbial community analysis of anodes from sediment microbial fuel cells powered by rhizodeposits of living rice plants. *Applied and Environmental Microbiology*, **76**(6), 2002-2008.

De Schamphelaire, L., Rabaey, K., Boeckx, P., Boon, N., Verstraete, W. 2008a. Outlook for benefits of sediment microbial fuel cells with two bio-electrodes. *Microbial Biotechnology*, **1**(6), 446-462.

De Schamphelaire, L., Van Den Bossche, L., Hai, S.D., Hofte, M., Boon, N., Rabaey, K., Verstraete, W. 2008b. Microbial fuel cells generating electricity from rhizodeposits of rice plants. *Environmental Science and Technology*, **42**(8), 3053-3058.

De Schamphelaire, L., Verstraete, W. 2009. Revival of the biological sunlight-to-biogas energy conversion system. *Biotechnology and Bioengineering*, **103**(2), 296-304.

Fontoynont, M., Dumortier, D., Heinemann, D., Hammer, A., Olseth, J., Skartveit, A., Ineichen, P., Reise, C., Page, J., Roche, L., Beyer, H.G., Wald, L. 1998. Satellight: A WWW server which provides high quality daylight and solar radiation data for Western and Central Europe. *Proceedings of the 9th Conference on Satellite Meteorology and Oceanography*, 434-437.

Gerbens-Leenes, W., Hoekstra, A.Y., Van Der Meer, T.H. 2009. The water footprint of bioenergy. *Proceedings of the National Academy of Sciences of the United States of America*, **106**(25), 10219-10223.

Getter, K.L., Rowe, D.B., Robertson, G.P., Cregg, B.M., Andresen, J.A. 2009. Carbon sequestration potential of extensive green roofs. *Environmental Science and Technology*, **43**(19), 7564-7570.

Girguis, P.R., Nielsen, M.E., Figueroa, I. 2010. Harnessing energy from marine productivity using bioelectrochemical systems. *Current Opinion in Biotechnology*, **21**.

Goldemberg, J., Khatib, H., Ba-N'Daw, S. 2004. World Energy Assessment: Energy and the challenge of sustainability. UNDP, UNDESA, WEC.

Gorby, Y.A., Yanina, S., McLean, J.S., Rosso, K.M., Moyles, D., Dohnalkova, A., Beveridge, T.J., Chang, I.S., Kim, B.H., Kim, K.S., Culley, D.E., Reed, S.B., Romine, M.F., Saffarini, D.A., Hill, E.A., Shi, L., Elias, D.A., Kennedy, D.W., Pinchuk, G., Watanabe, K., Ishii, S., Logan, B., Nealson, K.H., Fredrickson, J.K. 2006. Electrically conductive bacterial nanowires produced by *Shewanella oneidensis* strain MR-1 and other microorganisms. *Proceedings of the National Academy of Sciences of the United States of America*, **103**(30), 11358-11363.

Hamelers, H.V.M., Ter Heijne, A., Sleutels, T.H.J.A., Jeremiasse, A.W., Strik, D.P.B.T.B., Buisman, C.J.N. 2009. New applications and performance of bioelectrochemical systems. *Applied Microbiology and Biotechnology*, 1-13.

Hamelers, H.V.M., Ter Heijne, A., Sleutels, T.H.J.A., Jeremiasse, A.W., Strik, D.P.B.T.B., Buisman, C.J.N. 2010. New applications and performance of bioelectrochemical systems. *Applied Microbiology and Biotechnology*, **85**(6), 1673-1685.

Harnisch, F., Schröder, U. 2010. From MFC to MXC: Chemical and biological cathodes and their potential for microbial bioelectrochemical systems. *Chemical Society Reviews*, **39**(11), 4433-4448.

Harnisch, F., Warmbier, R., Schneider, R., Schröder, U. 2009. Modeling the ion transfer and polarization of ion exchange membranes in bioelectrochemical systems. *Bioelectrochemistry*, **75**(2), 136-141.

He, Z., Kan, J., Mansfeld, F., Angenent, L.T., Nealson, K.H. 2009. Self-sustained phototrophic microbial fuel cells based on the synergistic cooperation between photosynthetic microorganisms and heterotrophic bacteria. *Environmental Science and Technology*, **43**(5), 1648-1654.

Helder, M., Strik, D.P.B.T.B., Hamelers, H.V.M., Kuhn, A.J., Blok, C., Buisman, C.J.N. 2010. Concurrent bio-electricity and biomass production in three Plant-Microbial Fuel Cells using *Spartina anglica*, *Arundinella anomala* and *Arundo donax*. *Bioresource Technology*, **101**(10), 3541-3547.

Herrero, A., Flores, E. 2008. *The cyanobacteria: molecular biology, genomics, and evolution*. Caister Academic Press, Norfolk.

Holmes, D.E., Bond, D.R., O'Neil, R.A., Reimers, C.E., Tender, L.R., Lovley, D.R. 2004. Microbial communities associated with electrodes harvesting electricity from a variety of aquatic sediments. *Microbial Ecology*, **48**(2), 178-190.

Imhoff, M.L., Bounoua, L., Ricketts, T., Loucks, C., Harriss, R., Lawrence, W.T. 2004. Global patterns in human consumption of net primary production. *Nature*, **429**(6994), 870-873.

Janssen, M., Tramper, J., Mur, L.R., Wijffels, R.H. 2003. Enclosed outdoor photobioreactors: Light regime, photosynthetic efficiency, scale-up, and future prospects. *Biotechnology and Bioengineering*, **81**(2), 193-210.

Jones, D.L. 1998. Organic acids in the rhizosphere - A critical review. *Plant and Soil*, **205**(1), 25-44.

Jones, D.L., Nguyen, C., Finlay, R.D. 2009. Carbon flow in the rhizosphere: Carbon trading at the soil-root interface. *Plant and Soil*, **321**(1-2), 5-33.

Kaku, N., Yonezawa, N., Kodama, Y., Watanabe, K. 2008. Plant/microbe cooperation for electricity generation in a rice paddy field. *Applied Microbiology and Biotechnology*, **79**(1), 43-49.

Kazmerski, L.L. 2006. Solar photovoltaics R&D at the tipping point: A 2005 technology overview. *Journal of Electron Spectroscopy and Related Phenomena*, **150**(2-3), 105-135.

Kim, B.H., Kim, H.J., Hyun, M.S., Park, D.H. 1999. Direct electrode reaction of Fe(III)-reducing bacterium, *Shewanella putrefaciens*. *Journal of Microbiology and Biotechnology*, **9**(2), 127-131.

Larminie, J., Dicks, A. Fuel Cell Systems Explained (2nd Edition), John Wiley & Sons.

Larssen, T., Lydersen, E., Tang, D., He, Y., Gao, J., Liu, H., Duan, L., Seip, H.M., Vogt, R.D., Mulder, J., Shao, M., Wang, Y., Shang, H., Zhang, X., Solberg, S., Aas, W., Økland, T., Eilertsen, O., Angell, V., Liu, Q., Zhao, D., Xiang, R., Xiao, J., Luo, J. 2006. Acid rain in China. *Environmental Science and Technology*, **40**(2), 418-425.

Logan, B.E., Hamelers, B., Rozendal, R., Schröder, U., Keller, J., Freguia, S., Aelterman, P., Verstraete, W., Rabaey, K. 2006. Microbial fuel cells: Methodology and technology. *Environmental Science and Technology*, **40**(17), 5181-5192.

Logan, B.E., Regan, J.M. 2006. Microbial fuel cells - Challenges and applications. *Environmental Science and Technology*, **40**(17), 5172-5180.

Lovley, D.R. 2008. The microbe electric: conversion of organic matter to electricity. *Current Opinion in Biotechnology*, **19**(6), 564-571.

Lynch, J.M. 1990. *The Rhizosphere*. John Wiley & Sons, New York.

Malik, S., Drott, E., Grisdela, P., Lee, J., Lee, C., Lowy, D.A., Gray, S., Tender, L.M. 2009. A self-assembling self-repairing microbial photoelectrochemical solar cell. *Energy and Environmental Science*, **2**(3), 292-298.

Martin, J.H., Knauer, G.A., Karl, D.M., Broenkow, W.W. 1987. VERTEX: carbon cycling in the northeast Pacific. *Deep Sea Research Part A, Oceanographic Research Papers*, **34**(2), 267-285.

McGowan, J.G., Connors, S.R. 2000. Windpower: A turn of the century review. *Annual Review of Energy and the Environment*, **25**, 147-197.

Niachou, A., Papakonstantinou, K., Santamouris, M., Tsangrassoulis, A., Mihalakakou, G. 2001. Analysis of the green roof thermal properties and investigation of its energy performance. *Energy and Buildings*, **33**(7), 719-729.

Nishio, K., Hashimoto, K., Watanabe, K. 2010. Light/electricity conversion by a self-organized photosynthetic biofilm in a single-chamber reactor. *Applied Microbiology and Biotechnology*, **86**(3), 957-964.

Pabón Pereire, C.P. 2009. Anaerobic Digestion in Sustainable Biomass Chains. in: *Sub-department of Environmental Technology*, Vol. PhD, Wageningen University. Wageningen, pp. 262.

Pham, T.H., Aelterman, P., Verstraete, W. 2009. Bioanode performance in bioelectrochemical systems: recent improvements and prospects. *Trends in Biotechnology*, **27**(3), 168-178.

Pinton, R., Varanini, Z. 2007. *The rhizosphere: biochemistry and organic substances at the soil-plant interface*. CRC, Boca Raton.

Potter, M.C. 1911. Electrical Effects Accompanying the Decomposition of Organic Compounds. *Proceedings of the Royal Society of London. Series B, Containing Papers of a Biological Character*, **84**(571), 260-276.

Rabaey, K., Verstraete, W. 2005. Microbial fuel cells: Novel biotechnology for energy generation. *Trends in Biotechnology*, **23**(6), 291-298.

Reimers, C.E., Stecher Iii, H.A., Westall, J.C., Alleau, Y., Howell, K.A., Soule, L., White, H.K., Girguis, P.R. 2007. Substrate degradation kinetics, microbial diversity, and current efficiency of microbial fuel cells supplied with marine plankton. *Applied and Environmental Microbiology*, **73**(21), 7029-7040.

Richmond, A. 2004. *Handbook of Microalgal Culture: Biotechnology and Applied Phycology*. Blackwell Publishing, Oxford.

Rozendal, R.A., Hamelers, H.V.M., Euverink, G.J.W., Metz, S.J., Buisman, C.J.N. 2006. Principle and perspectives of hydrogen production through biocatalyzed electrolysis. *International Journal of Hydrogen Energy*, **31**(12), 1632-1640.

Rozendal, R.A., Hamelers, H.V.M., Rabaey, K., Keller, J., Buisman, C.J.N. 2008. Towards practical implementation of bioelectrochemical wastewater treatment. *Trends in Biotechnology*, **26**(8), 450-459.

Sleutels, T.H.J.A., Hamelers, H.V.M., Rozendal, R.A., Buisman, C.J.N. 2009a. Ion transport resistance in Microbial Electrolysis Cells with anion and cation exchange membranes. *International Journal of Hydrogen Energy*, **34**(9), 3612-3620.

Sleutels, T.H.J.A., Lodder, R., Hamelers, H.V.M., Buisman, C.J.N. 2009b. Improved performance of porous bio-anodes in microbial electrolysis cells by enhancing mass and charge transport. *International Journal of Hydrogen Energy*, **34**(24), 9655-9661.

Solomon, S., Qin D., Manning M. , Chen Z., Marquis M., Averyt K.B., Tignor M., Miller H.L. 2007. Climate change 2007: the physical science basis; Contribution of Working Group I to the Fourth Assessment Report of the Intergovernmental Panel on Climate Change. IPCC.

Steinbusch, K.J.J., Hamelers, H.V.M., Schaap, J.D., Kampman, C., Buisman, C.J.N. 2010. Bioelectrochemical ethanol production through mediated acetate reduction by mixed cultures. *Environmental Science and Technology*, **44**(1), 513-517.

Strik, D.P.B.T.B., Hamelers, H.V.M., Buisman, C.J.N. 2010. Solar energy powered microbial fuel cell with a reversible bioelectrode. *Environmental Science and Technology*, **44**(1), 532-537.

Strik, D.P.B.T.B., Hamelers, H.V.M., Snel, J.F.H., Buisman, C.J.N. 2008a. Green electricity production with living plants and bacteria in a fuel cell. *International Journal of Energy Research*, **32**(9), 870-876.

Strik, D.P.B.T.B., Terlouw, H., Hamelers, H.V.M., Buisman, C.J.N. 2008b. Renewable sustainable biocatalyzed electricity production in a photosynthetic algal microbial fuel cell (PAMFC). *Applied Microbiology and Biotechnology*, **81**(4), 659-668.

Stumm, W., Morgan, J.J. 1996. *Aquatic chemistry: chemical equilibria and rates in natural waters*. Wiley, New York.

Taiz, L., Zeiger, E. 2006. *Plant Physiology*. Sinauer Associates Inc., Sunderland.

Takanezawa, K., Nishio, K., Kato, S., Hashimoto, K., Watanabe, K. 2010. Factors affecting electric output from rice-paddy microbial fuel cells. *Bioscience, Biotechnology and Biochemistry*, **74**(6), 1271-1273.

Tanner, C.C. 1996. Plants for constructed wetland treatment systems - A comparison of the growth and nutrient uptake of eight emergent species. *Ecological Engineering*, **7**(1), 59-83.

Tender, L.M., Gray, S.A., Groveman, E., Lowy, D.A., Kauffman, P., Melhado, J., Tyce, R.C., Flynn, D., Petrecca, R., Dobarro, J. 2008. The first demonstration of a microbial fuel cell as a viable power supply: Powering a meteorological buoy. *Journal of Power Sources*, **179**(2), 571-575.

Ter Heijne, A., Hamelers, H.V.M., De Wilde, V., Rozendal, R.A., Buisman, C.J.N. 2006. A bipolar membrane combined with ferric iron reduction as an efficient cathode system in microbial fuel cells. *Environmental Science and Technology*, **40**(17), 5200-5205.

Timmers, R.A., Strik, D.P.B.T.B., Hamelers, H.V.M., Buisman, C.J.N. 2010. Long-term performance of a plant microbial fuel cell with *Spartina anglica*. *Applied Microbiology and Biotechnology*, **86**(3), 973-981.

Turkenburg W.C., 2001. World Energy Assessment Energy and the Challenge of Sustainability; Chapter 7 Renewable Energy Technologies.

Velasquez-Orta, S.B., Curtis, T.P., Logan, B.E. 2009. Energy from algae using microbial fuel cells. *Biotechnology and Bioengineering*, **103**(6), 1068-1076.

Velasquez-Orta, S.B., Yu, E., Katuri, K.P., Head, I.M., Curtis, T.P., Scott, K. 2011. Evaluation of hydrolysis and fermentation rates in microbial fuel cells. *Applied Microbiology and Biotechnology*, **90**(2), 789-798.

Weiland, P. 2010. Biogas production: Current state and perspectives. *Applied Microbiology and Biotechnology*, **85**(4), 849-860.

Whipps, J.M., Lynch, J.M. 1985. Energy losses by the plant in rhizodeposition. *Annual Proceeding in Phytochemical Society of Europe*, **26**, 59-71.

Zou, Y., Pisciotta, J., Baskakov, I.V. 2010. Nanostructured polypyrrole-coated anode for sun-powered microbial fuel cells. *Bioelectrochemistry*, **79**(1), 50-56.

Zou, Y., Pisciotta, J., Billmyre, R.B., Baskakov, I.V. 2009. Photosynthetic microbial fuel cells with positive light response. *Biotechnology and Bioengineering*, **104**(5), 939-946.

Part 1: Characterization of the Plant Microbial Fuel Cell

2. Rhizosphere anode model explains high oxygen levels during operation of a *Glyceria maxima* PMFC

This chapter has been published as:
Timmers RA, Strik DPBTB, Arampatzoglou C, Buisman CJN, Hamelers HVM, (2011) Rhizosphere anode model explains high oxygen levels during operation of a *Glyceria maxima* PMFC. Bioresource Technology doi:10.1016/j.biortech.2011.10.088

Abstract

In this paper, the effect of root oxygen loss on energy recovery of the plant microbial fuel cell (PMFC) is described. In this manner, advanced understanding of competing processes within the rhizosphere-anode interface was provided. A microscopic model was developed on the basis of exudation, oxygen loss, biological oxidation, and biological current generation. The model was successfully validated by comparison to oxygen concentration profiles, volatile fatty acid profiles, and chemical oxygen demand profiles measured in the anode compartment.

The model predicted oxic zones around roots in the anode of the plant microbial fuel cell. The results showed an increase in electrical power generation during dark periods. This indicated that production of organic compounds by plants (that is photosynthesis) was not required for electricity generation in the PMFC. This was consistent with the model which predicted that current was generated via hydrolysis of dead root-derived organic compounds. This result means that to optimize energy recovery of a PMFC, the plant selection should focus on high root biomass production combined with low oxygen loss.

Keywords: Plant Microbial Fuel Cell, Rhizodeposition, Radial oxygen loss, Substrate availability, *Glyceria maxima*

2 Rhizosphere anode model explains high oxygen levels during operation of a *Glyceria maxima* PMFC

Notation

Symbol	Unit	Value	Description
ΔE_{an}	[V]	-	anode overpotential
E_{an}^{th}	[V]	-	Theoretical anode potential
E_{an}	[V]	-	Measured anode potential
ΔG_r	[J]	-	Gibbs free energy for the specific conditions
n	[-]	-	Number of exchanged electrons in the reaction
E_A	[V]	-	Potential of electron acceptor
E_D	[V]	-	Potential of electron donor
Y_y^x	$\left[\frac{mol_y}{mol_{biomass}}\right]$	-	Yield of micro-organisms in a mol of substrate per mol of biomass
M_{O_2}	[mol_e]	-	Amount of oxygen in mol electron equivalents
A_{root}	[m^2]	-	Root surface area
$J_{O_2}^{in}$	[mol m^{-2}_{root} s^{-1}]	-	Oxygen loss into the rhizosphere
$J_{O_2}^{out}$	[mol m^{-2}_{root} s^{-1}]	-	Flux of oxygen into the bulk anolyte
r_{O_2}	[mol_e s^{-1}]	-	Oxygen consumption rate in the rhizosphere
M_x	[mol_e]	-	Biomass in mol equivalents

r_x	[mol s^{-1}]	-	Growth rate of biomass
b_x	[mol s^{-1}]	-	Decay rate of biomass
x	[-]	-	Type of biofilm, i.e., either aerobic (O_2) or electrochemically active (EAB)
M_{LMW}	[mol_e]	-	Amount of LMW rhizodeposits in mol
J_{LMW}^{in}	[mol m^{-2}_{root} s^{-1}]	-	Exudation into the rhizosphere
J_{LMW}^{out}	[mol m^{-2}_{root} s^{-1}]	-	Flux of LMW compounds out of the AB biofilm
r_{LMW}	[mol s^{-1}]	-	Exudate consumption rate in the rhizosphere
J_y^{in}	[mol m^{-2}_{root} s^{-1}]	-	Flux of y going in
J_y^{out}	[mol m^{-2}_{root} s^{-1}]	-	Flux of y going out
y	[-]	-	Exudates or oxygen
D_x	[s^{-1}]	2.3 10^{-6}	Decay rate of micro-organisms
C_x	[mol_e m^{-3}_{root}]	1087	Density of biomass on the root in mol electron equivalents
L_x	[m]	-	Thickness of the biofilm

2.1 Introduction

Depletion of fossil fuels, increased energy demand, and climate change have increased the need for renewable and sustainable energy sources. Bio-energy is one such renewable energy source (Demirbas, 2009). However, bio-energy is not sustainable in the case of competition with agricultural food production for arable land, water, and energy (Pimentel et al., 2009). Strik et al. (2008) proposed the Plant Microbial Fuel Cell (PMFC) for the production of renewable and sustainable bio-energy based on photosynthesis to avoid competition with agricultural food production. In the PMFC, plant roots grow in the anode of a microbial fuel cell where the roots lose exudates i.e., LMW organic compounds that are used as electron donors by electrochemically active bacteria (EAB). This process results in electrical power generation.

Roots are the key element in the PMFC because they serve as the primary source of organic compounds in the anode and play a vital role in the support of plant growth. Root-derived organic compounds consist exudates and a wide range of more complex organic compounds originating from border cells (i.e., root cap cells separated from the root apex) and root debris (i.e., cell contents, lysates) i.e., soluble and insoluble organic compounds. Typical substrates for EAB include LMW organic compounds such as organic acids, amino acids, and sugars (Hamelers et al., 2009). Exudation of LMW compounds is a continuous process that is driven by passive diffusion and migration (Jones, 1998; Pinton and Varanini, 2007).

To support plant growth, roots have three important functions: i) uptake of water and nutrients, ii) storage of metabolites and nutrients, and iii) physical support of the plant. To maintain these functions, energy that is typically generated by aerobic respiration in root cells is required. In anoxic soil conditions, roots cannot obtain the required oxygen from the soil gas phase and transform partly into aerenchyma. Aerenchyma, a specialized plant tissue, has large intracellular gas spaces that can account for up to 53% of root tissue of wetland plants. Moreover aerenchyma form a continuum with the atmosphere via stomata in plant leaves (Justin and Armstrong, 1987). Oxygen can diffuse via the stomata through the aerenchyma into the rhizosphere. This oxygen loss can result in an oxic

zone around the roots (Blossfeld et al., 2011; Soukup et al., 2007). Because the anode compartment of a microbial fuel cell is an anoxic environment, aerenchyma will be formed, which results in oxygen loss and subsequent formation of oxic zones in the anode of the PMFC.

In an MFC, energy recovery is negatively affected by oxygen in the anode because of parasitic processes involving chemical and biological oxygen reduction (Harnisch and Schröder, 2009; Jones, 1998). Chemical oxygen reduction to water and biological oxygen reduction processes consume electrons and lower the number of coulombs that are available for electrical current. In addition to the consumption of electrons, oxygen reduction has a high standard potential that can result in an increased anode potential and therefore result in a lower cell potential and energy output.

Living roots in the PMFC anode can thus be expected to affect current generation in the PMFC in two opposing ways. Whereas current generation is stimulated by roots via rhizodeposition of LMW rhizodeposits, which are a substrate for EAB, it is also suppressed by the roots via oxygen loss, which may negatively affects affect the energy recovery of a PMFC.

The objective of our study was to characterize the two opposing processes within the rhizosphere-anode interface of the PMFC. To do so, a microscopic model was developed based on the baseline rhizodeposition of LMW rhizodeposits, oxygen loss, biological oxidation, and biological current generation. In this manner, an indication of the extent to which exudates provide the EAB with electron donors was obtained. The model was validated by comparison to oxygen concentration profiles, volatile fatty acid (VFA) profiles, and chemical oxygen demand (COD) profiles measured in the anode compartment of the PMFC. Furthermore, the effect of oxygen in the PMFC was determined by injection of oxygen into the anode compartment.

2.2 Theory

2.2.1 Current generation in a PMFC

In the rhizosphere of the anode compartment of the PMFC, EAB oxidize the available organic rhizodeposits and produce electrons, protons, and

bicarbonate. The EAB transfer the liberated electrons to the conductive graphite electrode (De Schamphelaire et al., 2010). Subsequently, the electrons are transported via an electrical circuit to the cathode compartment, where they are captured by a reduction process (De Schamphelaire et al., 2008; Strik et al., 2008). Hamelers (2011) proposed a model that describes the kinetics of the electrochemically active biofilm as a function of anode overpotential and the concentration of electron donors on the basis of the Butler Volmer and Monod equations. In the Butler Volmer equation, the heterogeneous electron transfer to the graphite electrode is described as a function of the anode overpotential. The Monod equation describes the biochemical oxidation of the electron donor, which appears to be dependent on the anode overpotential. The anode overpotential is defined according to Sleutels (2009) as the difference between the theoretical anode potential and the measured anode potential $\left(\Delta E_{an} = E_{an} - E_{an}^{th}\right)$.

2.2.2 Preference for oxygen over the electrode as an electron acceptor

In competition for the same electron donor, assuming the same substrate affinity, micro-organisms with a higher yield will out-compete microorganisms with a lower yield. The yield of microorganisms is dependent on the Gibbs energy that they can derive from the reaction between the electron donor and electron acceptor. To estimate this yield, the Gibbs energy dissipation method described by Kleerebezem (2010) was used. The dissipation method uses the catabolic, anabolic, and dissipated Gibbs energies to calculate the yield. For a specific electron donor, the catabolic Gibbs energy depends on the actual electron acceptor, i.e., oxygen or the graphite electrode in this model. For oxygen, the catabolic Gibbs energy is a function of the activities of protons, oxygen, and electron donor whereas for the graphite electrode it is a function of the anode overpotential, and electron donor activity.

$$\Delta G_{cat} = nF\Delta E_{an} \qquad 1$$

In the above equation, ΔG_{cat} is the catabolic Gibbs energy (J mol^{-1}), n is the number of electrons involved in the reaction, F is the Faraday constant (96485 C mol^{-1}), and ΔE_{an} is the anode overpotential (V).

The yield of EAB is a function of the anode overpotential because the catabolic Gibbs energy is a function of the anode overpotential. An increase in anode overpotential results in an increase of the Gibbs energy of the catabolic reaction, and therefore more energy is available for biomass generation. Because of the increase in the energy available for biomass generation, the yield of EAB will increase with an increase of anode overpotential. On the basis of the estimated yield of aerobic bacteria (0.82 $mol_{biomass}$ / $mol_{acetate}$ at an oxygen concentration of 10^{-10} mol L^{-1}) as compared with that of EAB (0.31 $mol_{biomass}$ / $mol_{acetate}$ in case of an anode overpotential of 0.2 V), EAB are outcompeted by aerobic bacteria in the presence of oxygen. The calculation of the yield and the definition of the catabolic and anabolic reaction can be found in Appendix 2.1.

2.2.3 Rhizosphere anode model

2.2.3.1 The root as a source of exudates and oxygen

In the model, oxygen loss and exudation was related to microbial growth. Because oxygen is the preferred electron acceptor over the graphite electrode, aerobic bacteria out-compete EAB in the presence of oxygen. As described in the introduction, living roots release exudates (electron donors) and oxygen (electron acceptor). Therefore an AB will develop adjacent to the root. The EAB will develop only when oxygen is depleted by the aerobic biofilm and exudates are available. Figure 2.1 shows a schematic representation of the rhizosphere anode model. The amount of exudates available for the EAB is now equal to the flux of exudates out of the aerobic biofilm per mol m^{-2} s^{-1}. Acetate is chosen as a model exudate because it is a suitable substrate for EAB and is a major constituent of exudation (Albrecht et al., 1993; Strik et al., 2010).

The aerobic biofilm can now be described by following three mass balances: i) the mass balance of oxygen, ii) the mass balance of the electron donor, and iii) the mass balance of the biomass.

$$\frac{d}{dt}M_{O_2} = A_{root}\left(J_{O_2}^{in} - J_{O_2}^{out}\right) + r_{O_2} \quad 2$$

$$\frac{d}{dt}M_{LMW} = A_{root}\left(J_{LMW}^{in} - J_{LMW}^{out}\right) + r_{LMW,x} \quad 3$$

$$\frac{d}{dt}M_x = r_x + b_x \quad 4$$

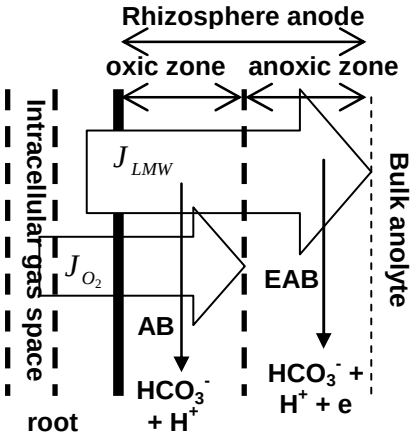

Figure 2.1: *Schematic representation of the microscopic rhizosphere anode model showing the flux of LMW rhizodeposits* $\left(J_{LMW}\right)$ *and oxygen loss* $\left(J_{O_2}\right)$ *into the rhizosphere and the aerobic (AB) and electrochemically active (EAB) biofilm. The bulk anolyte starts at the point where the LMW rhizodeposits are depleted.*

2.2.3.2 Steady-state oxic and anoxic zone

The PMFC has a long life span that is dictated by the duration of a typical growth season, which is large compared with the average lifetime of individual plant roots and doubling time of bacteria (Darrah and Staunton, 2000). Therefore, it is safe to assume a steady-state root system with a steady state biofilm, implying that there is no net change in root biomass, aerobic biofilm, or EAB biomass $\left(\frac{d}{dt}M_x = 0\right)$. Therefore, the growth rate equals the decay rate.

Oxygen and exudates diffuse through the root cell plasma membrane and the root epidermis into the rhizosphere. It can be assumed that concentrations of oxygen and electron donors in the rhizosphere are lower than those inside the root (Farrar et al., 2003). Thus, the main transport resistance is inside the root and that the flux of rhizodeposits $\left(J_{LMW}^{in}\right)$ and oxygen $\left(J_{O_2}^{in}\right)$ towards the rhizosphere is nominally constant, i.e., not influenced by the rate of consumption in the rhizosphere.

At this point, the thickness of the aerobic biofilm, i.e., the oxic zone can be calculated using the following relationships:

$$r_x = Y_y^x\left(J_y^{in} - J_y^{out}\right) \quad 5$$

$$b_x = D_x C_x L_x \quad 6$$

In steady state the growth rate equals the decay rate $\left(r_x = b_x\right)$ which makes it possible to calculate the thickness of the aerobic biofilm

$$L_x = \frac{Y_y^x.\left(J_y^{in} - J_y^{out}\right)}{D_x.C_x} \quad 7$$

Assumed all oxygen is consumed by the aerobic biofilm before EAB can grow. The flux of acetate available for EAB can now be determined using the calculated thickness of the aerobic biofilm.

$$J_y^{out} = J_y^{in} - \frac{L_y D_y.C_y}{Y_y^X} \quad 8$$

Subsequently, the thickness of the EAB biofilm can be estimated with Equation 7.

2.2.3.3 Flux of oxygen depends on root length

It is experimentally complicated to estimate the oxygen loss in the anode compartment of the PMFC. Armstrong (1975) developed a sleeving cylindrical oxygen electrode to measure the oxygen loss of individual roots. However, it is not physically possible to integrate a sleeving cylindrical

oxygen electrode into the anode of the PMFC, and therefore oxygen loss in the anode of the PMFC cannot be measured directly. Thus, experimental data provided by Soukup et al. (2007) were used to estimate the oxygen loss of *Glyceria maxima* into the anode of the PMFC.

Soukup et al. (2007) determined the oxygen loss of *G. maxima* at various distances from the root tip. The oxygen loss of *G. maxima* depends on the root length and decreases from $2.5 \cdot 10^{-7}$ mol O_2 m^{-2}_{root} s^{-1} at the root tip (0.002 m) to $2.6 \cdot 10^{-9}$ mol O_2 m^{-2}_{root} s^{-1} at 0.03 m behind the root tip, after which point the oxygen loss is stable. The average oxygen loss $\left(J_{O_2}^{in}\right)$ for multiple root lengths $\left(l_{root}\right)$ was calculated as a weighted moving average using the data provided by Soukup et al. (2007) and expressed in terms of moles per square meter per second (see Appendix 2.2). At an average root length of 0.04 m the oxygen loss is $7.8 \cdot 10^{-8}$ mol O_2 m^{-2}_{root} s^{-1}

2.2.3.4 Flux of exudates

It is experimentally complicated to determine the flux of LMW rhizodeposits in the anode compartment of the PMFC. Even experiments designed to estimate this flux are often influenced by the experimental method (Pinton and Varanini, 2007). Furthermore, exudation of LMW organic compounds is species-dependent and environmentally dependent. In the literature, a commonly found value for exudation is 10^{-9} $mol_{acetate}$ m^{-2} s^{-1} (Delhaize et al., 1993; Hoffland et al., 1989; Lu et al., 1999; Van Bodegom et al., 2001).

2.3 Material and Methods

2.3.1 PMFC construction

Four PMFCs were constructed as shown in Figure 2.2. The anode compartment of the PMFCs consisted of a glass cylinder (Schott, Duran) with a diameter of 35 mm and a height of 300 mm, with sampling points every 35 mm along each side of the cylinder. The glass cylinder was filled with 165 g of graphite granules that had diameters between 1 and 2 mm (le Carbone, Wemmel Belgium), to function as an electrode. The current collector was a 40 mm golden wire glued to a Teflon-coated copper wire. To separate the anode from the cathode, a cation exchange membrane (fumasep®, FKB) was fixed at the bottom of the glass cylinder. A Haber-Luggin capillary was placed at a depth of 0.14 m in the graphite granules. To measure the anode potential, the capillary was connected via a 3 M potassium chloride solution to an Ag/AgCl reference electrode (+205 mV versus NHE; Prosense Qis, Oosterhout, the Netherlands).

The cathode compartment consisted of PVC beakers with diameters of 110 mm, in which 6 mm thick graphite felt (Coidan Graphite Products LTD, York, United Kingdom), to which the current collector was connected, was placed. The catholyte was 50 mM ferric cyanide ($K_3[Fe(CN)]_6$ solution buffered with 8 mM potassium phosphate buffer (pH 6.8).

The PMFC was constructed by placing the anode on top of the graphite felt in the cathode. To close the electrical circuit, the current collectors were connected across an external resistance of 900 Ω.

2.3.2 Preparation of graphite granules

To develop EAB in the anode compartment, the setup was first operated without plants. To ensure the presence of EAB, the anode compartment was inoculated with 5 ml of an anolyte of an MFC operated with acetate. The medium used to grow EAB on the graphite granules was ½ Hoagland buffered with 8 mM potassium phosphate buffer solution (pH 6.8). Because of the large range of organic compounds excreted by plant roots (i.e., substrates), a different substrate was added to the medium. Potassium acetate (10 mM) was used for PMFCs 1 through 4, whereas glucose (10

mM) was used for PMFCs 5 through 8. The setups were operated using the artificial medium for 41 days, during which period the anolyte was refreshed with medium on day 18 and day 35. The average current density before the plants were introduced was 300 ± 30 mA m^{-2} for the acetate-operated PMFCs and 75 ± 10 mA m^{-2} for the glucose-operated PMFCs.

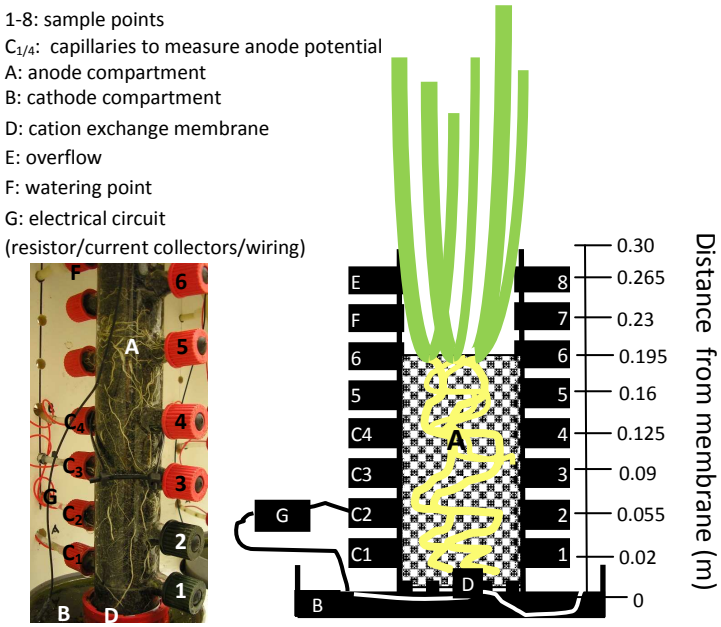

Figure 2.2: *Schematic representation of the anode and cathode compartment of the PMFC and picture of anode compartment of the PMFC.*

2.3.3 Plant-MFC operation

Before graphite granules with the electrochemically active biofilm were used for PMFCs, they were mixed and rinsed with tap water to remove any residual substrate. In total, there were 6 PMFCs. In each PMFC, one stem of *G. maxima* (D'n Bart Waterplanten, the Netherlands) with a mass between 4.4 g and 7.8 g was planted. The medium used to feed the PMFCs was ½ Hoagland buffered with 8 mM potassium phosphate buffer solution as described by Timmers et al. (2010) (pH 6.8, conductivity between 1.5 through 1.7 mS m^{-1}). The medium was fed from the top through sample point 8, which was located 0.07 m above the graphite granules. The applied flow rate was 0.17 ml s^{-1} throughout the experiment. The feeding frequency

of the PMFC with buffered ½ Hoagland medium was 5 minutes every 12 hours.

To determine the effect of oxygen in the PMFC, oxygen was injected in the anode of the PMFCs. Oxygen was injected at day 25 by feeding the medium through Sample Point 1, which was located at a depth of 0.175 m in the graphite granules. The oxygen concentration of the medium was 7.7 mg L^{-1}, which can potentially take up 4.72 Coulombs. The oxygen concentration profile in the anode was measured 1 hour after the feeding stopped.

Both the MFC and the PMFC setups were placed in a climate control cabinet (Microclima 1750 Snijders, Tilburg the Netherlands) under the following environmental conditions: the illumination period was 14 h d^{-1}, the average light density in the photo active region was 596 ± 161 µmol m^{-2} s^{-1}, temperature was 25 ^{o}C and humidity was 75%.

2.3.4 Measurements

Cell potential, anode potential, and temperature were measured online with a data acquisition instrument (Fieldpoint module FP-AI-112) connected to a personal computer with Labview software via the Fieldpoint Ethernet Controller Module FP-2000 (National Instruments, Austin, Texas, USA). Anode potential was measured at Sample Point 2 with respect to the silver/silver chloride (Ag/AgCl) reference electrodes (+205 mV vs. NHE ProSense QiS, Netherlands). Cathode potential was measured offline using a true RMS multimeter (Fluke 189, Fluke Europe B.V., the Netherlands) with respect to the silver/silver chloride (Ag/AgCl) reference electrodes (+205 mV vs. NHE ProSense QiS, Netherlands).

Volatile fatty acids and the chemical oxygen demand of samples were measured at depths of -0.175 m, -0.14 m, -0.105 m, -0.07 m, -0.035, and 0 m in the anode of the PMFC at days 40 and 44. Volatile fatty acid concentration and the chemical oxygen demand were measured as described by Timmers et al (2010). Oxygen concentration profiles in the anode were measured at days 40 and 44 at depths of -0.175 m, -0.14 m, -0.105 m, -0.07 m, -0.035, and 0 m in the anode of the PMFC.

Oxygen was measured using a needle-type oxygen micro-sensor with a sensor tip smaller than 50 µm. To measure oxygen in the anode, an optical needle-type oxygen micro-sensor was inserted in the sample points, after which the optical fiber sensor was pushed out of the needle into the anolyte. The optical needle-type oxygen sensor was connected to an OXY-4 micro, 4-channel fiber-optic oxygen meter (Presens Precision Sensing GmbH, Germany).

2.4 Results and discussion

2.4.1 Rhizosphere anode model predictions

2.4.1.1 No exudates available for current generation

The availability of exudates for EAB depends on the flux into the rhizosphere and the oxygen loss, which depends on root length. Figure 2.3 shows that no exudates are available for current generation at a commonly determined value for exudation of 10^{-9} mol m^{-2} s^{-1} (Delhaize et al., 1993; Hoffland et al., 1989; Lu et al., 1999; Van Bodegom et al., 2001) which is reflected by the negative availability. This indicated that production of organic compounds by plants (that is photosynthesis) was not required for electricity generation in the PMFC. Furthermore it showed that the aerobic biofilm is not limited by the availability of oxygen but is instead limited by the availability of exudates. Therefore, all exudates will be consumed by the aerobic biofilm rather than by EAB, and no exudates are available for current generation by EABs. Furthermore, the limitation of the aerobic biofilm by the availability of exudates instead of oxygen results in an oxygen flux from the root into the bulk anolyte. The flux of oxygen into the bulk anolyte varies between $2.5 \cdot 10^{-7}$ mol m^{-2} s^{-1} and $0.4 \cdot 10^{-7}$ mol m^{-2} s^{-1}, depending on the average root length.

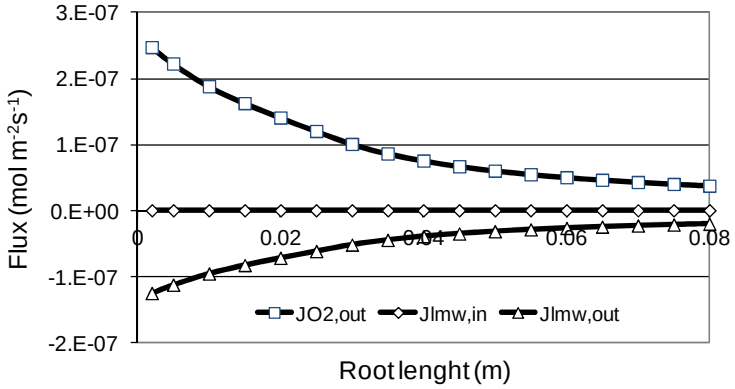

Figure 2.3: *The modeled flux of LMW compounds available for EAB* $\left(J_{LMW,out}\right)$*, oxygen loss into the bulk anolyte* $\left(J_{O_2,out}\right)$ *and exudation* $\left(J_{LMW,in}\right)$*. The figure shows that all exudates will be consumed by aerobic bacteria present in the rhizosphere and that the roots loose oxygen into the bulk anode solution.*

2.4.1.2 Current generation via hydrolysis of complex organic compounds

Current generation is a clear indication that LMW organic compounds are oxidized in the anode of the PMFC (see Fig. 4). This raises the question where do the LMW organic compounds come from since no exudates available for current generation. As described in the introduction roots are also the source of more complex organic compounds, consisting of soluble and insoluble organic carbon originating from sloughed-off border cells, dead roots, and dead microbial biomass. Plant biomass consist for 35 to 50% of cellulose (Lynd et al., 1999). EAB are not able to generate electricity directly from cellulose (Ren et al., 2008) and have a low energy conversion efficiency for complex organic compounds (< 3%). Therefore, it is likely that the hydrolysis of cellulose originating from root debris, sloughed-off border cells, and the aerobic biofilm is the source of LMW organic compounds required for current generation. The idea that current is generated via hydrolysis of cellulosic biomass and not directly from exudates is supported by the long start-up time required for the PMFC (Helder et al.; Strik et al., 2008; Strik et al., 2011). The long starts up times are in contrast with current generation based on exudation. Based on exudation only, current generation would start as soon as the roots are introduced in the anode of the PMFC. The model explains why no current is generated by living roots (see previous discussion 5.1.1); moreover they lose oxygen into the bulk

anolyte. In the bulk anolyte, oxygen will be consumed by chemical oxygen reduction or biochemical oxygen reduction of organic compounds originating from the hydrolysis of root-derived organic compounds. Therefore, to produce current, the production of LMW organic compounds should exceed the oxygen flux into the bulk. In anoxic conditions the production of LMW compounds is limited by the hydrolysis rate of cellulose (Pavlostathis and Giraldo-Gomez, 1991). The hydrolysis rate is proportional to the cellulose concentration (Eastman and Ferguson, 1981) and therefore there should be sufficient cellulose to produce sufficient LMW organic compounds to compensate for the oxygen loss by living roots. More specifically, the hydrolysis rate is directly related to the quantity of dead roots because they consist for 35 to 50% of cellulose (Lynd et al., 1999). It can be inferred that long start-up times are required for the accumulation of sufficient cellulose to reach the required hydrolysis rate to produce sufficient LMW organic compounds to compensate for the oxygen loss by living roots.

2.4.1.3 Low coulombic efficiency is due to poor biodegradability of insoluble organic carbon and the presence of alternative electron acceptors

The flux of more complex root-derived organic compounds consisting of soluble and insoluble organic carbon originating is $2.5 \cdot 10^{-6}$ mol_C m^{-2}_{root} s^{-1} (Darrah, 1991). The decrease of the availability of soluble and insoluble organic carbon due to oxygen is maximally 5%. Therefore a coulombic efficiency of 95% would be possible is all the soluble and insoluble organic carbon can be converted into current by EAB. The amount of available insoluble and soluble root-derived organic compounds is to an average current density of 1 A m^{-2}_{root}. In PMFC literature current density is expressed as current per geometric surface area. To convert the current density per root surface area to geometric surface area the root area index (root surface area per surface area) is used. *G. maxima* is a temperate aquatic grass. With a root area index for temperate grassland of 79 m^2_{root} $m^{-2}_{surface}$ (Jackson et al., 1997), the average current density would be 79 A $m^{-2}_{surface}$. The highest reported average current density generated by a PMFC is approximately 0.200 A $m^{-2}_{surface}$ (Timmers et al.). This result indicates that the coulombic efficiency in the PMFC is 0.25%, which is far below the

coulombic efficiency for cellulose in a MFC reported by Ren et al. (2008). The low coulombic efficiency is explained by a combination poor biodegradability of the insoluble organic carbon and the presence of alternative electron acceptors. The insoluble organic carbon made up 66 % of the root derived organic carbon. Furthermore it is likely that oxygen is not the only competing electron acceptor present in the rhizosphere anode, as nitrate ($3.7 \cdot 10^{-6}$ mol $m^{-2}_{surface}$ s^{-1} which potentially consumes 1.8 A $m^{-2}_{surface}$), sulfate ($6.1 \cdot 10^{-7}$ mol $m^{-2}_{surface}$ s^{-1} which potentially consumes 0.24 A $m^{-2}_{surface}$), and carbon dioxide are added with the medium and therefore also available. The yield of the competing micro-organisms will most likely determine the amount of LMW organic compounds available for EAB. The yield of various potentially competing microorganisms was calculated with the Gibbs energy dissipation as described by Kleerebezem et al. (2010) based on the concentration in the medium (see Appendix 2.1). The results show that EAB are outcompeted by aerobic bacteria and denitrifying bacteria at realistic anode overpotentials of up to 0.2 V (Hamelers et al., 2011). Methanogenic micro-organisms and sulfate reducing bacteria, however, can be outcompeted by EAB at anode overpotentials of 0.02 V and 0.03 V, respectively.

2.4.2 Rhizosphere anode model validation

2.4.2.1 No direct link between photosynthesis and current generation

There no obvious light-dark pattern observed in current generation (Figure 2.4), this was consistent with the findings of Timmers et al. (2010). The results showed an increase in electrical power generation during dark periods. This indicated that production of organic compounds by plants (that is photosynthesis) was not required for electricity generation in the PMFC. During dark periods there is no photosynthesis, however, in most cases current generation increased at the beginning of a dark period. Increase in current generation in dark periods can be explained by a decrease in oxygen loss in dark periods. The oxygen concentration around roots of aerenchymatous plants decreases at dark periods, this could indicate a decrease of oxygen loss by plant roots in dark periods (Nikolausz et al., 2008). The rhizosphere anode model predicted that a decrease in

oxygen loss will result in an increase of LMW organic compounds available for EAB and thus current generation.

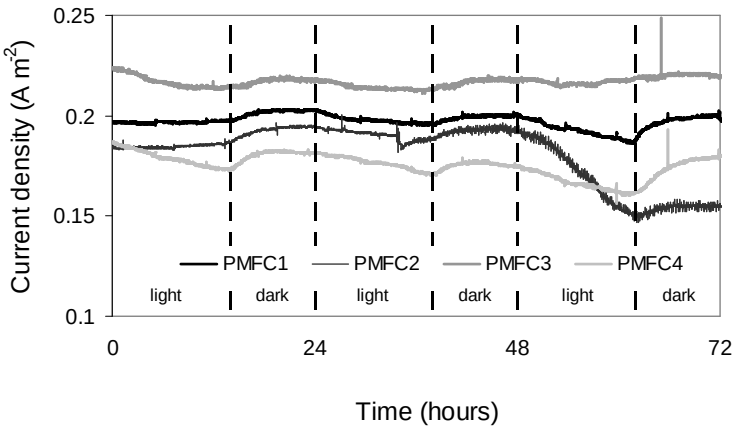

Figure 2.4: *No clear light-dark pattern in current generation of PMFC 1 through 4 from day 41 through 43.*

2.4.2.2 Oxygen profile is consistent with the rhizosphere anode model

In natural sediments, oxygen is depleted within a depth in the order of mm because of the degradation of organic matter and slow oxygen diffusion in the sediment (Frenzel et al. 1992). Based on a penetration depth in the order of mm the oxygen flux via the top of the PMFC into the anode is negligible compared to the oxygen loss via plant roots into the anode (see Appendix 2.3).

In the PMFC, oxygen is measured up to a depth of 0.175 m, which indicated that roots are the source of oxygen. Figure 2.5a shows the oxygen profiles measured in PMFC1 through PMFC4. The oxygen concentration decreased with an increase in depth in the graphite bed. Figure 2.5b shows a general picture of root growth in the anode compartment of a PMFC. Root density decreased with an increase in depth in the graphite bed. The rhizosphere anode model predicted the presence of oxic zones in the anode compartment. It is obvious that a higher root density resulted in a higher probability of detecting oxygen. It can be hypothesized that the oxic zones overlap and thus that high oxygen concentrations exist at depths of 0 through 0.035 m because of the high root density.

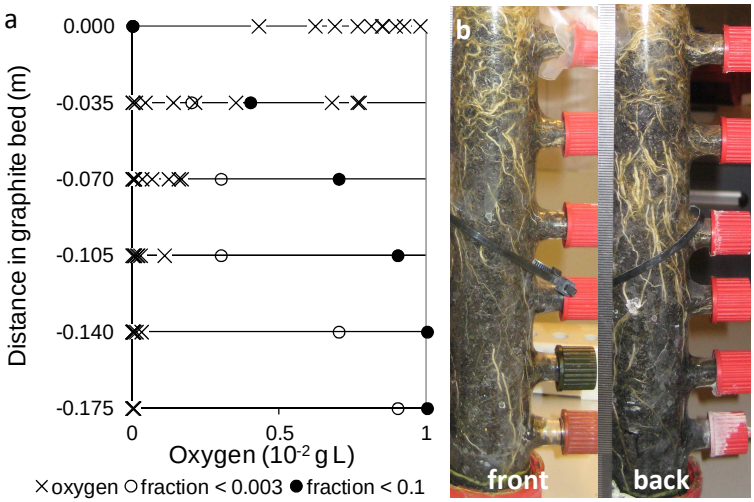

Figure 2.5: a) *Oxygen was present in anode compartment of the PMFC. Oxygen concentration in mg L^{-1} measured at a depth of 0, 0.035, 0.07, 0.105, 0.14, and 0.175 m in anode compartments of the PMFCs on day 40, and day 44 of the experiment.* ***Figure 2.5: b)*** *General root distribution throughout the anode compartment of a PMFC, picture is of PMFC1.*

Oxygen concentration in anode of PMFC1 through PMFC4 at current generation varied between 0.00 mg L^{-1} and 8.92 mg L^{-1}, 36 % of oxygen measurements were below 0.03 mg L^{-1}, 32 % of oxygen measurements were between 0.03 mg L^{-1} and 1 mg L^{-1}, and 32 % of oxygen measurements were above 1 mg L^{-1}. Oh et al. (2009) measured oxygen concentrations up to 0.03 mg L^{-1} in the anode of a MFC at periods of current generation, and suggest a threshold bulk oxygen concentration of 1 mg L^{-1} above which no current is generated. The relative high oxygen concentration in anode of the PMFC during current generation can be explained by the presence of oxic zones and anoxic zones in the PMFC. Anoxic zones (O_2 < 0.03 mg L^{-1}) were measured throughout the anode. The percentage of oxygen measurements below 0.03 mg L^{-1} increased with depth from 0 % at a depth of 0 m in the graphite bed through 90 % at a depth of 0.175 m in the graphite bed. The current that was generated during the oxygen measurements at day 40 was 0.18 mA for PMFC1, 0.11 mA for PMFC2, 0.21 mA for PMFC3, and 0.11 mA for PMFC4. At day 44, the current generated was 0.18 mA for PMFC1, 0.12 mA for PMFC2, 0.15 mA for PMFC3, and 0.04 mA for PMFC4.

2.4.2.3 VFA and COD concentrations are consistent with the rhizosphere anode model

The rhizosphere anode model predicts that the exudates are consumed within the biofilm i.e., the concentration in the anolyte is low. The VFA concentration is a measure of exudates present in the bulk anolyte. VFA measurements for all PMFCs were below the detection limit (2 mg L^{-1}). This low VFA concentration in the bulk anolyte is predicted by the model, as it is assumed that the EAB consume the available LMW organic compounds. The residual concentration of soluble COD (50 ± 25 mg L^{-1}) likely arises from a combination of the COD iron complex in the ½ Hoagland medium (10.4 mg L^{-1}) and the poorly hydrolysable cellulose present in the dead plant roots. The soluble COD concentration is low, which indicates that the *G. maxima* PMFC was limited by the hydrolysis rate of the insoluble cellulose.

2.4.2.4 Oxygen negatively affects current generation

The effect of the oxygen injection on the anode potential and current density is shown in Figure 2.6. Assuming that the current generation during oxygen injection is constant, the loss of electrons from the oxygen injection was estimated to be 1.2 C. The minimum amount of coulombs that was taken up by oxygen was 25% because as previously mentioned, the current likely increased because of an increase in anode overpotential (Hamelers et al., 2011). However, it is unlikely that the increased current generation explains the missing oxygen. The calculated anode overpotential before oxygen injection was 0.254 V (-0.247+0.501), and the maximum overpotential after the oxygen injection was 0.395 V (-0.106+0.501). Both overpotentials were in the region where the Butler-Volmer-Monod model of Hamelers (2011) predicts the maximum current, and thus the increase in overpotential negligibly affected the current. Trace amounts of oxygen can also have a positive effect on current generation through an increase in the hydrolysis rate (Johansen and Bakke, 2006). The increase in the hydrolysis rate may increase the availability of LMW organic compounds for EAB and thus increase current generation.

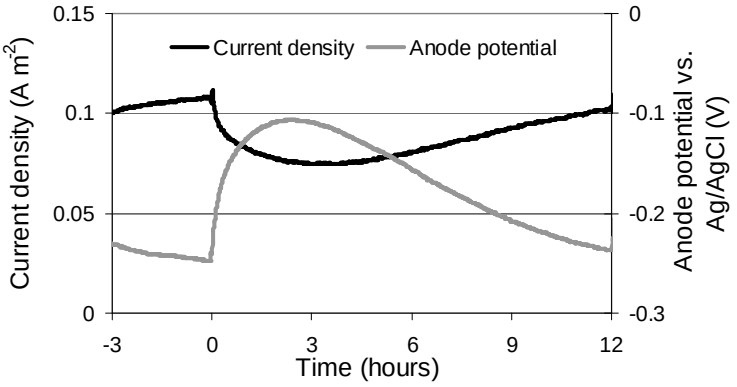

Figure 2.6: *Current density of the PMFC decreased and anode potential (vs. Ag/AgCl) increased due to oxygen injection. The oxygen was injected at Time = 0 (hours).*

It is unlikely, however, that the combined effect of the increased hydrolysis rate and the increased anode overpotential resulted in an increase of current sufficient to consume 75% of the injected oxygen. It is more likely that oxygen is also consumed by processes that do not consume exudates or electrons. These processes may be: i) biological oxidation of rhizodeposits that are not suitable as electron donors for EAB, such as cellulose, or ii) oxygen uptake by plant roots for aerobic respiration.

2.5 Conclusions

The model predicted that there is no direct link between current generation and photosynthesis. Furthermore that the exudates were consumed within the aerobic biofilm and therefore do not directly contribute to current generation in the PMFC. The LMW organic compounds needed for EAB to generate current originate from the hydrolysis of soluble and insoluble root-derived organic compounds. Plant selection should focus on high root biomass production to optimize the energy recovery of a PMFC.

The low coulombic efficiency is likely due to the poor biodegradability of insoluble organic carbon and the presence of alternative electron acceptors in the medium.

Acknowledgements

This research was funded by Senternovem, the Dutch governmental agency for sustainability and innovation in the Ministry of Finance (grant no. EOSLT06020), and supported by Alliander. The authors would like to thank Marjolein Helder, Kirsten Steinbusch, and Wouter Bac for their useful comments.

References

Albrecht, G., Kammerer, S., Praznik, W., Wiedenroth, E.M. 1993. Fructan content of wheat seedlings (*Triticum aestivum L.*) under hypoxia and following re-aeration. *New Phytol.*, **123**, 471.

Armstrong, W., Wright, E.J. 1975. Radial Oxygen Loss from Roots: Theoretical Basis for the Manipulation of Flux Data obtained by the Cylindrical Platinum Electrode Technique. *Physiol. Plant.*, **35**, 6.

Blossfeld, S., Gansert, D., Thiele, B., Kuhn, A.J., Lösch, R. 2011. The dynamics of oxygen concentration, pH value, and organic acids in the rhizosphere of Juncus spp. *Soil Biology and Biochemistry*.

Darrah, P.R. 1991. Models of the rhizosphere - I. Microbial population dynamics around a root releasing soluble and insoluble carbon. *Plant and Soil*, **133**(2), 187-199.

Darrah, P.R., Staunton, S. 2000. A mathematical model of root uptake of cations incorporating root turnover, distribution within the plant, and recycling of absorbed species. *European Journal of Soil Science*, **51**(4), 643-653.

De Schamphelaire, L., Cabezas, A., Marzorati, M., Friedrich, M.W., Boon, N., Verstraete, W. 2010. Microbial community analysis of anodes from sediment microbial fuel cells powered by rhizodeposits of living rice plants. *Applied and Environmental Microbiology*, **76**(6), 2002-2008.

De Schamphelaire, L., Van Den Bossche, L., Hai, S.D., Höfte, M., Boon, N., Rabaey, K., Verstraete, W. 2008. Microbial fuel cells generating electricity from rhizodeposits of rice plants. *Environmental Science and Technology*, **42**(8), 3053-3058.

Delhaize, E., Craig, S., Beaton, C.D., Bennet, R.J., Jagadish, V.C., Randall, P.J. 1993. Aluminium tolerance in wheat (*Triticum aestivum L.*). I.Uptake and distribution of aluminium in root apices. *Plant Physiology*, **103**(3), 685-693.

Demirbas, A. 2009. Political, economic and environmental impacts of biofuels: A review. *Applied Energy*, **86**(SUPPL. 1), S108-S117.

Eastman, J.A., Ferguson, J.F. 1981. Solubilization of particulate organic carbon during the acid phase of anaerobic digestion. *Journal of the Water Pollution Control Federation*, **53**(3 I), 352-366.

Farrar, J., Hawes, M., Jones, D., Lindow, S. 2003. How roots control the flux of carbon to the rhizosphere. *Ecology*, **84**(4), 827-837.

Hamelers, H.V.M., Ter Heijne, A., Sleutels, T.H.J.A., Jeremiasse, A.W., Strik, D.P.B.T.B., Buisman, C.J.N. 2009. New applications and performance of bioelectrochemical systems. *Applied Microbiology and Biotechnology*, 1-13.

Hamelers, H.V.M., ter Heijne, A., Stein, N., Rozendal, R.A., Buisman, C.J.N. 2011. Butler-Volmer-Monod model for describing bio-anode polarization curves. *Bioresource Technology*, **102**(1), 381-387.

Harnisch, F., Schröder, U. 2009. Selectivity versus mobility: Separation of anode and cathode in microbial bioelectrochemical systems. *ChemSusChem*, **2**(10), 921-926.

Helder, M., Strik, D.P.B.T.B., Hamelers, H.V.M., Kuhn, A.J., Blok, C., Buisman, C.J.N. Concurrent bio-electricity and biomass production in three Plant-Microbial Fuel Cells using *Spartina anglica, Arundinella anomala* and *Arundo donax*. *Bioresource Technology*.

Hoffland, E., Findenegg, G.R., Nelemans, J.A. 1989. Solubilization of rock phosphate by rape - II. Local root exudation of organic acids as a response to P-starvation. *Plant and Soil*, **113**(2), 161-165.

Jackson, R.B., Mooney, H.A., Schulze, E.D. 1997. A global budget for fine root biomass, surface area, and nutrient contents. *Proceedings of the National Academy of Sciences of the United States of America*, **94**(14), 7362-7366.

Johansen, J.E., Bakke, R. 2006. Enhancing hydrolysis with microaeration. in: *Water Science and Technology*, Vol. 53, pp. 43-50.

Jones, D.L. 1998. Organic acids in the rhizosphere - A critical review. *Plant and Soil*, **205**(1), 25-44.

Justin, S.H.F., Armstrong, W. 1987. The anatomical characteristics of roots and plant response to soil flooding. *New Phytol.*, **106**, 465.

Kleerebezem, R., Van Loosdrecht, M.C.M. 2010. A generalized method for thermodynamic state analysis of environmental systems. *Critical Reviews in Environmental Science and Technology*, **40**(1), 1-54.

Lu, Y., Wassmann, R., Neue, H.U., Huang, C. 1999. Impact of phosphorus supply on root exudation, aerenchyma formation and methane emission of rice plants. *Biogeochemistry*, **47**(2), 203-218.

Lynd, L.R., Wyman, C.E., Gerngross, T.U. 1999. Biocommodity engineering. *Biotechnology Progress*, **15**(5), 777-793.

Nikolausz, M., Kappelmeyer, U., Szàkely, A., Rusznyàk, A., Márialigeti, K., Kästner, M. 2008. Diurnal redox fluctuation and microbial activity in the rhizosphere of wetland plants. *European Journal of Soil Biology*, **44**(3), 324-333.

Oh, S.E., Kim, J.R., Joo, J.H., Logan, B.E. 2009. Effects of applied voltages and dissolved oxygen on sustained power generation by microbial fuel cells. *Water science and technology : a journal of the International Association on Water Pollution Research*, **60**(5), 1311-1317.

Pavlostathis, S.G., Giraldo-Gomez, E. 1991. Kinetics of anaerobic treatment. *Water Science and Technology*, **24**(8), 35-59.

Pimentel, D., Marklein, A., Toth, M.A., Karpoff, M.N., Paul, G.S., McCormack, R., Kyriazis, J., Krueger, T. 2009. Food versus biofuels: Environmental and economic costs. *Human Ecology*, **37**(1), 1-12.

Pinton, R., Varanini, Z. 2007. *The rhizosphere : biochemistry and organic substances at the soil-plant interface*. CRC, Boca Raton.

Ren, Z., Steinberg, L.M., Regan, J.M. 2008. Electricity production and microbial biofilm characterization in cellulose-fed microbial fuel cells. *Water Science and Technology* **58**(3), 617-622.

Sleutels, T.H.J.A., Hamelers, H.V.M., Rozendal, R.A., Buisman, C.J.N. 2009. Ion transport resistance in Microbial Electrolysis Cells with anion and cation exchange membranes. *International Journal of Hydrogen Energy*, **34**(9), 3612-3620.

Soukup, A., Armstrong, W., Schreiber, L., Franke, R., Votrubovaì, O. 2007. Apoplastic barriers to radial oxygen loss and solute penetration: A chemical and functional comparison of the exodermis of two wetland species, *Phragmites australis* and *Glyceria maxima*. *New Phytologist*, **173**(2), 264-278.

Strik, D.P.B.T.B., Hamelers, H.V.M., Buisman, C.J.N. 2010. Solar energy powered microbial fuel cell with a reversible bioelectrode. *Environmental Science and Technology*, **44**(1), 532-537.

Strik, D.P.B.T.B., Hamelers, H.V.M., Snel, J.F.H., Buisman, C.J.N. 2008. Green electricity production with living plants and bacteria in a fuel cell. *International Journal of Energy Research*, **32**(9), 870-876.

Strik, D.P.B.T.B., Timmers, R.A., Helder, M., Steinbusch, K.J.J., Hamelers, H.V.M., Buisman, C.J.N. 2011. Microbial solar cells: Applying photosynthetic and electrochemically active organisms. *Trends in Biotechnology*, **29**(1), 41-49.

Timmers, R.A., Strik, D.P.B.T.B., Hamelers, H.V.M., Buisman, C.J.N. Long-term performance of a plant microbial fuel cell with *Spartina anglica*. *Applied Microbiology and Biotechnology*, **86**(3)**,** 973-981.

Van Bodegom, P., Goudriaan, J., Leffelaar, P. 2001. A mechanistic model on methane oxidation in a rice rhizosphere. *Biogeochemistry*, **55**(2), 145-177.

Appendix 2.1: Yield calculated based on Appendix D: Generalized Growth and stoichiometric calculations (Kleerebezem & Van Loosdrecht, 2010)

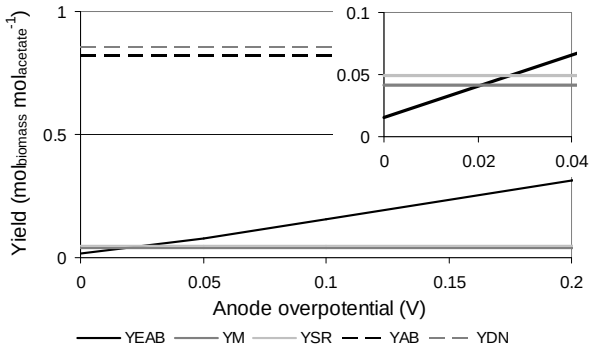

Figure A.2.1: *Theoretical yield, in mol biomass per mol acetate of competing microbial processes in PMFC versus anode overpotential. Y_{EAB} is the yield of electrochemically active bacteria, Y_{AB} is the yield of aerobic bacteria, Y_{DN} is the yield of the denitrifying bacteria, Y_{SR} is the yield of the sulfate reducing bacteria, and Y_M is the yield of the methanogens.*

Definition and calculation of stoichiometric coefficients determined according to Appendix D: Generalized Growth and stoichiometric calculations (Kleerebezem & Van Loosdrecht, 2010)

Definition of anabolic reaction

$$an* =$$
$$-0.525C_2H_3O_2^- - 0.2NH_4^+ - 0.3H^+ + CH_{1.8}O_{0.5}N_{0.2} + 0.4H_2O + 0.05HCO_3^- + 0.025e = 0$$
$$C = -0.525 \cdot 2 + 1 \cdot 1 + 0.05 \cdot 1 = 0$$
$$H = -0.525 \cdot 3 - 0.2 \cdot 4 - 0.3 \cdot 1 + 1 \cdot 1.8 + 0.4 \cdot 2 + 0.05 \cdot 1 = 0$$
$$O = -0.525 \cdot 2 + 1 \cdot 0.5 + 0.4 \cdot 1 + 0.05 \cdot 3 = 0$$
$$N = -0.2 \cdot 1 + 1 \cdot 0.2 = 0$$
$$e = -0.525 \cdot -1 - 0.2 \cdot 1 - 0.3 \cdot 1 + 0.025 \cdot -1 = 0$$
$$D = -C_2H_3O_2^- - 4H_2O + 2HCO_3^- + 9H^+ + 8e = 0$$
$$C = -1 \cdot 2 + 2 \cdot 1 = 0$$
$$H = -1 \cdot 3 - 4 \cdot 2 + 2 \cdot 1 + 9 \cdot 1 = 0$$
$$O = -1 \cdot 2 - 4 \cdot 1 + 2 \cdot 3 = 0$$
$$e = -1 \cdot -1 + 2 \cdot -1 + 9 \cdot 1 - 8 = 0$$
$$anabolic =$$
$$-0.6125C_2H_3O_2^- - 0.2NH_4^+ + CH_{1.8}O_{0.5}N_{0.2} + 0.05H_2O + 0.4875H^+ + 0.225HCO_3^- + 0.725e = 0$$

Calculation of Gibbs energy of anabolic reaction

$$\Delta G_R^1 = \Delta G_R^0 + RT\sum_{i=1}^{n} Y_{si}^R \ln(a_{Si})$$

formula 25 in (Kleerebezem & Van Loosdrecht, 2010)

$$\Delta G_{An}^1 = \Delta G_{An*}^1 - \frac{Y_e^{An*}}{Y_e^D}\Delta G_D^1$$

Appendix D of (Kleerebezem & Van Loosdrecht, 2010)

$$Y_e^{An*} = -\frac{0.2 \cdot 2 - 3 + 2 \cdot 2}{2} = -0.7$$

Appendix D of (Kleerebezem & Van Loosdrecht, 2010))

$$Y_e^D = 8$$

Catabolytic reaction Oxygen

$$D = -C_2H_3O_2^- - 4H_2O + 2HCO_3^- + 9H^+ + 8e = 0$$
$$C = -1 \cdot 2 + 2 \cdot 1 = 0$$
$$H = -1 \cdot 3 - 4 \cdot 2 + 2 \cdot 1 + 9 \cdot 1 = 0$$
$$O = -1 \cdot 2 - 4 \cdot 1 + 2 \cdot 3 = 0$$
$$e = -1 \cdot 1 - 2 \cdot 1 + 9 \cdot 1 - 8 = 0$$
$$A = -O_2 - 4H^+ - 4e + 2H_2O$$
$$H = -4 \cdot 1 + 2 \cdot 2 = 0$$
$$O = -1 \cdot 2 + 2 \cdot 1 = 0$$
$$e = -4 \cdot 1 - 4 \cdot -1 = 0$$

$$catabolic = -C_2H_3O_2^- - 2O_2 + 2HCO_3^- + H^+ = 0$$

Calculation of Gibbs energy of catabolic reaction oxygen

$$\Delta G_R^1 = \Delta G_R^0 + RT \sum_{i=1}^{n} Y_{si}^R \ln(a_{Si})$$

$$\Delta G_{Cat}^1 = \Delta G_A^1 - \frac{Y_e^A}{Y_e^D} \Delta G_D^1$$

$$Y_e^D = +8$$
$$Y_e^A = -4$$

Catabolic reaction Nitrate

$D = -C_2H_3O_2^- - 4H_2O + 2HCO_3^- + 9H^+ + 8e = 0$
$C = -1 \cdot 2 + 2 \cdot 1 = 0$
$H = -1 \cdot 3 - 4 \cdot 2 + 2 \cdot 1 + 9 \cdot 1 = 0$
$O = -1 \cdot 2 - 4 \cdot 1 + 2 \cdot 3 = 0$
$e = -1 \cdot 1 - 2 \cdot 1 + 9 \cdot 1 - 8 = 0$
$A = -2NO_{2\,3}^- - 12H^+ - 10e + N_{2+} + 6H_2O$
$N = -2 \cdot 1 + 1 \cdot 2 = 0$
$O = -2 \cdot 3 + 6 \cdot 1 = 0$
$H = -12 \cdot 1 + 6 \cdot 2 = 0$
$e = -2 \cdot -1 - 12 \cdot 1 - 10 \cdot -1 = 0$

$catabolic = -C_2H_3O_2^- - 1.6NO_3^- - 0.6H^+ + 0.8H_2O + 2HCO_3^- + 0.8N_2 = 0$

$Y_e^D = +8$
$Y_e^A = -10$

Catabolytic reaction Sulfate

$An: -C_2H_3O_2^- - 4H_2O + 2HCO_3^- + 9H^+ + 8e = 0$
$C: -1 \cdot 2 + 2 \cdot 1 = 0$
$H: -1 \cdot 3 - 4 \cdot 2 + 2 \cdot 1 + 9 \cdot 1 = 0$
$O: -1 \cdot 2 - 4 \cdot 1 + 2 \cdot 3 = 0$
$e: -1 \cdot 1 - 2 \cdot 1 + 9 \cdot 1 - 8 = 0$
$cat: -SO_4^{2-} - 9H^+ - 8e + HS^- + 4H_2O = 0$
$S: -1 \cdot 1 + 1 \cdot 1 = 0$
$O: -1 \cdot 4 + 4 \cdot 1 = 0$
$H: -9 \cdot 1 + 1 \cdot 1 + 4 \cdot 2 = 0$
$e: -1 \cdot -2 - 9 \cdot 1 - 8 \cdot -1 = 0$

$catabolic = -C_2H_3O_2^- - SO_4^{2-} + 2HCO_3^- + HS^- = 0$

$Y_e^D = +8$
$Y_e^A = -8$

Catabolytic reaction Methanogenesis

$Donor = -C_2H_3O_2^- - 4H_2O + 2HCO_3^- + 9H^+ + 8e = 0$
$C = -1 \cdot 2 + 2 \cdot 1 = 0$
$H = -1 \cdot 3 - 4 \cdot 2 + 2 \cdot 1 + 9 \cdot 1 = 0$
$O = -1 \cdot 2 - 4 \cdot 1 + 2 \cdot 3 = 0$
$e = -1 \cdot -1 + 2 \cdot -1 + 9 \cdot 1 - 8 = 0$
$Acceptor = -HCO_3^- - 9H^+ - 8e + CH_4 + 3H_2O$
$C = -1 \cdot 1 + 1 \cdot 1 = 0$
$H = -1 \cdot 1 - 9 \cdot 1 + 1 \cdot 4 + 3 \cdot 2 = 0$
$O = -1 \cdot 3 + 3 \cdot 1 = 0$
$e = -1 \cdot -1 - 9 \cdot 1 - 8 \cdot -1 = 0$

$catabolic = -C_2H_3O_2^- - H_2O + HCO_3^- + CH_4 = 0$

$$Y_e^D = +8$$
$$Y_e^A = -8$$

$$Y_{X/S}^{Met} = \frac{1}{Y_S^{An} + \lambda_{cat} \cdot Y_S^{cat}}$$

formula 37(Kleerebezem & Van Loosdrecht, 2010)

$$\lambda_{cat} = \frac{\Delta G_{An}^1 + \Delta G_{Dis}}{\Delta G_{Cat}^1}$$

formula 32(Kleerebezem & Van Loosdrecht, 2010)

$$\Delta G_{Dis} = 457.1 \quad kJmole^{-1}$$

(Kleerebezem & Van Loosdrecht, 2010)

Acceptor	ΔG_{An}^{0}	ΔG_{An}^{1}	ΔG_{Cat}^{0}	ΔG_{Cat}^{1}	$Y_{X/S}^{Met,0}$	$Y_{X/S}^{Met,1}$
O_2	11.75	34.12	-844.64	-711.12	-0.93	-0.82
NO_3^-	11.75	34.12	-793.7	-761.96	-0.90	-0.85
SO_4^{2-}	11.75	34.12	-48.14	-24.77	-0.10	-0.05
HCO_3^-	11.75	34.12	-26.65	-15.97	-0.06	-0.04

Standard conditions, activities of 1 M, pH = 7

Realistic conditions T = 298K

$C_2H_3O_2^- = 1\cdot10^{-6} \quad (M)$ $\quad H^+ = 1\cdot10^{-6} \quad (M)$

$NH_4^+ = 0.02 \quad (M)$ $\quad HCO_3^- = 0.05 \quad (M)$

$O_2 = 1\cdot10^{-10} \quad (M)$ $\quad NO_3^- = 0.014 \quad (M)$

$N_2 = 0.01 \quad (M)$ $\quad HS^- = 5\cdot10^{-3} \quad (M)$

$SO_4^{2-} = 1\cdot10^{-3} \quad (M)$ $\quad CH_4 = 0.0001 \quad (M)$

Kleerebezem, R., Van Loosdrecht, M.C.M. 2010. A generalized method for thermodynamic state analysis of environmental systems. *Critical Reviews in Environmental Science and Technology*, **40**(1), 1-54.

Appendix 2.2: Oxygen loss per square meter of root as a function of average root length based on data of (Soukup et al., 2007)

Root length (m)	Oxygen loss at specific root length(mol m^{-2} s^{-1}) (Soukup et al., 2007)	$J_{O_2}^{in}$ (mole m^{-2}_{root} s^{-1})	$J_{O_2}^{in}$ (mole$_e$ m^{-2}_{root} s^{-1})
0.002	2.5E-07	2.50E-7	1.0E-06
0.005	2.1E-07	2.25E-7	9.0E-07
0.01	1.6E-07	1.90E-7	7.6E-07
0.015	1.1E-07	1.65E-7	6.6E-07
0.02	7.8E-08	1.43E-7	5.7E-07
0.025	4.2E-08	1.23E-7	4.9E-07
0.03	5.2E-09	1.03E-7	4.1E-07
0.035	2.6E-09	0.90E-7	3.6E-07
0.04	2.6E-09	0.78E-7	3.1E-07
0.045	2.6E-09	0.70E-7	2.8E-07
0.05	2.6E-09	0.63E-7	2.5E-07
0.055	2.6E-09	0.58E-7	2.3E-07
0.06	2.6E-09	0.53E-7	2.1E-07
0.065	2.6E-09	0.50E-7	2.0E-07
0.07	2.6E-09	0.45E-7	1.8E-07
0.075	2.6E-09	0.43E-7	1.7E-07
0.08	2.6E-09	0.40E-7	1.6E-07

Soukup, A., Armstrong, W., Schreiber, L., Franke, R., Votrubova, O. 2007. Apoplastic barriers to radial oxygen loss and solute penetration: A chemical and functional comparison of the exodermis of two wetland species, Phragmites australis and Glyceria maxima. *New Phytologist*, **173**(2), 264-278.

Appendix 2.3: calculation of oxygen flux via the top of the PMFC based and Fick`s Law for diffusion

$$J = -D\frac{dC}{dx}$$

Where J is the oxygen flux via the top of the PMFC (mol $m^{-2}_{surface}$ s^{-1}), D is the diffusion coefficient of oxygen ($2.1 \cdot 10^{-9}$ $m^{2}_{surface}$ s^{-1} (Beckett, Armstrong et al. 2001)), $\frac{dC}{dx}$ is the oxygen concentration gradient (mol L^{-1} m^{-1}). The oxygen concentration gradient can be estimated based on a oxygen penetration depth of 1 mm (Frenzel, Rothfuss et al. 1992) (Gilbert and Frenzel 1998) and oxygen saturation at the air anolyte interface (about 9 mg L^{-1}). This results in an estimated oxygen flux in the anode of $5.9 \cdot 10^{-10}$ mol $m^{-2}_{surface}s^{-1}$.

Based on the minimum average oxygen loss of the roots $0.4 \cdot 10^{-7}$ mol m^{-2} s^{-} and a root surface area of 79 m^{2}_{root} $m^{-2}_{surface}$ (Jackson, Mooney et al. 1997). The oxygen flux via the top of the reactor into the anode is $5.9 \cdot 10^{-10}$ mol $m^{-2}_{surface}s^{-1}$ while the oxygen flux via the roots is $3.95 \cdot 10^{-6}$ mol $m^{-2}_{surface}s^{-1}$. This showed that the oxygen flux via the open top is likely negligible (about 0.02 %) compared to the oxygen flux via the roots.

Beckett, P. M., W. Armstrong, et al. (2001). Mathematical modelling of methane transport by phragmites: The potential for diffusion within the roots and rhizosphere. *Aquatic Botany* **69**(2-4): 293-312.

Frenzel, P., F. Rothfuss, et al. (1992). Oxygen profiles and methane turnover in a flooded rice microcosm. *Biology and Fertility of Soils* **14**(2): 84-89.

Gilbert, B. and P. Frenzel (1998). Rice roots and CH4 oxidation: The activity of bacteria, their distribution and the microenvironment. *Soil Biology and Biochemistry* **30**(14): 1903-1916.

Jackson, R. B., H. A. Mooney, et al. (1997). A global budget for fine root biomass, surface area, and nutrient contents. *Proceedings of the National Academy of Sciences of the United States of America* **94**(14): 7362-7366.

3. Microbial community structure elucidates performance of *Glyceria maxima* plant microbial fuel cell

This chapter has been published as:
Ruud A. Timmers, Michael Rothballer, David P.B.T.B. Strik, Marion Engel, Stephan Schulz, Michael Schloter, Anton Hartmann, Bert Hamelers, Cees Buisman, (2011) Microbial community structure elucidates performance of *Glyceria maxima* plant microbial fuel cell. Applied Microbiology and Biotechnology

Abstract

The plant microbial fuel cell (PMFC) is a technology in which living plant roots provide electron donor, via rhizodeposition, to a mixed microbial community to generate electricity in a microbial fuel cell. Analysis and localisation of the microbial community is necessary for gaining insight into the competition for electron donor in a PMFC. This paper characterises the anode-rhizosphere bacterial community of a *Glyceria maxima* (Reed Mannagrass) PMFC. Electrochemically active bacteria (EAB) were located on the root surfaces, but they were more abundant colonizing the graphite granular electrode. Anaerobic cellulolytic bacteria dominated the area where most of the EAB were found, indicating that the current was probably generated via the hydrolysis of cellulose. Due to the presence of oxygen and nitrate, short chain fatty acid-utilising denitrifiers were the major competitors for the electron donor. Acetate-utilising methanogens played a minor role in the competition for electron donor, probably due to the availability of graphite granules as electron acceptors.

Keywords: 454 amplicon sequencing / *Geobacter* / microbial community / plant microbial fuel cell / renewable energy / rhizosphere

3. Microbial community structure elucidates performance of *Glyceria maxima* plant microbial fuel cell

3.1 Introduction

The plant microbial fuel cell (PMFC) is a new technology that can potentially provide renewable and sustainable energy. The PMFC transforms solar energy into electricity through the oxidation of organic compounds originating from photosynthesis (De Schamphelaire et al., 2008; Strik et al., 2008). Electricity generation in the PMFC is based on the loss of organic compounds by plant roots (rhizodeposition) (Pinton & Varanini, 2007) and oxidation of these organic compounds by electrochemically active bacteria (EAB) (Potter, 1911). In the PMFC, electrons, proton and carbon dioxide are produced by oxidation of organic compounds lost by plant roots in the anode. The electrons that are transferred to the anode electrode are consumed in the cathode compartment by typically reduction of oxygen to water (Strik et al. 2011).

Several bacterial species are known to produce current in microbial fuel cells (MFC): *Shewanella putrefaciens* using lactate, pyruvate and formate as electron donor (Kim et al., 1999; Park & Kim, 2001); *Clostridium butyricum* and *Clostridium beijerinckii,* using glucose, starch, lactate and molasses (Niessen et al., 2004; Park et al., 2001); *Geobacter sulfurreducens*, using acetate and hydrogen (Bond & Lovley, 2002); *Rhodoferax ferrireducens,* using glucose (Chaudhuri & Lovley, 2003); *Geobacter metallireducens*, using acetate (Min et al., 2005); and *Rhodopseudomonas palustris*, using acetate, lactate, valerate, fumarate, ethanol, glycerol and yeast extract (Xing et al., 2008). *Alcaligenes faecalis, Enterococcus gallinarum,* and *Pseudomonas aeruginosa* are known to generate electricity by producing their own mediators, using glucose as an electron donor (Rabaey et al., 2004). To date, *Enterobacter cloacae* is the only pure culture that is known to generate electricity directly from more complex electron donors, such as cellulose (Rezaei et al., 2009).

Rhizodeposition is the loss and release of organic and inorganic compounds by plant roots into the rhizosphere (the soil volume affected by the presence of plant roots). Rhizodeposition provides a carbon and energy source, thus stimulating the development of bacterial communities in the rhizosphere. In anaerobic environments, rhizodeposition can also provide oxygen as an electron acceptor and may stimulate the development of

facultative anaerobic bacterial communities (Hartmann et al., 2009). In addition to prokaryotes (bacteria and archaea), eukaryotes (such as fungi, protozoa, nematodes, and meso- and macro-fauna) are also found in the rhizosphere (Phillips et al., 2003).

The genera *Geobacter* and *Desulfobulbus* have been found in PMFCs (De Schamphelaire et al. 2010). As both genera contain electrochemically active species that are enriched at the anode of MFCs (Holmes et al., 2004; Jung & Regan, 2007), it can be assumed that EAB may have been present in the PMFC. However, no studies have yet confirmed the presence of active EAB in PMFCs. The presence of active EAB is required to prove their role in electricity production by PMFCs.

In a PMFC, the plant roots are located at the anode of the MFC, where rhizodeposition provides EAB with electron donor. Together the MFC anode and the rhizosphere make up a complex system. In this complex system it is likely that different micro-organisms compete for electron donor. Competition for electron donor among the different micro-organisms results in a decrease of electron donor available for EAB and thus lower current generation. Analysis and localisation of the microbial community is needed to gain insight into the competition for electron donor in a PMFC.

In this study, we determined the microbial communities present in a PMFC rhizosphere and localised the active EAB in the rhizosphere and on the electrode of the PMFC. Additionally, we investigated the electron donor and electron pathways in the PMFC. We used 454 technology to sequence 16S rRNA gene amplicon libraries from bacteria and archaea. To prove the relevance of dominant pylogenetic groups and to localize those bacteria and archaea, fluorescent in situ hybridisation (FISH) in combination with confocal laser scanning microscopy (CLSM*)* was performed in samples of high-current-generating and low-current-generating *Glyceria maxima* (Reed Mannagrass) PMFC.

3.2 Materials and methods

3.2.1 Preparation of PMFC

The anode compartment of the PMFC consisted of 165 g of graphite granules with diameters between 1 and 2 mm (le Carbone, Wemmel, Belgium). The graphite granules were placed in a glass cylinder (Schott, Duran) with a diameter of 0.035 m and a height of 0.30 m. To separate the anode from the cathode, a cation exchange membrane (fumasep®, FKB, Fumatech GmbH, St. Ingbert, Germany) was fixed at the bottom of the glass cylinder. The anode was placed in the cathode, which consisted of a PVC beaker with a diameter of 0.11 m and a height 0.04 m that contained a 6-mm-thick graphite felt (Coidan Graphite Products LTD, York, United Kingdom). Figure 2.2 shows a schematic representation of the used setup.

To close the electrical circuit, two 4 cm golden wires glued to Teflon coated copper wire were connected over a resistance of 900 Ω. To create contact between the anode and the cathode, one of the gold wires was placed in between the graphite granules and the other was woven through the graphite felt.

3.2.2 Preparation of graphite granules

Eight setups were operated without plants to develop electrochemically active biofilms on the graphite granules. The anode was inoculated with 5 ml of anolyte from an MFC running on acetate (Dekker et al., 2009); the anolyte was extracted with a syringe. The setups were operated in batch mode. As nutrient solution ½ Hoagland Medium (Taiz and Zeiger 2006) buffered with an 8 mM potassium phosphate buffer solution (pH 6.8) was used. The electron donor was supplied by adding 10 mM potassium acetate to the nutrient solution of setups 1 through 4 and 10 mM glucose to the nutrient solution of 5 through 8. After 40 days, the acetate-fed setups generated a current density of 0.248 ± 0.004 A m^{-2}, and the glucose fed setups generated a current density of 0.151 ± 0.02 A m^{-2}. Current densities are expressed per square meter of cross sectional area of the PMFC (0.00096 m^2) throughout the document.

Before the graphite granules were used for the six PMFCs, they were thoroughly mixed to ensure the presence of micro-organisms able to generate electricity from acetate as well as glucose. After the mixing the graphite granules were rinsed with tap water to remove a large part of the residual electron donor. One stem of *G. maxima* (D'n Bart Waterplanten, Handel, the Netherlands) with a weight between 4.4 g and 7.8 g was planted in each PMFC.

3.2.3 Operation of PMFCs

The medium used to feed the PMFCs was ½ Hoagland buffered with 0.008 mol L^{-1} potassium phosphate buffer solution as described by Timmers et al. (2010) (pH 6.8, conductivity between 1.5 through 1.7 mS m^{-1}). The medium was fed through a sample point located 0.07 m above the graphite granules. The applied flow rate was 0.17 mL s^{-1} throughout the experimental period. The feeding frequency of the PMFC with buffered Hoagland medium was 5 minutes every 12 hours.

Both, MFC and PMFC, setups were placed in a climate control cabinet (Microclima 1750 Snijders, Tilburg, the Netherlands). In this manner, environmental conditions were fixed at illumination period of 14 h d^{-1}, average light density in the photo active region of 596 ± 161 µmol m^{-2} s^{-1}, temperature of 25 ^{o}C, and humidity of 75%.

3.2.4 Sample selection, preparation, and DNA extraction

Samples for analysis were taken from PMFC generating the highest current (PMFC2) and the PMFC generating the lowest current (PMFC1). Both PMFCs were dismantled 225 days after the start of the experiment. The anode compartments of both PMFCs were divided into bottom (0 to 0.15 m) and top (0.15 to 0.3) sections. Figure 2.2 shows a schematic representation of the PMFC and the sampling points. The root samples were taken from all of the sampling points in both PMFCs and stored at -80°C. DNA was extracted from a total of 500 mg of root material per sample following the protocol of Griffiths et al. (Griffiths et al., 2000) and using a BIO101 lysing matrix (MP Biomedicals, Illkirch, France) and a final purification step with the AllPrep Mini Kit by Qiagen (Munich, Germany). The amount of DNA in solution was quantified using a bioanalyser from Agilent (Böblingen, Germany).

3.2.5 PCR, 454 sequencing and data processing

If not otherwise mentioned, all the steps were performed according to the Roche 454 sequencing protocol for amplicons. To generate the amplicon library for bacteria and archaea, specific primers were selected according to two criteria: i) the fragment should span 600 bases of the 16S rRNA gene to receive sufficient phylogenetic information, and ii) the primers should bind to as many bacterial/archaeal sequences as possible without detecting non-target groups. To verify these criteria, the ARB probe match tool was used with the latest SILVA database (containing over 400,000 sequences), resulting in the following bacterial 16S primers: 926-F (5'-AAACTYAAAKGAATTGACGG-3', *Escherichia coli* position 907-926 (Lane, 1991)), and 630-R (5'-CAKAAAGGAGGTGATCC-3', *E. coli* position 1528-1544 (Juretschko et al., 1998)). The archaeal primers were rSAf(i) (5'-CCTAYGGGGCGCAGCAG-3', *E. coli* position 341-357 (Nicol et al., 2003)), and 958r (5'-YCCGGCGTTGAMTCCAATT-3', *E. coli* position 940-958 (Bano et al., 2004)). These primers were extended as amplicon fusion primers with respective A and B adapters, key sequence and multiplex identifiers (MID) as recommended and tested in initial PCR reactions to determine their optimal annealing temperatures (50°C, 54°C, 58°C), cycle numbers (20, 22, 25, 30) and amounts of template DNA (50 ng, 100 ng, 200 ng). The conditions under which a sufficient amount (approx. 10^{12} molecules) of specific amplicons of the right size was generated using the lowest number of cycles in all the samples were determined (50 °C, 22 cycles, 50 ng) for bacterial 16S rRNA genes. For archaeal 16S rRNA genes *30* cycles and the addition of 8% DMSO were necessary to obtain sufficient PCR product for archaea. These conditions were then used to produce four amplicon libraries each (top and middle/bottom part of the high and low current producing PMFC). The PCR products were purified with AMPure Beads (Agencourt, Beckman Coulter, Krefeld, Germany) and pooled in equimolar amounts.

Emulsion PCR (emPCR), emulsion breaking of DNA-enriched beads and sequencing run of the amplicon pools were performed on a second-generation pyrosequencer (454 GS FLX Titanium, Roche) using Titanium reagents and Titanium procedures as recommended by the developer following protocols for bidirectional amplicon sequencing.

Quality filtering of the pyrosequencing reads was performed using the automatic amplicon pipeline of the GS Run Processor (Roche) to remove failed and low quality reads from raw data and to remove adaptor sequences.

Newbler assembler v 2.3 (Roche) was used to batch sequences based on MID-identifiers and to combine corresponding sequences derived from forward and reverse reads with a similarity of 99% and an overlap of 400 bases for the bacterial sequences. Due to the low sequence diversity, a similarity value of 98% and an overlap of 200 bases were sufficient for archaeal sequences. The consensus sequences were inspected for chimera with the help of the Bellerophon software (http://foo.maths.uq.edu.au/_huber/bellerophon.pl) and putative chimera were removed from the dataset.

The alignment and phylogenetic analyses were performed using the ARB 5.1 software package (Strunk and Ludwig 1997). After phylogenetic allocation of the sequences down to the family or genus level, the sequences belonging to different phylogenetic groups were added together and depicted as a percentage of the total sequencing reads obtained from each sample. Phyla represented by less than 50 sequencing reads in all four libraries totalled were not included.

The assembled unique sequences with their phylogenetic allocation were deposited under the numbers JF731380 and JF732737 in GenBank.

3.2.6 Quantitative real-time PCR (qRT-PCR) of archaeal and bacterial 16S rRNA genes

For Sybr®Green based qRT-PCR the same primers as for the 454 sequencing were used, but without the 454 specific adaptor, the key and the MID sequences. For standard generation PCRs using these specific primers were performed with the same conditions as for the amplicon library amplification. The resulting products were cloned into a pSC-A-Amp/Kan Vector using the StrataCloneTM PCR Cloning Kit (Agilent, Palo Alto, CA, USA) after manufacturer's instructions. In each case, eight resulting clones were picked, the inserts sequenced and subsequently allocated by the ARB software package. Sequences either related to the genus

Methanobacterium (archaea) or to the genus *Clostridium* (bacteria) were chosen as standards, as both sequences represented genera commonly found in a large proportion in all four amplicon libraries.

Subsequently, abundances of archaeal and bacterial 16S rRNA genes were measured on the ABI Prism 3300 system (Applied Biosystems, Foster City, CA, USA) under comparable conditions (10 min 95 °C, 40 cycles of 20 s 95 °C, 1 min. 50 °C and 30 s 72 °C) in triplicates. Signal acquisition was done at 78 °C to overcome bias due to primer dimers. PCR reaction mixtures (25 µl volume) contained 2 mM $MgCl_2$, 0.1 µM of respective primers (forward and reverse), 1x Power Sybr®Green (Applied Biosystems, Foster City, CA, USA) and 4 ng of template DNA. Curves for both standards were linear ($r^2 > 0.99$) over five orders of magnitude and amplification efficiencies were comparable at 87 %.

3.2.7 Fluorescent in situ hybridization (FISH) and confocal laser scanning microscopy (CLSM)

Fixed bacterial samples were stained for 10 minutes in the dark with the DNA binding dye Syto Orange 80 (Molecular Probes, Invitrogen, Carlsbad, USA) at a concentration of 5 µM in 10 mM Tris, 1 mM EDTA (pH 8.0) and subsequently washed twice with ultrapure water.

For the FISH, the washed root samples were fixed for 2 hours at room temperature (Amann et al., 1990) with either 50% ethanol in ultrapure water for Gram-positive bacteria or 4% paraformaldehyde for Gram-negative bacteria. Hybridisation with fluorochrome (Cy3, Cy5)-labelled oligonucleotide probes was carried out following the protocols described by (Manz et al., 1992) and (Amann et al., 1992). For the microscopic observations, the FISH stained root pieces (ca. 5-10 mm long) were embedded in Citifluor (Citifluor Ltd., Canterbury, UK) and observed by CLSM without further cutting.

rRNA-targeted oligonucleotide probes were synthesised and labelled by Sigma-Aldrich (Steinheim, Germany). EUB338-I (Amann et al., 1990) and EUB338-II and III (Daims et al., 1999) were used in an equimolar mixture at different formamide concentrations. To detect the genus *Geobacter*, an equimolar mixture of the 16S rRNA targeted probes Geo1A and Geo1B was

used at a 35% formamide concentration. Geo1A is specific for *G. sulfurreducens*, *Geobacter hydrogenophilus*, *Geobacter grbiciae*, and *G. metallireducens*; Geo1B detects most other *Geobacter* species (Demaneche et al., 2008). To detect the Ruminococcaceae group members *Ruminococcus bromii*, *Clostridium sporosphaeroides*, and *Clostridium leptum*, the Rbro730 probe (Harmsen et al., 2002) was applied in the presence of 20% formamide. To detect most members of *Clostridium* clusters I and II, the Chis150 probe (Collins et al., 1994; Franks et al., 1998) was used with 35% formamide.

The fluorescently labelled cells were detected using a Zeiss LSM510 CLSM. An argon ion laser supplied 488-nm illumination to excite the fluorescein, and two helium-neon lasers provided 543 nm for Cy3 and 633 nm for Cy5. For each hybridisation probe, an EUB338 mix labelled with Cy5 (blue) was combined with another group-specific probe labelled with Cy3 (red). The binding of both probes resulted in a magenta staining of the target cells. The green channel (fluorescein) served as a negative control that showed only autofluorescence by the root or other particles. Syto Orange was detected by excitation with the 488 nm and 543 nm laser wavelengths, resulting in a yellow/orange fluorescence signal in the target cells; the negative control was the blue channel (excitation at 633 nm).

The optical sectioning of the root was achieved by moving the focus position deeper into the sample in 1 µm steps, which produced z-stacks of individual pictures from the same xy-area with a penetration depth of up to 60 µm. The resulting set of pictures was displayed as an orthogonal view using the LSM510 software package that was provided by Zeiss.

3.3 Results

3.3.1 Energetic performance of PMFCs

The daily average current density was 0.067 ± 0.058 A m^{-2} for the low-current PMFC and 0.164 ± 0.065 A m^{-2} for the high-current PMFC (Figure 3.1). The daily average current density was substantially higher than the 0.009 A m^{-2} reported for fresh water sediment microbial fuel cells (Holmes et al., 2004). Furthermore, the daily average current density was in the range of average current densities reported in literature for PMFCs (De Schamphelaire et al., 2008; Helder et al., 2010; Kaku et al., 2008; Strik et al., 2008; Timmers et al., 2010). An examination of the standard deviations revealed that both PMFCs had relatively large fluctuations in current density over time. The maximum power density, with an external resistance of 900 Ω, was 32 mW m^{-2} for the low-current PMFC and 80 mW m^{-2} for the high-current PMFC. The high-current PMFC produced a total of 522 J, and the low-current PMFC produced a total of 124 J.

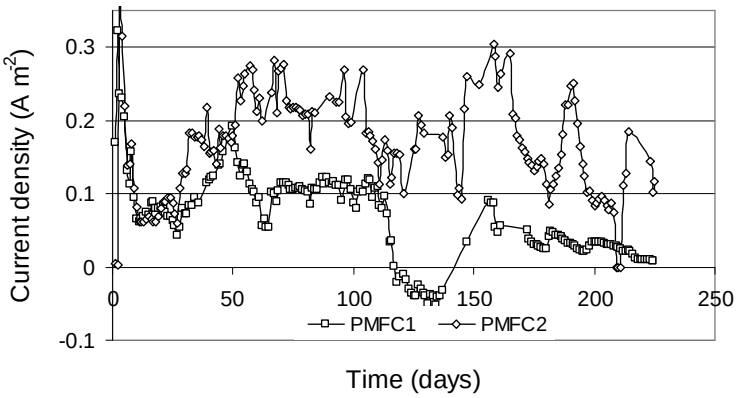

Figure 3.1: *Current density versus time of the low current density PMFC (PMFC1) and high current density PMFC (PMFC2).*

3.3.2 Differences in the 454 sequencing of bacterial and archaeal 16S rRNA gene fragments between PMFCs

A bidirectional sequencing approach of the four pooled bacterial 16S rRNA gene amplicon libraries (top section low-current PMFC, middle/bottom section low-current PMFC, top section high-current PMFC, middle/bottom section high-current PMFC) resulted in a total of 140000 reads with 114000 key pass reads and 46000 reads that passed all of the internal quality filters of the 454 software. An average read length of 517 bases and almost no reads shorter than 500 bases were obtained. The sequencing of the bacterial amplicon libraries was repeated once for verification of the results with slightly lower output and read lengths but no major differences in bacterial abundance. The assembly resulted in 495 unique sequences for bacteria and 863 for archaea, which were then phylogenetically allocated by the ARB software package. Figure 3.2 (a) shows the bacterial classes and families found in both PMFCs. In the bottom section of the high-current PMFC, the major portion (54%) of the bacterial 16S rDNA belonged to the Ruminococcaceae family, with considerable amounts (25%) belonging to the Clostridiaceae family. Within the Ruminococcaceae family, almost all the sequences clustered around *C. sporosphaeroides*. Although unambiguous species-level assignment is difficult using the 16S rDNA fragment lengths of 600 bp that were obtained, this analysis enabled the selection of suitable FISH probes for verification of the sequencing results.

In the top section of the high-current PMFC, the major portion (36%) of the bacterial 16S belonged to Comamonadaceae, and considerable amounts could be assigned to the Rhodocyclaceae (10%) and Clostridiaceae families (13%).

The bottom and top sections of the low-current PMFC were dominated (54% and 35%, respectively) by members of the Comamonadaceae family, but also representatives of the Rhodocyclaceae family were frequently detected (13% and 23%).

Figure 3.2 (b) shows the archaeal genera found in both PMFCs. In the high-current PMFC, the genus *Methanobacterium* made up over 95% of the archaeal community. In the low-current PMFC, the archaeal community was

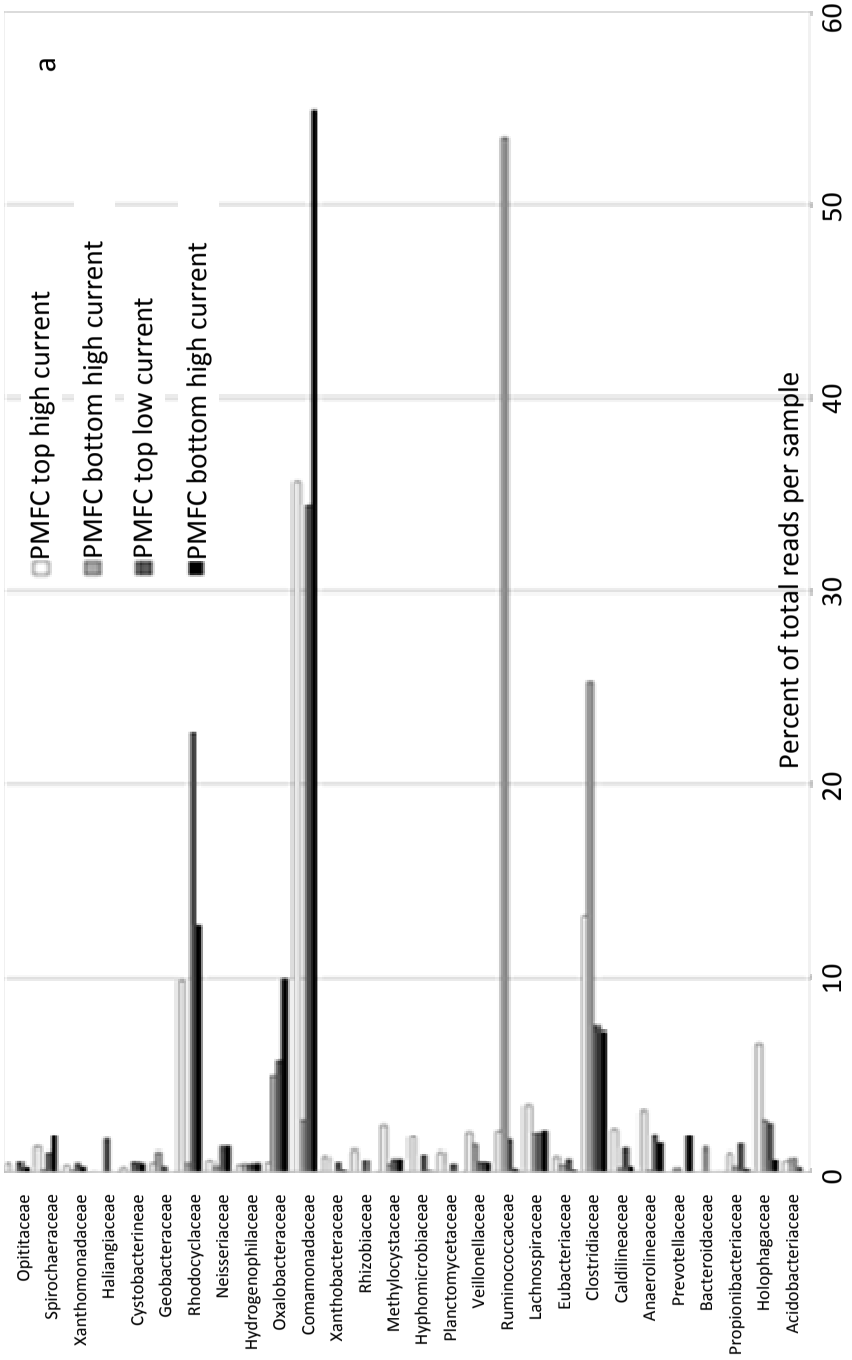
a
PMFC top high current
PMFC bottom high current
PMFC top low current
PMFC bottom high current
Percent of total reads per sample
0
10
20
30
40
50
60
Opititaceae
Spirochaeraceae
Xanthomonadaceae
Haliangiaceae
Cystobacterineae
Geobacteraceae
Rhodocyclaceae
Neisseriaceae
Hydrogenophilaceae
Oxalobacteraceae
Comamonadaceae
Xanthobacteraceae
Rhizobiaceae
Methylocystaceae
Hyphomicrobiaceae
Planctomycetaceae
Veillonellaceae
Ruminococcaceae
Lachnospiraceae
Eubacteriaceae
Clostridiaceae
Caldilineaceae
Anaerolineaceae
Prevotellaceae
Bacteroidaceae
Propionibacteriaceae
Holophagaceae
Acidobacteriaceae

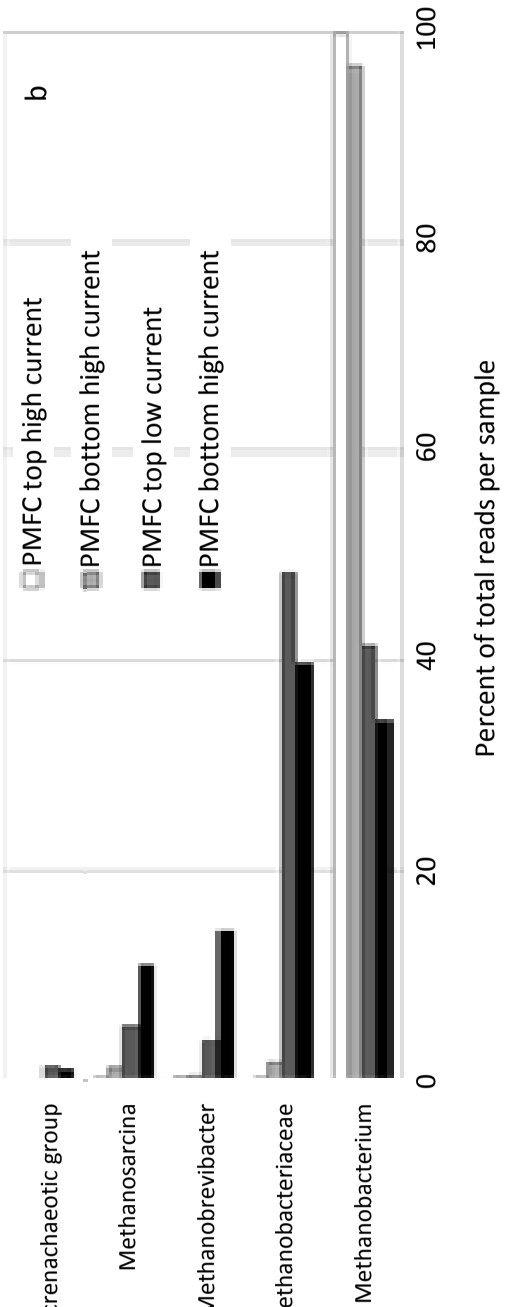

Figure 3.2: *454 sequencing reads in percent of total reads per sample phylogenetically allocated to different bacterial families /genera by the ARB software package. Phyla represented by less than 50 sequencing reads in all four libraries are not included.*

(a) Bacteria

(b) Archaea

more diverse and mainly consisted of the genus *Methanobacterium* and uncultured Methanobacteriaceae. Furthermore, *Methanosarcina* was found to account for 5 % of the archaeal community in the top section and up to 10% in the bottom section of the low-current PMFC.

The quantification of archaeal and bacterial 16S rRNA genes revealed great differences in the abundances of about two to three orders of magnitude. Gene copy numbers of bacterial 16S rRNA genes per ng extracted DNA were (top section, low current; middle/bottom section, low-current; top section, high current; middle/bottom section, high-current) 0.9, 2.4, 0.7 and 1.2 x 10^6, respectively. In comparison, gene copy numbers of archaeal 16S rRNA were 5.6, 4.9, 1.4 and 0.8 x 10^3, respectively. While the abundances of bacteria differed by a maximum of factor 2, when comparing the same sections of the high and the low-current PMFCs, there were 4 to 6 times more archaeal 16S genes in the low-current than in the high-current PMFC.

3.3.3 Localization of characteristic PMFC bacteria by FISH and CLSM

A biofilm was detected, particularly in roots from the upper sections of both PMFCs, where the film completely surrounded the root and was 5 to 10 µm thick. No visual differences in the structure or amount of the biofilms were observed between the PMFCs. For the low-current PMFC, however, fungal hyphae were clearly detected in the biofilms of all observed samples.

FISH was used to localise *Geobacter*, Clostridiaceae, and Ruminococcaceae species that were previously detected by 454 sequencing of the 16S rRNA gene. The *Geobacter* probe set enabled detection of fluorescent *Geobacter* cells, which appeared more frequently on the graphite granules than on the root surfaces. With probe Geo1A, specific only for *G. sulfurreducens*, *G. metallireducens*, *G. grbiciae*, and *G. hydrogenophilus*, positive signals were identified on both roots and granules from both PMFCs. Furthermore, the positive signal was more frequently observed on samples from the bottom layer of the high-current PMFC. A Clostridia cluster I and II specific probe yielded very few positive signals, and no clear differences were observed between the individual samples. With probe Rbro730, specific for the three Ruminococcaceae species *R. bromii*, *C. sporosphaeroides* and *C. leptum*,

small numbers of cells were positively identified on the root surfaces, but fluorescent signals were detected to a much greater extent in the outer cortex layers of roots of the high-current PMFC.

3.4 Discussion

3.4.1 The presence of electrochemically active bacteria in the PMFCs

The current generation was likely due to the presence of the active *G. sulfurreducens* and *G. metallireducens* that were detected in both the PMFCs (Figure 3.3 c). Pure cultures of both *G. sulfurreducens* and *G. metallireducens* are known to generate electricity in an MFC (Bond & Lovley, 2002; Min et al., 2005). In particular, *G. sulfurreducens* has been shown to colonise the anodes of MFCs in structured biofilms (Holmes et al., 2004; Jung & Regan, 2007; Reguera et al., 2006). The same probe also detected active *G. grbiciae* and *G. hydrogenophilus*. These species have not been shown to be capable of generating electricity in an MFC, but they are able to reduce Fe(III) (Lovley et al., 2000), a property that is also exhibited by EAB such as *S. putrefaciens, G. sulfurreducens, G. metallireducens* (Coates et al., 2001), and *R. ferrireducens* (Finneran et al., 2003).

In the bottom section of the high-current PMFC, *G. sulfurreducens* or one of its close relatives (*G. metallireducens*, *G. grbiciae*, and *G. hydrogenophilus)* were observed frequently on the graphite granules. The roots in the bottom section of the high-current PMFC were also colonised, although less frequently than the graphite granules (Figure 3.3 c and f). In the low-current PMFC, *G. sulfurreducens* or one of its close relatives (*G. metallireducens*, *G. grbiciae*, and *G. hydrogenophilus*) were observed less frequently in the top section, and no signal at all was detected in the bottom section.

The difference in the presence of the genus *Geobacter* between the PMFC types was supported by the differences in the presence of the Geobacteraceae family to which the *Geobacter* genus belongs (Figure 3.3 a). An average of 0.74 % of the obtained 16S rRNA gene fragment sequences belonged to Geobacteraceae in the high-current PMFC, while an average of only 0.13 % belonged to Geobacteraceae in the low-current PMFC.

3.4.2 Anaerobic Ruminococcaceae were predominant in the bottom section of the high-current PMFC

Ruminococcaceae accounted for over half of the bacterial rhizosphere sequences in the bottom section of the high current PMFC. The members of this family have not been reported to be electrochemically active, but they are known to hydrolyse cellulose into hydrogen and low-molecular-weight organic compounds. In MFCs, the hydrolysis of cellulose generates electron donors that are suitable for *G. sulfurreducens* (Maki et al., 2009; Ren et al., 2007).

Based on their cellulolytic activity, the Ruminococcaceae species probably played an important role in electricity generation in the PMFC. They probably hydrolysed the cellulose, originating from dead roots, into suitable electron donors for EAB. Typically, 35-50% of dry-plant weight consists of cellulose (Lynd et al., 1999), which stresses the importance of cellulolytic activity in generating a suitable electron donor for EAB.

The main species of the Ruminococcaceae family was probably *C. sporosphaeroides*, which is able to ferment glutamate to ammonia, CO_2, acetate, butyrate and hydrogen via the hydroxyglutamate pathway (Hsiao et al., 2009). Furthermore, this species has been used to improve the hydrolysis rates of cellulose and hemicelluloses in a biomass fermenter (patent no. WO/2010/072219).

C. sporosphaeroides was mainly found in the root cells of the outer root cortex in the high-current PMFC (see Figure 3.3 e). Due to the large surface area of the outer root cortex, the presence of *C. sporosphaeroides* there probably resulted in a high rate of hydrolysis (Lynd et al., 2002). It could not be determined whether *C. sporosphaeroides* acted as a moderate pathogen and actively killed root cells or was simply colonising dead plant material. *E. cloacae,* able to generate current from complex electron donors as a pure culture was not detected in the PMFCs (Rezaei et al., 2009). This is another indication that current was likely generated via the hydrolysis of complex electron donors into suitable electron donor for *G. sulfurreducens*. The importance of the hydrolysis of cellulose for electricity generation is supported by the results of Ren et al. (2007). They demonstrated that a

binary culture of *Clostridium cellulolyticum* and *G. sulfurreducens* (with carboxymethyl cellulose and MN301 cellulose as electron donors) produced current, while single cultures of these bacteria did not.

The lack of dominance by obligate anaerobes in the top section of the high-current PMFC and in the top and bottom sections of the low-current PMFC indicates the presence of oxygen. Therefore hydrolysis in the low-current PMFC was likely performed by fungi and/or facultative anaerobic cellulolytic bacteria, such as the Rhodocyclaceae family (Schellenberger et al., 2010). In contrast, the bottom section of the high-current PMFC was dominated by the obligate anaerobe Ruminococcaceae, indicating that cellulose hydrolysis was predominantly carried out by members of this family.

3.4.3 Short chain fatty acid-utilizing denitrifiers are major competitors for electron donor

Except for the bottom section of the high-current MFC, Rhodocyclaceae and Comamonadaceae were the dominant families observed on the PMFCs. Rhodocyclaceae and Comamonadaceae are known to be facultative anaerobic short chain fatty acid-utilising denitrifiers (Ginige et al., 2005; Nielsen et al., 2006; Thomsen et al., 2007). Nevertheless, both Comamonadaceae and Rhodocyclaceae have been previously observed in MFCs. Comamonadaceae have been found to dominate the bacterial community in the anode of a cellulose-fed MFC (Rismani-Yazdi et al., 2007). Rhodocyclaceae have been found to dominate the bacterial community in the anode of an acetate-fed MFC with an open air cathode (Borole et al., 2009). Furthermore, *Comamonas denitrificans* and *R. ferrireducens* species belonging to the Comamonadaceae family are able to generate electricity in an MFC in the absence of oxygen and nitrate (Xing et al., 2010; Xing et al., 2008).

In our PMFC, both oxygen and nitrate were probably present due to the diffusion of oxygen through the roots and the addition of nitrate through the medium. The nitrate flux into the anode was equivalent to 140 g N m^{-2} d^{-1} ($2 \cdot 10^{-3}$ $mol_{nitrate}$ d^{-1}, assuming that there was no medium overflow), which is about 125 times higher than the maximum reported rate of nitrogen

uptake by emergent macrophytes in a constructed wetland containing *G. maxima* (Tanner, 1996). Therefore, a large portion of the added nitrate was denitrified by facultative anaerobic activity as long as short-chain fatty acids were available as electron donors. Short-chain fatty acids were probably generated by the aerobic cellulolytic activity of Oxalobacteraceae (Lynd et al. 2002) and the anaerobic cellulolytic activity of Rhodocyclaceae (Schellenberger et al., 2010). Offre et al. (2007) associated the presence of Oxalobacteraceae and Comamonadaceae with mycorrhizal roots and suggested a possible symbiosis between both bacterial families and fungi. The presence of fungi in the outer cortex of the roots in the low-current PMFC was consistent with these findings.

The presence of Rhodocyclaceae and Comamonadaceae probably had a negative effect on current generation, as these families do not contribute to electricity generation in the presence of oxygen and nitrate. Furthermore, these families consume short chain fatty acids, which decreases the amount of short chain fatty acids available for current generation and thus negatively affect current generation. The difference in current generation between the high and low current generating PMFC could likely be attributed to difference in presence of Rhodocyclaceae and Comamonandaceae in the bottom part of both PMFC. In the bottom part of the high current PMFC Rhodocyclaceae and Comamonandaceae were almost absent while they were more abundant in the bottom part of the low current PMFC. As these families consume short chain fatty acids it is likely that their presence resulted in lower current generation because less substrate is available for EAB.

The absence of fungi in the outer cortex of roots in the bottom section of the high-current PMFC, together with possible nitrate depletion, may have allowed strictly anaerobic cellulolytic micro-organisms (Clostridiaceae and Ruminococcaceae) and EAB, such as *G. sulfurreducens,* and *G. metallireducens*, to proliferate.

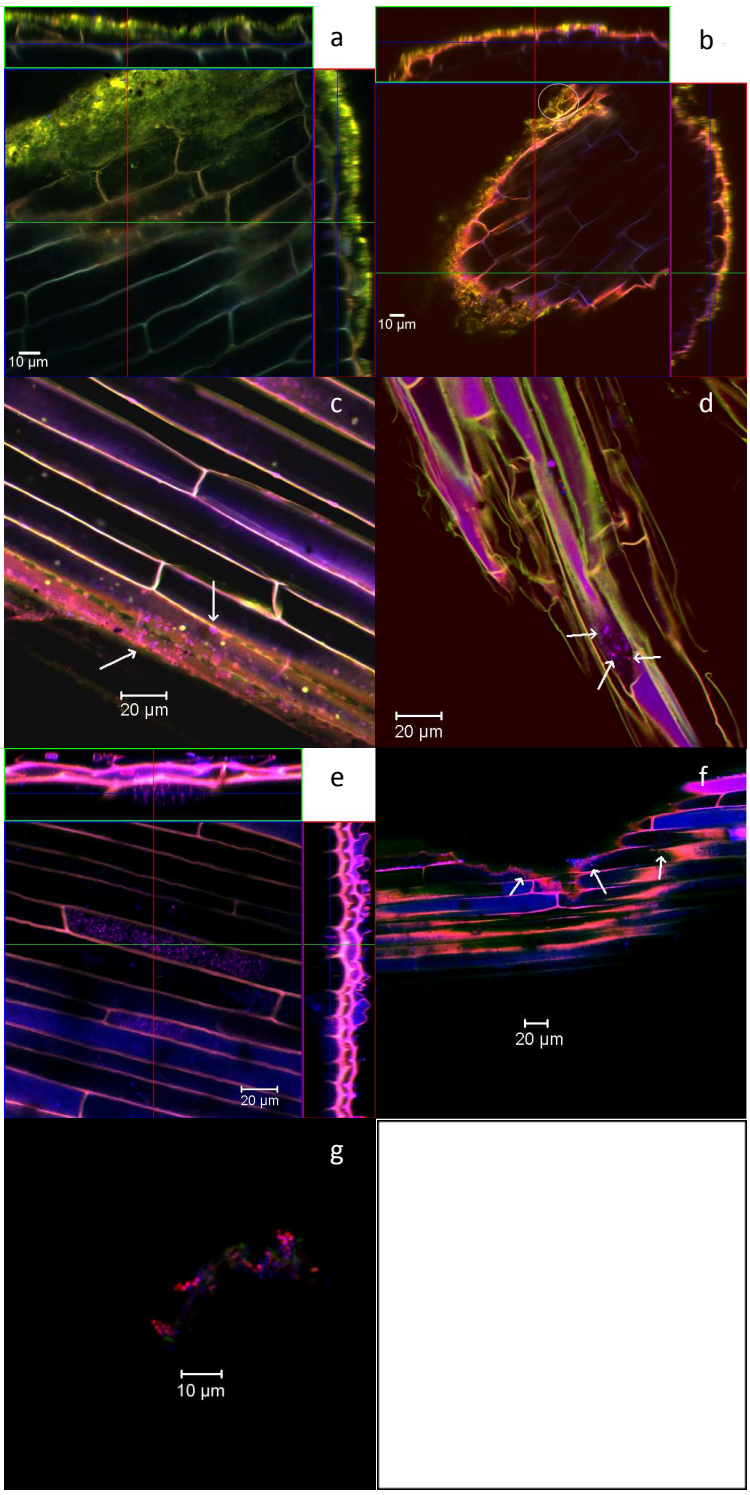
a
10 µm
b
10 µm
c
20 µm
d
20 µm
e
20 µm
f
20 µm
g
10 µm

Figure 3.3: *CLSM images of FISH or SYTO orange stained roots from the two PMFCs. All FISH staining was performed with probe Eub338Mix labeled in Cy5 (blue) in combination with a group specific probe labeled in Cy3 (red). Target cells appear in magenta (combination of red and blue). If three dimensional z-stacks were prepared, pictures are shown in orthogonal views. The top view, framed in blue, gives one picture from the middle of this z-stack. The red and green lines represent vertical optical cuts through the stack, which result in the side view images framed in red and green, respectively. In these side views the blue line marks the vertical position, where the top view image is located within the z-stack*

(a) Syto orange stained biofilm on a root from high current producing PMFC, upper part
(b) Syto orange stained biofilm on a root from low current producing PMFC, upper part; fungal hyphae are marked by white circle
(c) FISH stained root with probe set Geo1A and Geo1B (G. genus) from high current PMFC, bottom part (indicated by white arrows)
(d) Root from same sample as 4C; Geo1A (detecting only G sulfurreducens, G. metallireducens, G. grbiciae or G. hydrogenophilus, indicated by white arrows)
(e) FISH stained root with probe Rbro730 (C. sporosphaeroides, C. leptum, R. bromii) from high current PMFC, middle part
(f) FISH staining with probe set Geo1A and Geo1B (G. genus) of a graphite granule of high current PMFC (not visible); small cluster of Geobacter is detected on the surface of the graphite granules (indicated by white arrows)
(g) CLSM picture of a FISH stained root from high current PMFC, bottom part; probe Chis150 (Clostridiaceae)

3.4.4 Methanogenesis plays a minor role in competition for electron donor

Methanogens can compete with *G. sulfurreducens* and *G. metallireducens* for electron donors, as they are able to use acetate, formate, methanol, methylamine, H_2, and CO_2 (Ishii et al., 2008; Thauer et al., 2008; Thomsen et al., 2007). Quantitative real time PCR amplification with bacterial and archaeal primers using the same DNA template indicated that considerably less of the DNA present in the sample was derived from archaea than from bacteria. The higher abundance of bacterial DNA compared to archaeal DNA was probably due to the presence of alternative acceptors in the medium, such as oxygen, nitrate and sulphate. As long as these acceptors are present, methanogenic archaea are outcompeted by aerobic bacteria, denitrifiers and/or sulphate-reducing bacteria (Scheid et al., 2004; Thauer et al., 2008). Timmers et al. (2011) did not measure acetate concentrations above 2 mg L^{-1} (the limit of detection) in the PMFCs of which the biological community was analysed. This finding indicated that hydrolysis is the rate-limiting step in that type of cell. Assuming that electricity in the PMFC is generated via fermentation of hydrolyses products to acetate and the subsequent oxidation of acetate by *G*. *sulfurreducens* and *G.*

metallireducens. The majority of the methanogenic archaeal community, Methanobacteriacea*,* are unable to utilize acetate (Thauer et al. 2008). And therefore do not compete with *G*. *sulfurreducens* and *G. metallireducens* for acetate. This restriction is supported by the finding that of all the archaeal genera found in both PMFCs, only the *Methanosarcina* genera belong to acetate-utilising methanogens (Thauer et al., 2008). *Methanosarcina* comprised, on average, less than 10% of the archaeal DNA in the low-current PMFC and were barely observed in the high-current PMFC. The relative higher abundance of *Methanosarcina* in the low-current PMFC compared to the high-current PMFC likely contributed to competition for acetate. The competition for acetate between *G*. *sulfurreducens* and *G. metallireducens* and *Methanosarcina* likely contributed to the difference in current generation, however less than Rhodocyclaceae and Comamonandaceae. Furthermore, *Methanosarcina* is a methanogen with cytochrome, which generally have a threshold partial hydrogen pressure above 10 Pa. This consideration may indicate that products other than acetate were formed by fermentation, leading to less acetate production and thus likely a decrease in availability of acetate for generation of current. In addition the overall abundance of archaeal 16S rRNA genes was considerably lower in the high-current PMFC than in the low-current PMFC. This result leads to the conclusion that the methanogens likely did not consume a major portion of the acetate available for *G*. *sulfurreducens* and *G. metallireducens*.

De Schamphelaire (2010) performed a phylogenetic community analysis on archaea and found that 45% of the archaeal clone sequence was not related to any of the known methanogenic lineages. Of the archaeal clone sequences related to methanogenic lineages, 20% belonged to Methanobacteriaceae*,* 18 % to *Methanosarcina,* and 10% to Methanosaetaceae*.* In this study, the amounts of the acetate-utilising methanogens *Methanosarcina* and Methanosaetaceae were considerably lower (an average of <10% versus an average of 28%). One possible explanation for this discrepancy is the difference in the availability of graphite as an electron acceptor. De Schamphelaire (2010) used a graphite felt in sediment as the anode electrode for the PMFC, whereas in our setups we used graphite granules (without sediment) as electrodes. The use of graphite granules may have resulted in the increased availability of

graphite as an electron acceptor. The limited availability of the graphite felt as an electron acceptor may have given the acetate-utilising methanogens a competitive advantage over EAB. In case the availability of graphite as an electron acceptor indeed limits the competitive advantage of EAB over acetate-utilising methanogens. The availability of graphite as an electron acceptor will be an important factor in the reduction of methanogenesis by the PMFC (De Schamphelaire et al., 2008; Strik et al., 2008).

3.4.5 Possible electron sinks and electron donor transfer pathways

Five terminal electron acceptors were present at the anodes of the PMFCs: graphite granules, oxygen, nitrate, sulphate, and carbon dioxide. Of these, the latter four are possible electron sinks that do not contribute to current generation. The microbial community at the anode of the PMFC did not contain a large population of sulphate-reducing bacteria, indicating that they were out-competed for electron donor by the facultative anaerobic denitrifiers (such as Rhodocyclaceae and Comamonadaceae) and EAB (such as *G. sulfurreducens* and *G. metallireducens*) that were present in the anode of the PMFC. This finding is consistent with observations from natural fresh water sediments and wastewater treatment facilities, where the terminal electron acceptors are used in the following order of preference: O_2, NO_3^-, Mn(IV) oxides, Fe(III) oxides, SO_4^{2-}, and CO_2. Most EAB, such as *G. sulfurreducens* and *G. metallireducens*, reduce Fe(III) oxides in natural sediments (Holmes et al.). Iron reducers have a higher rate of conversion of acetate and hydrogen than sulphate-reducing bacteria and methanogens, which gives them a competitive advantage (Van Bodegom & Scholten, 2001). Despite the competitive advantage of EAB, however, acetate-utilising methanogens (*Methanosarcina)* were found. The presence of acetate-utilising methanogens might be explained by the availability of CO_2 at the root surface, as it is released by the plant roots as the result of metabolic processes. In contrast to CO_2, graphite granules have limited availability at the root surface due to the porous structure of the anode, which means that not all root surface was in direct contact with graphite granules. Figure 3.4 shows a schematic presentation of electron donor pathways and electron sinks.

Anaerobic cellulolytic bacteria dominated the area where most of the EAB were found, and more EAB were found on the graphite granules than on the root surface. This result implies that current was generated via the hydrolysis of cellulose and not directly from low-molecular-weight rhizodeposits. When optimising electricity generation in a PMFC, therefore, the focus should be on root biomass production and effective hydrolysis of the biomass.

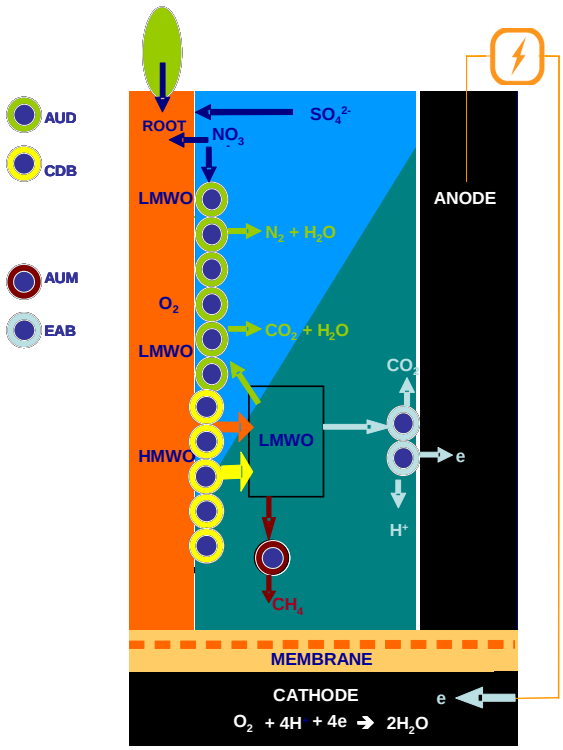

Figure 3.4: *Schematic presentation of the possible oxidation pathways of high molecular weight organic compounds (HMWO) and low molecular weight organic compounds (LMWO) in the anode of the plant microbial fuel cell (PMFC). The orange arrow represented the LMWO lost by the plant root, the yellow arrow represented the LMWO produced by cellulose degrading bacteria (CDB). The green, light blue and brown arrows represented the possible oxidation pathways and products of the oxidation of LMWO compounds .The blue colour represents the volume of the PMFC anode where electrochemically active bacteria (EAB) are out-competed by acetate utilizing denitrifiers (AUD) for LMWO. The green colour represents the volume of the PMFC anode where EAB are present and thus compete for LMWO with acetate utilizing methanogens (AUM).*

Acknowledgements

This research received funding from the European community's 7th framework programme FP7/2007-2013 under grant agreement no. 226532, as well as from Senternovem, the Dutch governmental agency for sustainability and innovation from the Ministry of Finance (grant no. EOSLT06020), and was supported by Alliander. The authors would like to thank Marjolein Helder and Kirsten Steinbusch for their useful comments.

References

Amann, R.I., Krumholz, L., Stahl, D.A. 1990. Fluorescent-oligonucleotide probing of whole cells for determinative, phylogenetic, and environmental studies in microbiology. *Journal of Bacteriology*, **172**(2), 762-770.

Amann, R.I., Zarda, B., Stahl, D.A., Schleifer, K.H. 1992. Identification of individual prokaryotic cells by using enzyme-labeled, rRNA-targeted oligonucleotide probes. *Applied and Environmental Microbiology*, **58**(9), 3007-3011.

Bano, N., Ruffin, S., Ransom, B., Hollibaugh, J.T. 2004. Phylogenetic Composition of Arctic Ocean Archaeal Assemblages and Comparison with Antarctic Assemblages. *Applied and Environmental Microbiology*, **70**(2), 781-789.

Bond, D.R., Lovley, D.R. 2002. Reduction of Fe(III) oxide by methanogens in the presence and absence of extracellular quinones. *Environmental Microbiology*, **4**(2), 115-124.

Borole, A.P., Hamilton, C.Y., Aaron, D.S., Tsouris, C. 2009. Investigating microbial fuel cell bioanode performance under different cathode conditions. *Biotechnology Progress*, **25**(6), 1630-1636.

Coates, J.D., Bhupathiraju, V.K., Achenbach, L.A., McInerney, M.J., Lovley, D.R. 2001. *Geobacter hydrogenophilus*, *Geobacter chapellei* and *Geobacter grbiciae*, three new, strictly anaerobic, dissimilatory Fe(III)-reducers. *International Journal of Systematic and Evolutionary Microbiology*, **51**(2), 581-588.

Collins, M.D., Lawson, P.A., Willems, A., Cordoba, J.J., Fernandez-Garayzabal, J., Garcia, P., Cai, J., Hippe, H., Farrow, J.A.E. 1994. The phylogeny of the genus Clostridium: Proposal of five new genera and eleven new species combinations. *International Journal of Systematic Bacteriology*, **44**(4), 812-826.

Chaudhuri, S.K., Lovley, D.R. 2003. Electricity generation by direct oxidation of glucose in mediatorless microbial fuel cells. *Nature Biotechnology*, **21**(10), 1229-1232.

Daims, H., Brähl, A., Amann, R., Schleifer, K.H., Wagner, M. 1999. The domain-specific probe EUB338 is insufficient for the detection of all bacteria: Development and evaluation of a more comprehensive probe set. *Systematic and Applied Microbiology*, **22**(3), 434-444.

De Schamphelaire, L., Cabezas, A., Marzorati, M., Friedrich, M.W., Boon, N., Verstraete, W. 2010. Microbial community analysis of anodes from sediment microbial fuel cells powered by rhizodeposits of living rice plants. *Applied and Environmental Microbiology*, **76**(6), 2002-2008.

De Schamphelaire, L., Van Den Bossche, L., Hai, S.D., Hofte, M., Boon, N., Rabaey, K., Verstraete, W. 2008. Microbial fuel cells generating electricity from rhizodeposits of rice plants. *Environmental Science and Technology*, **42**(8), 3053-3058.

Dekker, A., Ter Heijne, A., Saakes, M., Hamelers, H.V.M., Buisman, C.J.N. 2009. Analysis and improvement of a scaled-up and stacked microbial fuel cell. *Environmental Science and Technology*, **43**(23), 9038-9042.

Demaneche, S., Sanguin, H., Poté, J., Navarro, E., Bernillon, D., Mavingui, P., Wildi, W., Vogel, T.M., Simonet, P. 2008. Antibiotic-resistant soil bacteria in transgenic plant fields. *Proceedings of the National Academy of Sciences of the United States of America*, **105**(10), 3957-3962.

Finneran, K.T., Johnsen, C.V., Lovley, D.R. 2003. *Rhodoferax ferrireducens* sp. nov., a psychrotolerant, facultatively anaerobic bacterium that oxidizes acetate with the reduction of Fe(III). *International Journal of Systematic and Evolutionary Microbiology*, **53**(3), 669-673.

Franks, A.H., Harmsen, H.J.M., Raangs, G.C., Jansen, G.J., Schut, F., Welling, G.W. 1998. Variations of bacterial populations in human feces measured by fluorescent in situ hybridization with group-specific 16S rRNA-targeted oligonucleotide probes. *Applied and Environmental Microbiology*, **64**(9), 3336-3345.

Ginige, M.P., Keller, J., Blackall, L.L. 2005. Investigation of an acetate-fed denitrifying microbial community by stable isotope probing, full-cycle rRNA analysis, and fluorescent in situ hybridization-microautoradiography. *Applied and Environmental Microbiology*, **71**(12), 8683-8691.

Griffiths, R.I., Whiteley, A.S., O'Donnell, A.G., Bailey, M.J. 2000. Rapid method for coextraction of DNA and RNA from natural environments for analysis of ribosomal DNA- and rRNA-based microbial community composition. *Applied and Environmental Microbiology*, **66**(12), 5488-5491.

Harmsen, H.J.M., Raangs, G.C., He, T., Degener, J.E., Welling, G.W. 2002. Extensive set of 16S rRNA-based probes for detection of bacteria in human feces. *Applied and Environmental Microbiology*, **68**(6), 2982-2990.

Hartmann, A., Schmid, M., van Tuinen, D., Berg, G. 2009. Plant-driven selection of microbes. *Plant and Soil*, **321**(1-2), 235-257.

Helder, M., Strik, D.P.B.T.B., Hamelers, H.V.M., Kuhn, A.J., Blok, C., Buisman, C.J.N. 2010. Concurrent bio-electricity and biomass production in three Plant-Microbial Fuel Cells using *Spartina anglica, Arundinella anomala* and *Arundo donax*. *Bioresource Technology*, **101**(10), 3541-3547.

Holmes, D.E., Bond, D.R., O'Neil, R.A., Reimers, C.E., Tender, L.R., Lovley, D.R. 2004. Microbial communities associated with electrodes harvesting electricity from a variety of aquatic sediments. *Microbial Ecology*, **48**(2), 178-190.

Hsiao, C.L., Chang, J.J., Wu, J.H., Chin, W.C., Wen, F.S., Huang, C.C., Chen, C.C., Lin, C.Y. 2009. Clostridium strain co-cultures for biohydrogen production enhancement from condensed

molasses fermentation solubles. *International Journal of Hydrogen Energy*, **34**(17), 7173-7181.

Ishii, S., Hotta, Y., Watanabe, K. 2008. Methanogenesis versus electrogenesis: Morphological and phylogenetic comparisons of microbial communities. *Bioscience, Biotechnology and Biochemistry*, **72**(2), 286-294.

Jung, S., Regan, J.M. 2007. Comparison of anode bacterial communities and performance in microbial fuel cells with different electron donors. *Applied Microbiology and Biotechnology*, **77**(2), 393-402.

Juretschko, S., Timmermann, G., Schmid, M., Schleifer, K.H., Pommerening-Röser, A., Koops, H.P., Wagner, M. 1998. Combined molecular and conventional analyses of nitrifying bacterium diversity in activated sludge: *Nitrosococcus mobilis* and Nitrospira-like bacteria as dominant populations. *Applied and Environmental Microbiology*, **64**(8), 3042-3051.

Kaku, N., Yonezawa, N., Kodama, Y., Watanabe, K. 2008. Plant/microbe cooperation for electricity generation in a rice paddy field. *Applied Microbiology and Biotechnology*, **79**(1), 43-49.

Kim, B.H., Kim, H.J., Hyun, M.S., Park, D.H. 1999. Direct electrode reaction of Fe(III)-reducing bacterium, *Shewanella putrefaciens. Journal of Microbiology and Biotechnology*, **9**(2), 127-131.

Lane, D.J. 1991. 16S/23S rRNA sequencing. in: *Nucleic Acid Techniques in Bacterial Systematics*, pp. 115-175.

Lovley, D.R., Kashefi, K., Vargas, M., Tor, J.M., Blunt-Harris, E.L. 2000. Reduction of humic substances and Fe(III) by hyperthermophilic microorganisms. *Chemical Geology*, **169**(3-4), 289-298.

Lynd, L.R., Weimer, P.J., Van Zyl, W.H., Pretorius, I.S. 2002. Microbial cellulose utilization: Fundamentals and biotechnology. *Microbiology and Molecular Biology Reviews*, **66**(3), 506-577.

Lynd, L.R., Wyman, C.E., Gerngross, T.U. 1999. Biocommodity engineering. *Biotechnology Progress*, **15**(5), 777-793.

Maki, M., Leung, K.T., Qin, W. 2009. The prospects of cellulase-producing bacteria for the bioconversion of lignocellulosic biomass. *International Journal of Biological Sciences*, **5**(5), 500-516.

Manz, W., Amann, R., Ludwig, W., Wagner, M., Schleifer, K.-H. 1992. Phylogenetic oligodeoxynucleotide probes for the major subclass of *Proteobacteria*: problems and solutions. *Systematic and Applied Microbiology*, **15**, 593-600.

Min, B., Cheng, S., Logan, B.E. 2005. Electricity generation using membrane and salt bridge microbial fuel cells. *Water Research*, **39**(9), 1675-1686.

Nicol, G.W., Glover, L.A., Prosser, J.I. 2003. Molecular analysis of methanogenic archaeal communities in managed and natural upland pasture soils. *Global Change Biology*, **9**(10), 1451-1457.

Nielsen, J.L., Klausen, C., Nielsen, P.H., Burford, M., Jørgensen, N.O.G. 2006. Detection of activity among uncultured Actinobacteria in a drinking water reservoir. *FEMS Microbiology Ecology*, **55**(3), 432-438.

Niessen, J., Schröder, U., Scholz, F. 2004. Exploiting complex carbohydrates for microbial electricity generation - A bacterial fuel cell operating on starch. *Electrochemistry Communications*, **6**(9), 955-958.

Offre, P., Pivato, B., Siblot, S., Gamalero, E., Corberand, T., Lemanceau, P., Mougel, C. 2007. Identification of bacterial groups preferentially associated with mycorrhizal roots of *Medicago truncatula*. *Applied and Environmental Microbiology*, **73**(3), 913-921.

Park, D.H., Kim, B.H. 2001. Growth Properties of the Iron-reducing Bacteria, *Shewanella putrefaciens* IR-1 and MR-1 Coupling to Reduction of Fe(III) to Fe(II). *Journal of Microbiology*, **39**(4), 273-278.

Park, H.S., Kim, B.H., Kim, H.S., Kim, H.J., Kim, G.T., Kim, M., Chang, I.S., Park, Y.K., Chang, H.I. 2001. A novel electrochemically active and Fe(III)-reducing bacterium phylogenetically related to *Clostridium butyricum* isolated from a microbial fuel cell. *Anaerobe*, **7**(6), 297-306.

Phillips, D.A., Ferris, H., Cook, D.R., Strong, D.R. 2003. Molecular control points in rhizosphere food webs. *Ecology*, **84**(4), 816-826.

Pinton, R., Varanini, Z. 2007. *The rhizosphere : biochemistry and organic substances at the soil-plant interface*. CRC, Boca Raton.

Potter, M.C. 1911. Electrical Effects Accompanying the Decomposition of Organic Compounds. *Proceedings of the Royal Society of London. Series B, Containing Papers of a Biological Character*, **84**(571), 260-276.

Rabaey, K., Boon, N., Siciliano, S.D., Verhaege, M., Verstraete, W. 2004. Biofuel cells select for microbial consortia that self-mediate electron transfer. *Applied and Environmental Microbiology*, **70**(9), 5373-5382.

Reguera, G., Nevin, K.P., Nicoll, J.S., Covalla, S.F., Woodard, T.L., Lovley, D.R. 2006. Biofilm and nanowire production leads to increased current in *Geobacter sulfurreducens* fuel cells. *Applied and Environmental Microbiology*, **72**(11), 7345-7348.

Ren, Z., Ward, T.E., Regan, J.M. 2007. Electricity production from cellulose in a microbial fuel cell using a defined binary culture. *Environmental Science and Technology*, **41**(13), 4781-4786.

Rezaei, F., Xing, D., Wagner, R., Regan, J.M., Richard, T.L., Logan, B.E. 2009. Simultaneous cellulose degradation and electricity production by E*nterobacter cloacae* in a microbial fuel cell. *Applied and Environmental Microbiology*, **75**(11), 3673-3678.

Rismani-Yazdi, H., Christy, A.D., Dehority, B.A., Morrison, M., Yu, Z., Tuovinen, O.H. 2007. Electricity generation from cellulose by rumen microorganisms in microbial fuel cells. *Biotechnology and Bioengineering*, **97**(6), 1398-1407.

Scheid, D., Stubner, S., Conrad, R. 2004. Identification of rice root associated nitrate, sulfate and ferric iron reducing bacteria during root decomposition. *FEMS Microbiology Ecology*, **50**(2), 101-110.

Schellenberger, S., Kolb, S., Drake, H.L. 2010. Metabolic responses of novel cellulolytic and saccharolytic agricultural soil Bacteria to oxygen. *Environmental Microbiology*, **12**(4), 845-861.

Strik, D.P.B.T.B., Hamelers, H.V.M., Snel, J.F.H., Buisman, C.J.N. 2008. Green electricity production with living plants and bacteria in a fuel cell. *International Journal of Energy Research*, **32**(9), 870-876.

Tanner, C.C. 1996. Plants for constructed wetland treatment systems - A comparison of the growth and nutrient uptake of eight emergent species. *Ecological Engineering*, **7**(1), 59-83.

Thauer, R.K., Kaster, A.K., Seedorf, H., Buckel, W., Hedderich, R. 2008. Methanogenic archaea: Ecologically relevant differences in energy conservation. *Nature Reviews Microbiology*, **6**(8), 579-591.

Thomsen, T.R., Kong, Y., Nielsen, P.H. 2007. Ecophysiology of abundant denitrifying bacteria in activated sludge. *FEMS Microbiology Ecology*, **60**(3), 370-382.

Timmers, R.A., Strik, D.P.B.T.B., Hamelers, H.V.M., Buisman, C.J.N. 2010. Long-term performance of a plant microbial fuel cell with *Spartina anglica*. *Applied Microbiology and Biotechnology*, **86**(3), 973-981.

Van Bodegom, P.M., Scholten, J.C.M. 2001. Microbial processes of CH_4 production in a rice paddy soil: Model and experimental validation. *Geochimica et Cosmochimica Acta*, **65**(13), 2055-2066.

Xing, D., Cheng, S., Logan, B.E., Regan, J.M. 2010. Isolation of the exoelectrogenic denitrifying bacterium *Comamonas denitrificans* based on dilution to extinction. *Applied Microbiology and Biotechnology*, **85**(5), 1575-1587.

Xing, D., Zuo, Y., Cheng, S., Regan, J.M., Logan, B.E. 2008. Electricity generation by *Rhodopseudomonas palustris* DX-1. *Environmental Science and Technology*, **42**(11), 4146-4151.

4 Characterization of the internal resistance of a plant microbial fuel cell

This chapter has been published as:
Ruud A. Timmers, David P.B.T.B. Strik, Bert Hamelers, Cees Buisman, (2012) Characterization of the internal resistance of the plant microbial fuel cell. Electrochimica Acta

Abstract

Increase of energy demand and depletion of fossil fuels result in a need for renewable energy sources. The Plant Microbial Fuel Cell (PMFC) is a technology that has the potential to fulfil this need. To fulfil this need the power output should be improved and therefore the internal resistance must be reduced. It is not clear how the internal resistance of the PMFC is built up; therefore, the objective was to clarify the internal resistance of the PMFC. To characterize internal resistances of the PMFC current interrupt and polarization were used, and partial resistances were calculated. The internal resistance consisted mainly of anode resistance and membrane resistance which both decreased during current interrupt. The anode resistance was the result of mass transfer resistance in the electrochemically active biofilm. The membrane resistance was the result of accumulation of cations in the cathode. The polarization showed a distinct hysteresis which was explained by the increase of the internal resistance during polarization. The increase of this resistance makes it difficult to interpret the maximum power output of the PMFC.

Keywords: plant microbial fuel cell / current interrupt/ polarization / internal resistance / anode resistance / membrane resistance

4 Characterization of the internal resistance of the plant microbial fuel cell

4.1 Introduction

Increase of energy demand and depletion of fossil fuels result in a need for more renewable energy sources. Growing plants to produce renewable and sustainable bio-energy is an option because plant growth is based on photosynthesis which is renewable. The Plant Microbial Fuel Cell (PMFC) is a technology that has the potential to fulfil the need for a clean renewable energy source (Strik et al., 2008) (Timmers et al., 2010) (Strik et al., 2011). It is renewable because is driven by solar radiation (photosynthesis). The PMFC technology is clean because energy generation is based on bio-catalysts and therefore does not require the use of toxic catalysts and mediators. The advantage of the PMFC over conventional renewable energies based on plant growth is that it can be integrated with food production (De Schamphelaire et al., 2008) (Kaku et al., 2008) and can be applied at locations unsuitable for food production like green roofs (Strik et al., 2011).

In the PMFC, the plant roots are integrated in the anode of a microbial fuel cell (MFC) (Strik et al., 2008), where roots provide electrochemically active bacteria with substrate via rhizodeposition (loss of (in)organic material by roots). Electrochemically active bacteria transfer electrons to anode electrode via oxidation of substrate which yields carbon dioxide, protons, and electrons (De Schamphelaire et al., 2010). Subsequently the electrons flow through an electrical circuit and power harvester to the cathode, where they are consumed by typically oxygen reduction. The produced carbon dioxide is converted again into substrate for electrochemically active bacteria by photosynthesis. In this manner, the PMFC produces in situ renewable electrical power in a clean manner.

Based on the highest reported values for photosynthesis, rhizodeposition and energy recovery in a MFC, the maximum power production of the PMFC is 3.2 W m^{-2} (28,000 kWh ha^{-1} $year^{-1}$) (Strik et al., 2011). Nevertheless, the reported power production of different PMFCs setups ranged from 0.22 to 0.0060 W m^{-2} (De Schamphelaire et al., 2008) (Kaku et al., 2008) (Strik et al., 2008) (Helder et al., 2010) (Timmers et al., 2010) which is less than 10% of the maximum. The power output of the PMFC is a combination of the coulombic efficiency and voltage efficiency. The coulombic efficiency of the

PMFC is affected by the presence of alternative electron acceptors (Timmers et al.) and microorganisms (Timmers et al., 2011). Helder et al. (Helder et al., 2011) showed that the power output increased in the absence of nitrate in the medium for the PMFC. Until now there is no clear insight in the voltage efficiency of the PMFC, although this is required to improve the power output. The voltage efficiency is determined by the potential losses during current generation and thus the internal resistance. Reported internal resistances of the PMFC are determined as the slope of the polarization curve and show a large variance between 21 Ωm^2 (Kaku et al., 2008) and 0.5 Ωm^2 (Strik et al., 2008). To increase the power production the internal resistance of the PMFC must be decreased. Until now there is no explanation for the high internal resistance of the PMFC compared to the internal resistance of the microbial fuel cells. In addition, the polarization behaviour of the PMFC showed a typical very distinct hysteresis which is not reported for MFC.

The objective of this study was to clarify the internal resistance of the PMFC. In order to do the current interrupt method and polarization technique were used. In order to calculate the partial resistances the cell, cathode, and anode potential were measured together with the pH, and conductivity in the anode of a PMFC. To determine whether or not the internal resistance and polarization behaviour was unique for the PMFC, a MFC setup without (plant)roots was also evaluated.

4.2 Material and methods

4.2.1 Experimental set-up

Figure 2.2 shows a schematic representation of the experimental set-up. The anode compartment of the set-up consisted of glass cylinder with diameter of 0.035 m, height of 0.3 m, and two sample points opposite to each other at 0.02, 0.055, 0.09, 0.125, 0.16, 0.195, 0.23, 0.265 m from the bottom of the cylinder. At the bottom of the cylinder, a cation exchange membrane (fumasep®, FKB FuMA-Tech GmbH, St Ingbert, Germany) was fixed to separate the anode from the cathode compartment. The glass cylinder was filled with 165 g of graphite granules with a BET surface of 0.5 m^{-2} g to function as anode electrode. The cathode compartment consisted

of a PCV beaker with diameter of 0.11 m, and height of 0.04 m. This beaker included graphite felt to function as cathode electrode. The anode compartment was placed in the PVC beaker on top of the graphite felt. A gold wire glued to a Teflon coated copper wire was used as current collector in both the anode and cathode. Current collectors were connected over a resistance of 900 Ω to close the electrical circuit.

Before the plant *Glyceria maxima* was planted, the set-up was operated as a MFC fed with 0.02 mol L^{-1} acetate. The medium used to grow electrochemically active bacteria on the graphite granules was ½ Hoagland buffered with 0.008 mol L^{-1} potassium phosphate buffer solution (pH 6.8).

Before graphite granules with the electrochemically active biofilm were used for PMFCs, they were mixed and rinsed with tap water to remove any residual substrate. In total, there were 6 PMFCs. In each PMFC, one stem of *G. maxima* (D'n Bart Waterplanten, the Netherlands) with a mass between 4.4 g and 7.8 g was planted. The medium used to feed the PMFCs was ½ Hoagland buffered with 0.008 mol L^{-1} potassium phosphate buffer solution as described by Timmers et al. (2010) (pH 6.8, conductivity between 1.5 through 1.7 mS m^{-1}). The medium was fed through a sample point located 0.07 m above the graphite granules. The applied flow rate was 0.17 mL s^{-1} throughout the experimental period. The feeding frequency of the PMFC with buffered Hoagland medium was 5 minutes every 12 hours.

Both, MFC and PMFC, setups were placed in a climate control cabinet (Microclima 1750 Snijders, Tilburg the Netherlands). In this manner, environmental conditions were fixed at illumination period of 14 h d^{-1}, average light density in the photo active region of 596 ± 161 µmol m^{-2} s^{-1}, temperature of 25 ^{o}C, and humidity of 75%.

4.2.2 Measurements

Cell potential (E_{cell}) was measured every 60 seconds online with data acquisition instrument (Fieldpoint module FP-AI-112) connected to a personal computer with Labview software via a Fieldpoint Ethernet Controller Module FP-2000 (National Instuments, Austin USA). Similarly, anode potentials and cathode potential were measured versus silver/silverchloride (Ag/AgCl) reference electrodes (3 mol L^{-1}KCl electrode,

ProSense QiS, Oosterhout, the Netherlands, +205 mV vs. NHE). To determine the anode potential profile, the anode potentials were measured at 0.02, 0.055, 0.09, and 0.125 m from the membrane.

Samples were taken with a syringe (2 mL) through a septum. pH, conductivity and volatile fatty acids were measured in the samples. The pH was measured with a pH-electrode (Prosense Qis, Oosterhout, the Netherlands) together with a pH-meter (Metrohm 691 pH-meter Herisau, Switzerland). Conductivity was measured with a ProLine Plus conductivity meter (Prosense Qis, Oosterhout, the Netherlands). Volatile fatty acids concentrations were measured as described by Timmers et al (2010).

4.2.3 Electrochemical characterization

To see the effect of the current interrupt method on the cell, anode, and cathode potential the current was interrupted by disconnecting the cathode from the resistance for about four hours.

To acquire polarization curves, chronoamperometry was performed with an IviumStat potentiostat and IviumSoft software (IVIUM technologies B.V. Eindhoven, the Netherlands). The controlled cell potential was decreased stepwise from 0.4 V to 0.005 V (via 0.2 V, 0.1 V, and 0.05 V), and further raised again stepwise from 0.05 to 0.4 (via 0.05 V, 0.1 V, and 0.2 V). Each controlled cell potential was maintained for 5 or 60 minutes to study the effect of time on the power output. To measure the pH profile, pH-electrodes (Prosense Qis, Oosterhout, the Netherlands) were inserted at 0.02, 0.055, 0.09 and 0.125 m from the CEM in the PMFC. The pH electrodes were connected to a pH controller (Liquisis M CPM 253, Endress+Hauser, Reinach, Switzerland) which was connected to the Fieldpoint Ethernet Controller Module FP-2000 (National Instuments, Austin USA).

4.3 Calculations

4.3.1 Profile gradients

Profile gradients of anode, pH and conductivity were defined as the slope of the linear trend line fitted to the profile. The anode potential gradient $\frac{dE_{an}}{dx}$ was expressed in V m^{-1}, the pH gradient was expressed as $\frac{dpH_{an}}{dx}$ in pH m^{-1}, and the conductivity gradient was expressed as $\frac{d\sigma_{an}}{dx}$ in S m^{-2}.

4.3.2 Time constants of transport in electrochemically active biofilm and anode compartment

To characterize the response of the MFC and PMFC to the current interrupt time constants for mass transfer in the electrochemically active biofilm and bulk anolyte were defined. Mass transfer in the electrochemically active biofilm at open circuit is diffusion driven. The characteristic diffusion length, for diffusion in the electrochemically biofilm is the biofilm thickness, which is in the range of 10^{-6} through 10^{-3} m. Mass transfer in the bulk anolyte compartment was also diffusion driven, because the anode compartment was not mixed, and the cation exchange membrane was non-porous. The characteristic diffusion length, for diffusion in the anode compartment was defined as half the height of the graphite bed (0.5·0.1 = 0.05 m). With the characteristic diffusion length for the electrochemically active biofilm, and the anode compartment the time constant was calculated according to the following equation:

$$\tau = \frac{L_d^2}{4D} \qquad 1$$

In the above equation τ is the time constant (s), L_d is the characteristic diffusion length (m), and D is the diffusion coefficient (m^2 s^{-1}). The diffusion coefficient for simple ions is in the range of 10^{-9} m^2 s^{-1} through 10^{-8} m^2 s^{-1}.

The time constant for mass transfer in the electrochemically active biofilm was estimated to be in the range of $2.5 \cdot 10^{-5}$ s through 2.5 s, The time

constant for mass transfer in the bulk anolyte was estimated to be in the range of $6.25 \cdot 10^4$ s (≈17 h) through $6.25 \cdot 10^5$ s (≈170 h),

4.3.3 Internal resistance

In |MFCs, the cell potential is linear function of the maximum theoretical cell potential approximated to the open cell potential, the current density and the internal resistance (Logan et al., 2006).

$$E_{cell} = E_{OCP} - iR_{\text{int}} \quad (2)$$

In the above equation E_{cell} is the measured cell potential in V, E_{OCP} is the open cell potential in V, i is the current density in A m^{-2}, and R_{int} is the internal resistance in Ω m^2.

The internal resistance consists of resistances due to the cathode overpotential, anode overpotential, and current dependent potential losses such as ionic losses and transport losses (Logan et al., 2006) which are measured as the membrane potential (Harnisch et al., 2009) (Bard & Faulkner, 1980). Therefore, combining this with equation (1), E_{cell} (cell potential) can be calculated as:

$$E_{cell} = E_{OCP} - \eta_{cath} - \eta_{an} - i(R_M) \quad (3)$$

Where η_{cath} is the cathode overpotential (V), η_{an} is the anode overpotential (V), and R_M is membrane resistance (Ω m^2). According to (Sleutels et al., 2009), cathode and anode overpotential can be calculated as:

$$\eta_{cath} = E_{OCP,cath} - E_{cath} \quad (4)$$

$$\eta_{an} = E_{an} - E_{OCP,an} \quad (5)$$

Where E_{cath} is the measured cathode potential (V), $E_{OCP,cath}$ is the cathode potential at open cell potential (V), $E_{OCP,an}$ is the anode potential at open cell potential (V), and E_{an} is the measured anode potential (V). The

anode potential at open circuit is about equal to the theoretical anode potential (Logan et al., 2006) which can be calculated by the Nernst equation.

$$E_{OCP,an} = E_{an}^{0} - \frac{RT}{nF} \ln \frac{\left[CH_3COO^-\right]}{\left[H^+\right]^9 \left[HCO_3^-\right]^2} \quad 6$$

Where E_{an}^{0} is the standard potential (V), R is the universal gas constant (8.314 J mol^{-1} K^{-1}), T is the temperature (K), n is the number of electrons involved in the reaction (-), F is Faraday's constant (96485 C mol^{-1}), $\left[CH_3COO^-\right]$ is the acetate activity (mol L^{-1}), $\left[H^+\right]$ is the proton activity (mol L^{-1}), and $\left[HCO_3^-\right]$ is the bicarbonate activity (mol L^{-1}).

The membrane potential is defined as difference between reference electrodes in the anode and the cathode (Ter Heijne et al., 2006). In this manner, membrane potential loss was calculated according to Sleutels (2009):

$$E_M = E_{cath} - E_{an} - E_{cell} \quad 7$$

In the above equation E_M is the membrane potential loss (V), E_{cath} is the measured cathode potential (V), E_{an} is the measured anode potential (V), and E_{cell} is the measured cell potential (V). In this set-up, the anode potential was measured at 0.02 m, 0.055 m, 0.09 m and, 0.125 m from the membrane. Consequently, there were four different anode overpotential losses and thus four membrane potential losses.

The partial internal resistances were calculated by Ohm's law, i.e. by dividing the partial potential losses by the current density. Therefore as alternative to equation 2, the internal resistance was also calculated by adding up the cathode overpotential resistance, anode overpotential resistance and membrane resistance.

4.3.4 Capacitive current

Electrons are stored in the electrical double layer of the PMFC anode. The electrical double layer is able to release or take up electrons when the anode potential changes. The release of electrons results in an increase in current generation whereas capture of electrons results in a decrease in current generation. The capacitive current is proportional to the rate of change of the anode potential $\left(dE/dt\right)$ which was calculated according to:

$$\frac{dE_i}{dt} \approx \frac{\Delta E_i}{\Delta t} \qquad 8$$

where E_i is the anode potential of a specific section (V). The rate of change of the anode potential (capacitive current) was estimated by assuming that the anode potential of each section was equal to the measured anode potential in the specific section.

The capacitance of the graphite electrode, i.e. the proportionality constant is in the order of 0.034 F m^{-2} (per square meter of BET surface) (Qu & Shi, 1998). Knowing the BET surface area (0.5 m^2 g), the mass of the graphite granules (165 g), the capacitance (0.034 F m^{-2}) and the rate of change of the anode potential, the capacitive current can be calculated. Again, since anode potential was measured at 0.02, 0.055, 0.09, and 0.125 m from the membrane, four different rates of change for the anode potential were calculated. To calculate the capacitive current, the anode was divided into 4 sections, namely from 0 to 0.0375 m, from 0.0375 to 0.0725 m, from 0.0725 to 0.1025, and from 0.1025 to 0.195 m. The BET surface of graphite granules of each section was calculated by dividing the height of the specific section by the total height of the graphite bed which was multiplied with the total BET area of the graphite granules in the anode (82.5 m^{-2}). Subsequently, the capacitance of the specific section was calculated by multiplying the BET area and the capacitance. The capacitive current for each section was calculated by multiplying of the rate of change of the anode potential by the capacitance.

$$cc = C_i \frac{\Delta E_i}{\Delta t} \quad 9$$

where cc is the capacitive current (A), C_i is the capacitance of the specific section. The total capacitive current was the sum of the capacitive currents of each section.

4.4 Results and discussion

4.4.1 Current interrupt

4.4.1.1 Mass transfer in bulk anolyte governed response to current interrupt.

The current interrupt technique is used to determine the ohmic potential loss of the (P)MFC in which current generation is interrupted by opening the electrical circuit. The ohmic potential loss is proportional to the current and therefore disappears immediately at open circuit (Bard & Faulkner, 1980) (Logan et al., 2006). Figure 4.1 shows the typical response of the cell, anode, and cathode potential to open circuit (i.e. no current was generated) of the PMFC (A) and MFC (B) setup. The cell potential increased, the anode potential decreased, and the cathode potential remained stable for both the PMFC and the MFC. The immediate response of the anode and cathode potential was small which indicated that the ohmic loss (and thus resistance) was negligible (Logan et al., 2006). The anode potentials of the PMFC and the MFC showed a similar response to open circuit (Figure 4.1 a and b), all anode potentials decreased during open circuit. The anode potentials reached its final value after a time span in the order of hours in both setups. This response suggested that acetate, proton, and bicarbonate concentration continued to change at the electrode surface for hours because these concentrations determine the anode potential at open circuit (equation 6). Based on the time constants (for diffusion in the electrochemically active biofilm, and the time constant for diffusion in the bulk anolyte) it was likely that the response of the anode potential to open circuit was governed by transport processes in the bulk anolyte. The transport processes in the bulk anolyte subsequently affected the

concentration of protons, bicarbonate and substrate (acetate) at the electrode surface and thus the anode potentials.

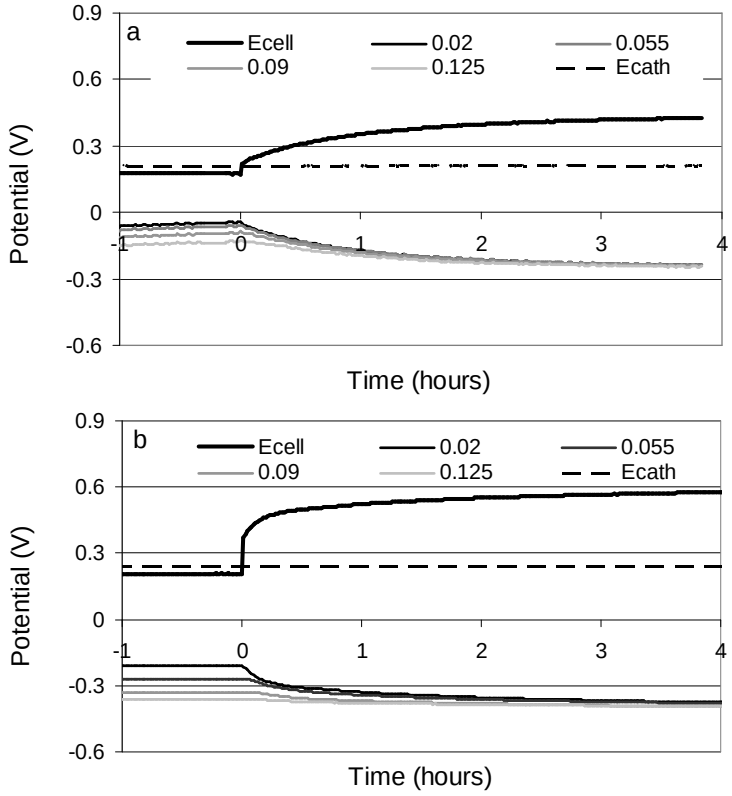

Figure 4.1: *Increase of cell potential (E_{cell}), decrease of anode potential versus Ag/AgCl (0.02, 0.055, 0.09, 0.125) and constant cathode potential versus Ag/AgCl (E_{cath}) during current interrupt of the PMFC (a) and the MFC (b) during current interrupt, at t = 0 the electrical circuit was opened.*

4.4.1.2 Current generation driving force for anode potential gradient

A distinct feature of Figure 4.1 is that at current generation (t<0) the anode potential increased closer to the cation exchange membrane, and thus that the anode potential gradient was negative (-0.8 ± 0.01 V m^{-1} for the PMFC and -1.5 ± 0.002 V m^{-1} for the MFC). During open circuit, however, the anode potential gradients increased to -0.08 V m^{-1} for the PMFC and, -0.003 V m^{-1} for the MFC. This showed that the difference between the measured anode potentials disappeared. Based on the cell potential, anode potential,

and cathode potential, the membrane potential was calculated (equation 7). The membrane potential showed the opposite trend as the anode potential i.e., the gradient was positive. During open circuit the membrane potential gradient continuously decreased. As stated before the membrane potential consists of ohmic potential loss and transport potential loss (Sleutels et al., 2009). The ohmic losses are proportional to current and disappear immediately at open circuit (Bard & Faulkner, 1980) (Logan et al., 2006). Therefore if ohmic losses would cause the anode potential profile, than the anode potential gradient should become zero immediately at open circuit. However, the anode potential gradient, and thus membrane potential gradient, did not become zero immediately at open circuit. This finding indicated that transport potential losses resulted in the anode potential profile and thus membrane potential profile. Transport potential loss is the potential loss due to charge transfer through the membrane and the adjacent stagnant layer (Harnisch et al., 2009) (Sleutels et al., 2009) and is nothing more than the potential gradient that is the driving force for migration (Bard & Faulkner, 1980). Migration of cations was required to maintain electro-neutrality in the system. Transport of cations through a non-porous cation exchange membrane is the sum of diffusion and migration. This is commonly described by the Nernst-Planck flux equation (Rozendal, 2007). This equation states that diffusion is driven by a concentration gradient, and migration is driven by a potential gradient. Due to the concentration gradient of potassium over the cation exchange membrane, at the start of the experiment (catholyte 0.16 mol L^{-1}, anolyte (0.014 mol L^{-1}), diffusional transport of positive charge opposed the direction of transport to maintain electro neutrality. Therefore, when current was generated, migration and thus a potential gradient was required to drive transport of cations against the concentration gradient towards the cathode. The measured anode potential gradient represented the membrane potential required to drive transport of cations to the cathode.

Migration, is not ion specific, therefore all cations, and thus protons, were transported towards the cathode. As migration drove cations towards the cathode, the concentration of anions also had to increase closer to the cathode to maintain electro neutrality throughout the anode. Migration, therefore, explained the conductivity gradient as well as the pH gradient in

PMFC and MFC. In both set-ups, the conductivity and proton concentration increased towards the membrane. More specifically, the conductivity gradient was always negative –3.14 ± 1.95 S m^{-2} for the PMFC, and -1.94 ± 1.96 S m^{-2} for the MFC. The pH profile in the PMFC and MFC exhibited always a positive gradient 14.5 ± 8.6 pH m^{-1} for the PMFC, and 8.8 ± 5.1 pH m^{-1} for the MFC.

The presence of the anode potential, pH, and conductivity profiles indicated that the diffusion layer adjacent to the cation exchange membrane extended throughout the anode compartment of the PMFC and MFC i.e., a large part of the anode compartment could be seen as a diffusion layer. The similarity in anode potential, pH, and conductivity profiles in the PMFC and the MFC indicated that plant roots did not cause the profiles.

4.4.1.3 Anode potential negatively affected by plant roots

The plant roots did not cause the anode potential profile, however, the average anode potential in the PMFC was higher than the average anode potential of the MFC (Figure 4.1 a and b). The open circuit anode potential approaches the Nernst-potential and is determined by the substrate (acetate), proton, and bicarbonate activities at the electrode surface at a given temperature (Logan et al., 2006). The difference in average anode potential (0.15 V) between the PMFC and MFC at open circuit could partly be attributed to the lower average pH in the anolyte of the PMFC. The average pH was 5.4 ± 1.1 in the PMFC versus 6.8 ± 0.5 in the MFC. The 1.4 difference in pH unit accounts for 0.09 V (0.06 V per pH unit) of the difference in average anode potential. The difference in the acetate concentration in the anolyte of the PMFC and MFC was maximally 0.016 mol L^{-1}. The acetate concentration in the PMFC is around detection limit (3.4 10^{-5} mole L^{-1}) (Timmers et al., 2010) while the acetate concentration in the MFC was 0.016 ± 0.01 mole L^{-1}. According to the Nernst equation (equation 6) the difference in acetate concentration accounted for 0.02 V of the difference in average anode potential. The remaining difference (0.04 V) was likely due to the fact that plant roots loose oxygen into the rhizosphere in submerged conditions(Jackson & Armstrong, 1999). Oxygen in the anode of the PMFC could increase the anode potential due to chemical oxygen reduction.

4.4.1.4 Anode resistance decreased during current interrupt

The average anode resistance decreased with 99% during open circuit, from 0.9 Ω m^2 to 0.01 Ω m^2 in the PMFC, and from 0.5 Ω m^2 to 0.002 Ω m^2 in the MFC. In MFCs, the anode resistance is mainly due to an increase of proton concentration at the anode electrode surface due to the resistance to proton transport out of the electrochemically active biofilm and the adjacent stagnant diffusion layer (Torres et al., 2008) . During open circuit no current was produced by the electrochemically active biofilm, hence no protons were generated at the anode electrode surface. Because there was no production of protons the concentration in the electrochemically active biofilm decreased, and therefore the anode resistance. In the PMFC substrate accumulation might have contributed to the decrease of anode resistance because during open circuit no substrate is consumed by electrochemically active bacteria while it was produced by rhizodeposition of low molecular weight compounds and hydrolysis of dead plant material. However, the accumulation of substrate was highly unlikely because, the anode potential in the MFC reached its final in about the same time as the anode potential in the PMFC. This fact indicated that substrate accumulation played a minor because in the MFC there was no substrate accumulation. In addition other microbes than electrochemically bacteria are present in the PMFC (De Schamphelaire et al., 2010). These microbes likely continue to consume acetate during open circuit and likely consume the acetate not consumed by electrochemically active bacteria. Additionally electrochemically active bacteria only make up small part of the biofilm in the PMFC (< 1.%). Therefore it was highly unlikely that substrate accumulated during open circuit. These facts indicated that substrate accumulation played a minor because in the MFC there was no substrate accumulation.

4.4.1.5 Membrane resistance decreased during current interrupt

The average membrane resistance decreased also spectacular during open circuit, from 0.6 Ω m^2 to 0.1 Ω m^2 in the PMFC, and from 1.3 Ω m^2 to 0.3 Ω m^2 in the MFC. The decrease in membrane resistance can be explained by transport processes in the anode compartment. No current was generated during open circuit, thus there is no need for charge transfer to maintain

electro neutrality. Because there was no charge transfer, the accumulation of cations in the cathode stopped. Moreover the accumulation of cations decreased due to diffusion from the cathode to the anode. Due to the decrease in accumulation, the membrane resistance decreased during open circuit. The decrease in membrane resistance was less than the decrease of the anode resistance this finding was consistent with the estimated time constants for diffusion. Diffusion in the electrochemically active biofilm had an estimated time constant in the order of seconds whereas diffusion through the anode had an estimated time constant in the order of hours.

4.4.2 Polarization curves of the PMFC

4.4.2.1 Hysteresis explained by increase in internal resistance and capacitive currents during polarization

The PMFC showed a consistent hysteresis in the polarization curves, and power curves. Figure 4.2 shows the polarization behaviour of the PMFC and capacitive currents when the controlled potentials were maintained for 5 minutes and when the controlled potentials were maintained for 60 minutes (a), and the power curves (b). The hysteresis during polarization could be due to capacitive currents which can be produced when the anode potential increased and can be consumed when the anode potential decreased (see Appendix 4.1). Figure 4.2 a clearly shows that the capacitive current, when the controlled potentials were maintained for 60 minutes, was negligible (>2%) compared to the measured current and therefore hardly contributed to the hysteresis in the polarization and power curve. When the controlled potentials were maintained for 5 minutes the contribution of the capacitive current to the measured current was not negligible at the maximum power output (30 %) and thus contributed to the hysteresis of the polarization and power curve. However it did not totally explain the difference in power output. The maximum power output during the increase of the controlled potential was only 31 % of the maximum power output reached when the controlled potential was decreased.

Figure 4.2 shows the development of the partial and total internal resistance during polarization when the controlled potentials were maintained for 60 minutes (a) and when the controlled potentials were

maintained for 5 minutes (b). The Figure clearly shows that the total internal resistance increased during polarization. According to equation 1, a higher internal resistance results in a lower current density and thus a lower power density at the same controlled potential. The increase in the internal resistance explained not only the hysteresis of the polarization and consequently the power curve but also the difference between the 5 and 60 minutes. The internal resistance at 5 minutes was lower compared to 60 minutes which resulted in a higher power output. Therefore, in the present study, the hysteresis at 60 minutes was explained by the increase in internal resistance while the hysteresis at 5 minutes was explained by the increase in internal resistance in combination with capacitive currents.

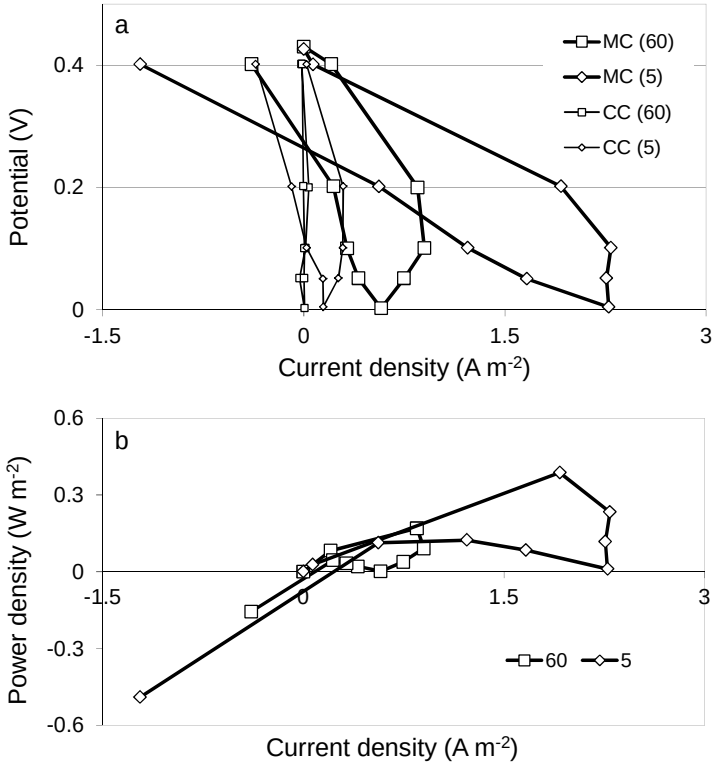

Figure 4.2: *Hysteresis in polarization and power curves.*
(a) *Polarization curves of the PMFC when the controlled potential was maintained for 60 minutes (MC (60)) and for 5 minutes (MC (5)) and the released capacitive current (CC (60) and CC(5)).*
(b) *Power curves of the PMFC when the controlled potential was maintained for 5 minutes (5) and for 60 minutes (60).*

4.4.2.2 Anode resistance increased during polarization

During polarization the anode resistance increased continuously to 0.7 Ω m^2 at 60 minutes and 0.3 at 5 minutes (Figure 4.3 a and b (AR)). The increase in anode resistance was likely due to proton production in the electrochemically active biofilm during current generation. The proton production resulted in an increase of the proton concentration in the electrochemically active biofilm and thus an increase in anode resistance. The continuous increase of the anode resistance indicated that the proton concentration in the electrochemically active biofilm continuously increased. This was likely due to the limited buffer capacity of the anolyte and limited proton transfer out of the anode to the cathode. This resulted in a continuous increase of the proton concentration in the anolyte and therefore a continuous increase in proton concentration in the electrochemically active biofilm and thus an increase in anode resistance. This explained not only the continuous increase of the anode resistance, but also the higher anode resistance at 60 minutes. Because at 60 minutes more coulombs, and thus protons, were generated than at 5 minutes which resulted in a higher anode resistance.

4.4.2.3 Membrane resistance increased during polarization

In contrast to the anode resistance the membrane resistance did not increase continuously during polarization but decreased when the controlled potential was decreased from 0.4 to 0.2 V (Figure4.3 a and b (MR)). However, after the initial decrease the membrane resistance increased as long as the cumulative coulombs increased. The increase of the membrane resistance was likely due to a continuous increase of accumulation of cations in the cathode compartment during current generation. The increase in accumulation resulted in a continuous increase of the concentration gradient. Due to the increase in the concentration gradient a larger potential gradient, and thus membrane potential, was required to drive cations against the concentration gradient into the cathode.

The membrane resistance decreased when the controlled potential was decreased from 0.4 to 0.2 V (Figure4.3 a and b (MR)). It can be

hypothesized that this was due the contribution of protons to the charge transport. As stated before, there was no migration during open circuit, because no current was generated there was no charge transport required to maintain electroneutrality. Therefore the protons diffused not only to the cathode but also in the anode away from the membrane and thus the proton concentration decreased, close to the membrane. Therefore, at the start of current generation the proton concentration was low compared to before open circuit. The low proton concentration resulted in a smaller diffusional transport of protons and therefore other cations were transported to the cathode against the concentration gradient which explained the relatively high membrane resistance. On the other hand, during current generation, protons are produced in the anode and migrate to towards the membrane again which could increase the proton concentration at the anode side of the membrane. The supposed increase of proton concentration would cause an increase in diffusion of protons from the anode to the cathode which might explain the decrease in membrane resistance at the initial stage of polarization.

In addition, the membrane resistance decreased, when the cumulative coulombs decreased (Figure4.3 a and b). The decrease in cumulative coulombs was due to negative currents i.e., electrons were transported from the cathode to the anode (see Appendix 4.2). Therefore, to maintain electro neutrality, positive charge must be transported from the cathode to the anode which was along the concentration gradient. This resulted in a decrease of accumulated cations in the cathode and thus a reduction of the concentration gradient which opposed the required transport direction. The reduction to the concentration gradient resulted in a decrease of the membrane resistance

4.4.2.4 Increase in internal resistance during polarization makes interpretation of maximum power output difficult

The maximum power output was 0.39 W m^{-2} (Figure 4.2 b), which is highest reported power output (Strik et al., 2011). This maximum power output was reached when the controlled potential was decreased. When the controlled potential was increased, the maximum power output was much lower (0.12 W m^{-2}). The same tendency was seen when the potentials were controlled

for 60 minutes however the power output was lower, (Figure 4.2 b). The decrease in the maximum power output was the result of the increase in internal resistance during polarization. The increase of internal resistance made it difficult to interpret the maximum power output and extrapolate this to average power output.

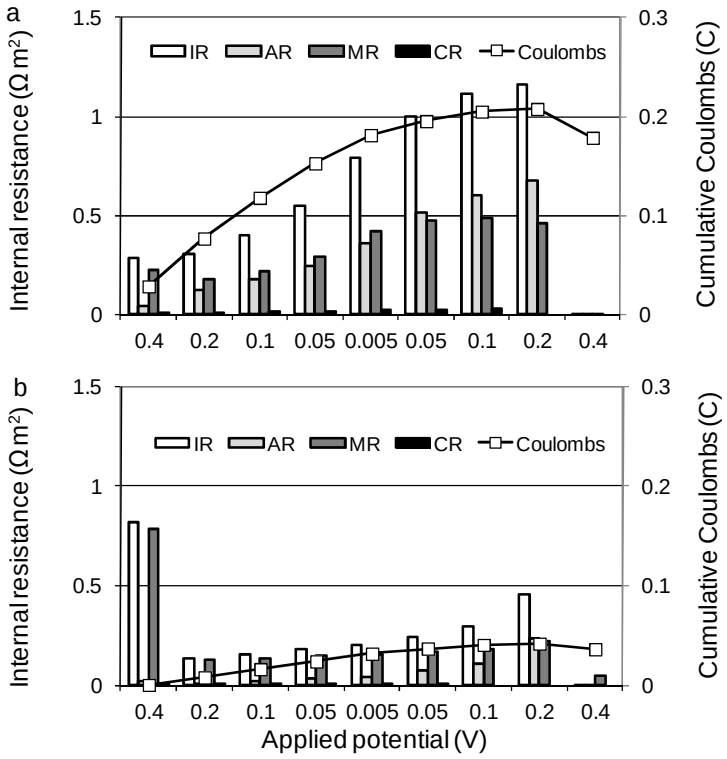

Figure 4.4: *Development of internal resistance (IR), cathode resistance (CR), anode resistance (AR), membrane resistance (MR) and the cumulative coulombs (coulombs) during polarization when the controlled potential was maintained for 60 minutes (A) and for 5 minutes*

4.5 Conclusions

The internal resistance consisted mainly of anode resistance and membrane resistance which both decreased during current interrupt. The anode resistance was the result of mass transfer resistance in the electrochemically active biofilm. The membrane resistance was the result of accumulation of cations in the cathode. The polarization showed a distinct

hysteresis which was explained by the increase of the internal resistance during polarization. The increase of this resistance makes it difficult to interpret the maximum power output of the PMFC.

Acknowledgements

This research was funded by Senternovem, the Dutch governmental agency for sustainability and innovation in the Ministry of Finance (grant no. EOSLT06020), and supported by Alliander. The authors would like to thank Cristina Arampatzoglou, Marjolein Helder, Kirsten Steinbusch, and Wouter Bac for their useful comments.

References

Bard, A.J., Faulkner, L.R. 1980. *Electrochemical methods : fundamentals and applications*. Wiley, New York.

De Schamphelaire, L., Cabezas, A., Marzorati, M., Friedrich, M.W., Boon, N., Verstraete, W. 2010. Microbial community analysis of anodes from sediment microbial fuel cells powered by rhizodeposits of living rice plants. *Applied and Environmental Microbiology*, **76**(6), 2002-2008.

De Schamphelaire, L., Van Den Bossche, L., Hai, S.D., Höfte, M., Boon, N., Rabaey, K., Verstraete, W. 2008. Microbial fuel cells generating electricity from rhizodeposits of rice plants. *Environmental Science and Technology*, **42**(8), 3053-3058.

Harnisch, F., Warmbier, R., Schneider, R., Schröder, U. 2009. Modeling the ion transfer and polarization of ion exchange membranes in bioelectrochemical systems. *Bioelectrochemistry*, **75**(2), 136-141.

Helder, M., Strik, D.P.B.T.B., Hamelers, H.V.M., Kuhn, A.J., Blok, C., Buisman, C.J.N. 2010. Concurrent bio-electricity and biomass production in three Plant-Microbial Fuel Cells using Spartina anglica, Arundinella anomala and Arundo donax. *Bioresource Technology*, **101**(10), 3541-3547.

Helder, M., Strik, D.P.B.T.B., Hamelers, H.V.M., Kuijken, R.C.P., Buisman, C.J.N. 2011. New plant-growth medium for increased power output of the Plant-Microbial Fuel Cell. *Bioresource Technology*.

Jackson, M.B., Armstrong, W. 1999. Formation of aerenchyma and the processes of plant ventilation in relation to soil flooding and submergence. *Plant Biology*, **1**(3), 274-287.

Kaku, N., Yonezawa, N., Kodama, Y., Watanabe, K. 2008. Plant/microbe cooperation for electricity generation in a rice paddy field. *Applied Microbiology and Biotechnology*, **79**(1), 43-49.

Logan, B.E., Hamelers, B., Rozendal, R., Schröder, U., Keller, J., Freguia, S., Aelterman, P., Verstraete, W., Rabaey, K. 2006. Microbial fuel cells: Methodology and technology. *Environmental Science and Technology*, **40**(17), 5181-5192.

Qu, D., Shi, H. 1998. Studies of activated carbons used in double-layer capacitors. *Journal of Power Sources*, **74**(1), 99-107.

Rozendal, R.A. 2007. Hydrogen production through biocatalyzed electrolysis, *Dissertation* Wageningen.

Sleutels, T.H.J.A., Hamelers, H.V.M., Rozendal, R.A., Buisman, C.J.N. 2009. Ion transport resistance in Microbial Electrolysis Cells with anion and cation exchange membranes. *International Journal of Hydrogen Energy*, **34**(9), 3612-3620.

Strik, D.P.B.T.B., Hamelers, H.V.M., Snel, J.F.H., Buisman, C.J.N. 2008. Green electricity production with living plants and bacteria in a fuel cell. *International Journal of Energy Research*, **32**(9), 870-876.

Strik, D.P.B.T.B., Timmers, R.A., Helder, M., Steinbusch, K.J.J., Hamelers, H.V.M., Buisman, C.J.N. 2011. Microbial solar cells: Applying photosynthetic and electrochemically active organisms. *Trends in Biotechnology*, **29**(1), 41-49.

Ter Heijne, A., Hamelers, H.V.M., De Wilde, V., Rozendal, R.A., Buisman, C.J.N. 2006. A bipolar membrane combined with ferric iron reduction as an efficient cathode system in microbial fuel cells. *Environmental Science and Technology*, **40**(17), 5200-5205.

Timmers, R.A., Rothballer, M., Strik, D.P.B.T.B., Engel, M., Schulz, S., Schloter, M., Hartmann, A., Hamelers, B., Buisman, C. 2011. Microbial community structure elucidates performance of Glyceria maxima plant microbial fuel cell. *Applied Microbiology and Biotechnology*.

Timmers, R.A., Strik, D.P.B.T.B., Arampatzoglou, C., Buisman, C.J.N., Hamelers, H.V.M. Rhizosphere anode model explains high oxygen levels during operation of a Glyceria maxima PMFC. *Bioresource Technology*(0).

Timmers, R.A., Strik, D.P.B.T.B., Hamelers, H.V.M., Buisman, C.J.N. 2010. Long-term performance of a plant microbial fuel cell with Spartina anglica. *Applied Microbiology and Biotechnology*, **86**(3), 973-981.

Torres, C.I., Marcus, A.K., Rittmann, B.E. 2008. Proton transport inside the biofilm limits electrical current generation by anode-respiring bacteria. *Biotechnology and Bioengineering*, **100**(5), 872-881.

Appendix 4.1: Anode potentials at 0.02, 0.055, 0.09, and 0.125 m from the cation exchange membrane during polarization when the controlled potential was maintained for 60 minutes (a), and when the potential was applied for 5 minutes (b)

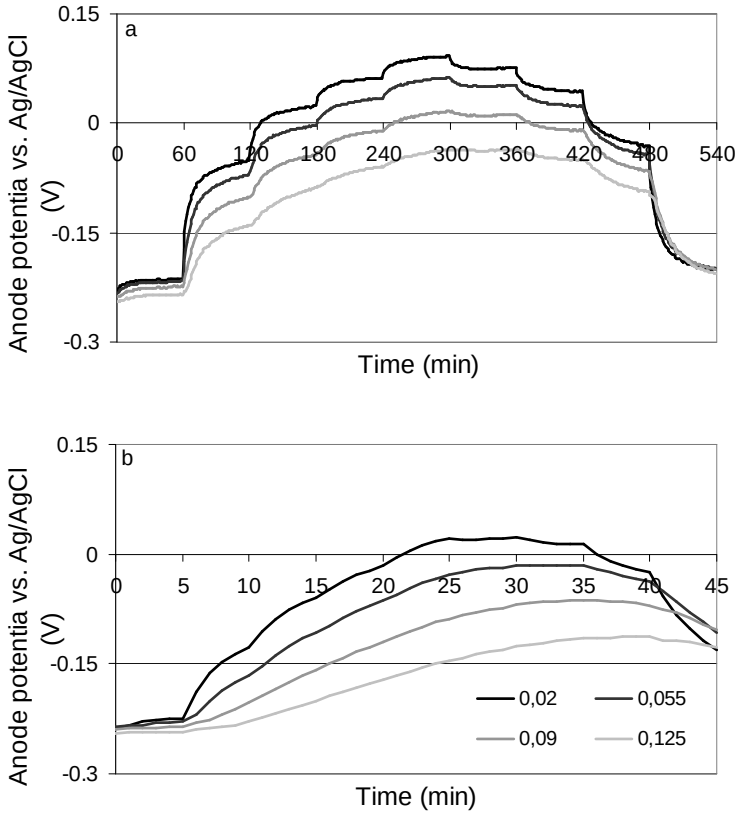

Figure A.4.1: *Anode potentials at 0.02, 0.055, 0.09, and 0.125 m from the cation exchange membrane during polarization*

Appendix 4.2: Current density during polarization when the controlled potential was maintained for 60 minutes (a), and when the potential was applied for 5 minutes (b)

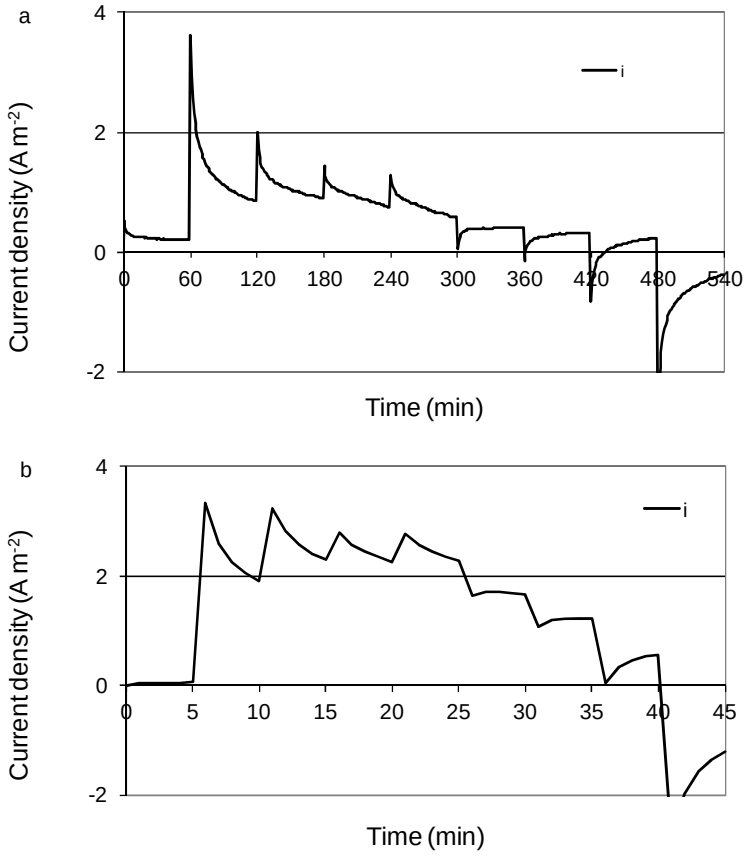

Figure A.4.2: *Current density during polarization when the controlled potential was maintained for 60 minutes (a), and when the potential was applied for 5 minutes (b)*

Part 2: Improvement of the Plant Microbial Fuel Cell design

5 Increase of power output by change of ion transport direction in a (Plant) Microbial Fuel Cell

Abstract

The Plant Microbial Fuel Cell (PMFC) is a technology for the production of renewable and clean bio-energy based on photosynthesis. To increase the power output of the PMFC the internal resistance must be reduced. The objective of the present study was to reduce the membrane resistance by changing the transport direction of cations in the direction of the established concentration gradient. To demonstrate the effect of changing the transport direction a MFC and PMFC were designed with one anode and two cathode compartments. This design allowed changing the direction of transport of cations by switching the cathode compartment that functions as cathode. The change between cathode 1 and cathode 2 enhanced the power output of the PMFC by 398 %.

The increase in power output was due to the reduction of internal from 4.3 $\Omega\ m^2$ to 1.2 $\Omega\ m^2$ in the PMFC after the change between cathode 1 and cathode 2.

Repeated changes of between cathode 1 and cathode 2 resulted in an increase of power generated with cathode 1 and a decrease of the power generated with cathode 2. However the average power output remained constant 0.036 ± 0.0005 W $m^{-2}_{membrane}$, this was 246 % higher than the initial power output with cathode 1.

Keywords: Plant Microbial Fuel Cell, Rhizodeposition, Mass transfer resistance, membrane resistance, *Glyceria maxima.*

5 Increase of power output by change of ion transport direction in a (Plant) Microbial Fuel Cell

5.1 Introduction

The increase in energy demand of the world population in combination with depletion of fossil fuels has risen the need for renewable energy sources. Growing plants for bio-energy is potentially a renewable energy source since plant production is based on photosynthesis. The Plant Microbial Fuel Cell (PMFC) is a technology for the production of renewable and clean bio-energy based on photosynthesis (Strik et al., 2008). The PMFC is a clean bio-energy source because electrical power is generated by electrochemically active bacteria, which prevents the use of toxic catalysts and mediators. Furthermore in closed PMFC systems nutrients are recycled which enables long term power generation without depletion of nutrients. PMFC do emit carbon dioxide, however, the emitted carbon does not increase greenhouse gas emission because this carbon dioxide is part of the short carbon cycle. Additionally, the PMFC technology can be integrated with food production and therefore does not compete with food production (De Schamphelaire et al., 2008; Kaku et al., 2008). Furthermore the PMFC can be applied at locations unsuitable for food production such as green roofs (Strik et al., 2011). This prevents deforestation with the aim to produce arable land, which is the second most important source of greenhouse gas emissions in the world (von Witzke, 2008).

The PMFC technology is based on two well-known principles, loss of organic compounds by plant roots (rhizodeposition) and electricity generation by electrochemically active bacteria in a microbial fuel cell (MFC). In the PMFC, the plant roots are integrated in the anode compartment of a MFC. Plant roots provide the electrochemically active bacteria with substrate via rhizodeposition. The electrochemically active bacteria present in the anode compartment of the PMFC, convert the substrate into carbon dioxide, protons and donate the electrons to the graphite electrode located in the anode (De Schamphelaire et al., 2010). Subsequently, the electrons flow through an electrical circuit and power harvester to the cathode compartment where they are consumed.

Based on reported high values for photosynthesis, rhizodeposition, and energy recovery in a microbial fuel cell, the theoretical maximum electrical power production of a PMFC is 3.2 W m^{-2} which is 28,000 kWh ha^{-1} $year^{-1}$

(Strik et al., 2011). Until now, the maximum experimental electrical power output reported is 0.22 W m^{-2} (Helder et al., 2010). The relative low electrical power output compared to the theoretical maximum is likely the result of substrate limitation for the electrochemically active bacteria, in combination with a high internal resistance which is mainly due to a high internal resistance (Timmers et al., 2010) (Strik et al., 2011) (Kaku et al., 2008). Therefore, to increase the electrical power output the internal resistance must be decreased.

In PMFCs, the internal resistance is a combination of anode resistance and membrane resistance in case the cathode is limiting (Timmers et al., 2010) (Timmers submitted). The anode resistance is the result of mass transfer limitations in the electrochemically active biofilm and the adjacent stagnant boundary layer. The membrane resistance is, also, the result of mass transfer resistance through the membrane and the adjacent stagnant boundary layer. Therefore to decrease the internal resistance mass transfer should be improved. One option to improve mass transfer is to increase the flow rate in the anode (Sleutels et al., 2011). Improved mass transfer in the electrochemically active biofilm and the adjacent stagnant boundary layer reduces the anode resistance (Ter Heijne et al., 2011b). Furthermore, improved mass transfer between anode and cathode reduces the membrane resistance (Sleutels et al., 2009b). Another option to enhance proton transfer in the electrochemically active biofilm as well as from the anode to the cathode is to increase the buffer concentration in the bulk anolyte (Jeremiasse et al., 2009).

In the PMFC the anode compartment is a sediment-like structure (De Schamphelaire et al., 2008; Kaku et al., 2008; Strik et al., 2008). Therefore it is unlikely that increasing the flow rate in the anode will be an energy efficient option. Whereas increasing flow rates in sediments requires an energy input, which will diminish power generation by the PMFC. Increase of the buffer in the anode of the PMFC requires addition of large amounts of buffer. The addition of large amount of buffer is not sustainable (Rozendal et al., 2008), furthermore it negatively affects plant growth and thus electrical power output (Helder et al).

The membrane resistance of the PMFC is due to the accumulation of cations in the cathode of the PMFC (Timmers et al., 2010). This accumulation of cations results in a driving force for diffusion opposite the required transport direction (Harnisch et al., 2009) (Sleutels et al., 2009a). During current generation, this driving force increases during current generation due to the continuous accumulation. As a consequence, the potential gradient needed to overcome diffusion continuously increases which results in a continuous increase of the membrane resistance.

The objective of the present study was to reduce the membrane resistance by changing the transport direction of cations in the direction of the established concentration gradient. To demonstrate the effect of changing the transport direction a MFC and PMFC were designed with one anode and two cathode compartments (Figure 5.1). This design allowed changing the direction of transport of cations by switching the cathode compartment that functions as cathode.

5.2 Material and Methods

5.2.1 Bicathode setup

The setup consisted of a polyvinyl chloride reduced T-piece (Figure 5.1) in which two cation exchange membranes (fumasep®, FKB, diameter 0.07 m) were fixed to separate the anode from the cathode compartments. The total volume of the anode compartment was 0.95 L. Figure 5.1 shows a schematic representation of the setup. The anode compartment was filled with 750 g of graphite granules with a diameter between 1 and 2 mm (le Carbone, Wemmel Belgium) to function as an electrode. The current collector was a 40 mm golden wire glued to a teflon-coated copper wire. To measure the anode potential, Haber-Luggin capillaries were placed in the anode at a distance of 0.025 m, 0.05 m, and 0.075 m from the cation exchange membrane. To measure the anode potential, the capillaries were connected via a 3 M potassium chloride solution to an Ag/AgCl reference electrode (+205 mV versus NHE; Prosense Qis, Oosterhout, the Netherlands).

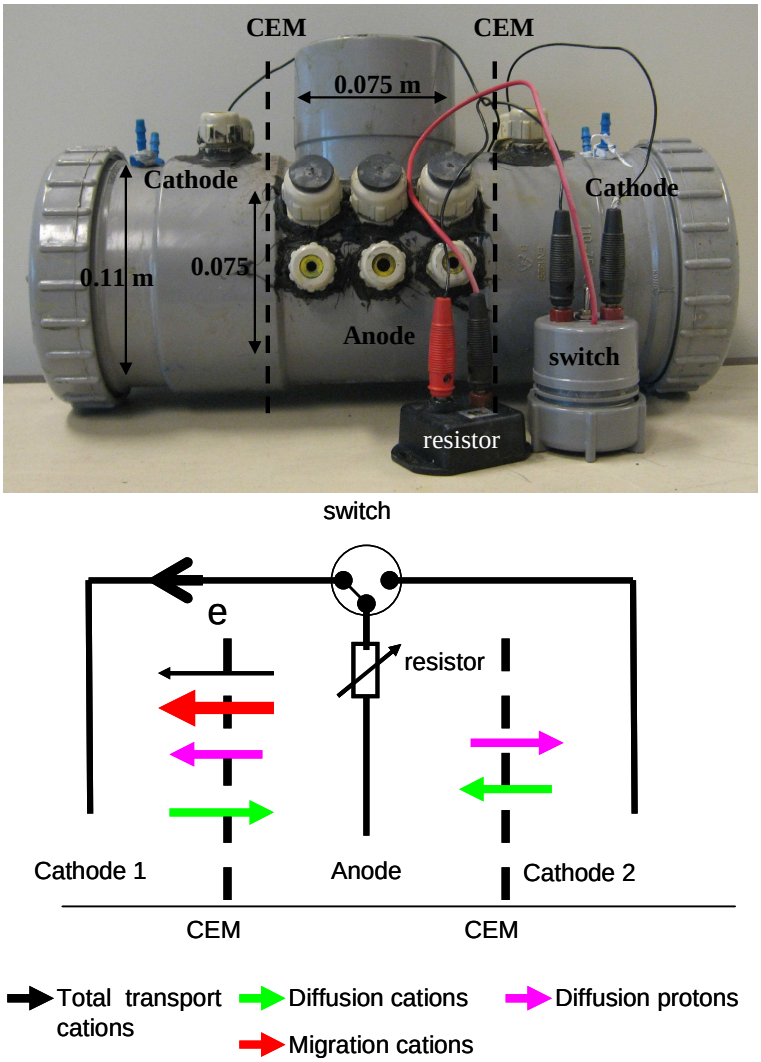

Figure 5.1: *Picture and schematic representation of the bicathode setup and the transport processes during current generation with cathode 1.*

The cathode compartment consisted of two polyvinyl chloride end-pieces (diameter 110 mm) with a screw cap fixed in the T-piece. The volume of a single cathode compartment was 0.95 L. The cathode electrode consisted of 2.8 mm thick graphite felt (Grade WDF, National Specialty Products Carbon and Graphite Felt, Taiwan). The catholyte was 0.05 M ferric cyanide ($K_3[Fe(CN)]_6$) solution buffered with 0.01 M potassium phosphate buffer (pH 6.8). The current collector used was similar to the ones used in the anode. To measure the cathode potential, one Haber-Luggin capillary was placed in

both cathode compartments at a distance of 0.02 m from the cation exchange membrane. The capillary was connected via a 3 M potassium chloride solution to an Ag/AgCl reference electrode (+205 mV versus NHE; Prosense Qis, Oosterhout, the Netherlands). The current collectors of the cathode compartments were connected to a single pole double through switch (Figure 5.1). To close the electrical circuit the com signal of the single pole through switch was connected to the anode current collector over an external resistance of 500 Ω or 50 Ω.

5.2.2 Operation

5.2.2.1 MFC

The bicathode MFC setup was fed with the adapted ½ Hoagland solution as described by Helder et al. (2011) to which 0.02 M acetate was added (pH 6.8, conductivity between 3.5 through 3.7 mS m^{-1}). The MFC setup was inoculated with 5 mL of an acetate operated MFC (Ter Heijne et al., 2011a). The MFC setups were placed in a climate control cabinet (Microclima 1750 Snijders, Tilburg the Netherlands) an illumination period of 14 h d^{-1}, an average light density in the photo active region of 596 ± 161 µmole m^{-2} s^{-1}, a temperature of 25 ^{o}C, and a humidity of 75%.

5.2.2.2 PMFC

Before the plant *Glyceria maxima* was planted in the PMFC, the setup was operated as a MFC fed with 0.02 mole L^{-1} acetate to ensure the presence of electrochemically active bacteria. Before graphite granules and electrochemically active biofilm were used for the PMFC, they were mixed and rinsed with tap water to remove any residual substrate. In the PMFC, several stems of *G. maxima* (D'n Bart Waterplanten, the Netherlands) with a total mass of 83 g were planted. The medium used to feed the PMFC was the same adapted ½ Hoagland (pH 6.8, conductivity between 1.5 through 1.7 mS m^{-1}) without the acetate. The medium was fed from the top with a flow rate of 0.17 mL s^{-1}. The feeding frequency of the PMFC with the adapted ½ Hoagland medium was 5 minutes every 6 hours.

The PMFC setups were placed in a climate control cabinet (Microclima 1750 Snijders, Tilburg the Netherlands) an illumination period of 14 h d^{-1}, an

average light density in the photo active region of 596 ± 161 µmole m^{-2} s^{-1}, a temperature of 25 ^{o}C, and a humidity of 75%.

5.2.2.3 Change of transport direction

To change the direction of cation transport within the anode, the single pole double through switch was either connected to cathode 1 or cathode 2 (Figure 5.1). The MFC and PMFC were started up with cathode 1. To see the effect of the change in transport direction the MFC and PMFC were switched to cathode 2 for approximately 200 seconds. To see the effect of repeated changes of transport on the power output of the PMFC, the PMFC was changed back to cathode 1. The change between cathode was repeated 3 times, at which each cathode was functioning for approximately 200 seconds as cathode.

5.2.3 Measurements

Cell potential, anode potential, cathode potential and temperature were measured online with a data acquisition instrument (Fieldpoint module FP-AI-112) connected to a personal computer with Labview software via the Fieldpoint Ethernet Controller Module FP-2000 (National Instruments, Austin, Texas, USA). As mentioned previously, anode potentials were measured at 0.025 m, 0.05 m, and 0.075 m from the cation exchange while the cathode potential was measured at 0.02 m from the cation exchange membrane.

5.2.4 Calculations

5.2.4.1 Power density

The current density was calculated via Ohm´s Law and divided by the membrane area of one membrane (0.038 m^2).

$$i = \frac{E_{cell}}{R_{ext}} \qquad 1$$

In the above equation i is the current density (A m^2_{mem}), E_{cell} is the cell potential (V), and R_{ext} is the external resistance (Ω).

Subsequently the current density was used to calculate the power density via Joule´s Law

$$P = E_{cell} i \qquad 2$$

In the above equation P is the power density (W m^{-2}).

5.2.4.2 Profile gradients

Gradients of anode, pH and conductivity profile were defined as the slope of the linear trend line fitted to the profile. The anode potential gradient $\frac{dE_{an}}{dx}$ was expressed in V m^{-1}, the pH gradient was expressed as $\frac{dpH_{an}}{dx}$ in pH m^{-1}, and the conductivity gradient was expressed as $\frac{d\sigma_{an}}{dx}$ in S m^{-2}.

5.2.4.3 Internal resistance

In microbial fuel cells, the cell potential is a linear function of the maximum theoretical cell potential approximated by the open cell potential, the current density and, the internal resistance (Logan et al., 2006).

$$E_{cell} = E_{OCP} - iR_{\text{int}} \qquad 3$$

Thus the internal resistance can be calculated with:

$$R_{\text{int}} = \frac{E_{OCP} - E_{cell}}{i} \qquad 4$$

In the above equation R_{int} is the internal resistance in Ω m^2, E_{OCP} is the open cell potential in V, E_{cell} is the measured cell potential in V, and i is the current density in A m^{-2}.

The internal resistance consists of resistances due to the cathode overpotential, anode overpotential, and current dependent potential losses. Those losses include ionic and transport losses (Logan et al., 2006) which are measured as membrane potential (Harnisch et al., 2009).

$$E_{cell} = E_{OCP} - \eta_{cath} - \eta_{an} - i(R_M) \quad 5$$

In the above equation, E_{cell} is the measured cell potential (V), η_{cath} is the cathode overpotential (V), η_{an} is the anode overpotential (V), and R_M is membrane resistance (Ω m^2).

The cathode overpotential is defined as the cathode potential at open cell potential subtracted from the measured cathode potential while the anode overpotential is the measured anode potential subtracted from the anode potential at open cell potential (Sleutels et al., 2009a).

$$\eta_{cath} = E_{OCP,cath} - E_{cath} \quad 6$$

$$\eta_{an} = E_{an} - E_{OCP,an} \quad 7$$

In the above equations, E_{cath} is the measured cathode potential (V), $E_{OCP,cath}$ is the cathode potential at open cell potential (V), $E_{OCP,an}$ is the anode potential at open cell potential (V), and E_{an} is the measured anode potential (V).

The membrane potential loss is defined as the difference between reference electrodes in the anode and the reference electrode in the cathode (Ter Heijne et al., 2006). More specifically, membrane potential loss was calculated according to Sleutels (2009):

$$E_M = E_{cath} - E_{an} - E_{cell} \quad 8$$

where E_M is the membrane potential loss (V), E_{cath} is the measured cathode potential (V), E_{an} is the measured anode potential (V), and E_{cell} is the measured cell potential (V). In this setup, the anode potential was measured at 0.025 m, 0.05 m, and 0.075 from the cation exchange membranes. Consequently, there were 3 different anode overpotential losses and membrane potential losses. The average anode overpotential and membrane potential loss was defined as the average over the sample points. The average anode overpotential and average membrane potential before and after the change between cathode 1 and cathode 2 were the

average of 200 s before and 200 s after the change. The partial internal resistances were calculated by Ohm's law, i.e. by dividing the partial potential losses by the current density.

5.3 Results and discussion

5.3.1 Change of cathode increased power output of MFC and PMFC

The MFC and PMFC were start up with cathode 1, after the change from cathode 1 to cathode 2 (t = 0), the cell potential of the MFC and the PMFC setup increased immediately (Figure 5.2 a and b). Both setups exhibited a peak in cell potential immediately after the change from cathode 1 to cathode 2. Next, the cell potential output decreased steadily along with time.

The increase in cell potential resulted in an increase of power output of 167 % for the MFC and 398 % for the PMFC. More specifically, before the change from cathode 1 to cathode 2 (-200 > t > 0) the average power output was 0.31 W m^2_{mem} for the MFC, and 0.015 W m^2_{mem} for the PMFC. After the change from cathode 1 to cathode 2 (0 < t < 200) the average power output increased to 0.51 W m^2_{mem} for the MFC, and 0.058 W m^2_{mem} for the PMFC. The increase in power output was the result of the decrease of internal resistance. The internal resistance in the MFC decreased from 0.37 Ω m^2 to 0.25 Ω m^2 while the internal resistance in the PMFC decreased from 4.3 Ω m^2 to 1.2 Ω m^2. The observed internal resistance of the PMFC was in the range of the internal resistances reported in literature (Strik et al., 2011).

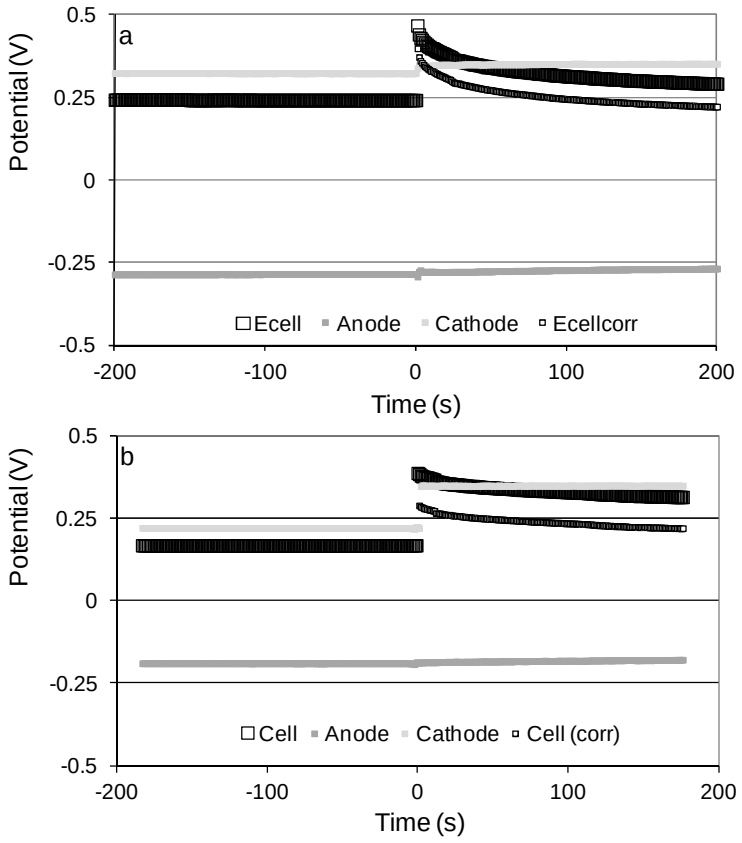

Figure 5.2: *Increase in cell potential, and cathode potential of the MFC (a) and PMFC (c) after change between cathode 1 and 2 (t > 0). The anode potential slightly increased after the change between cathode 1 and 2.*

Besides the cell potential Figure 5.2 shows the cathode potential, and the average anode potential. The cathode potential increased immediately after the change from cathode 1 to cathode 2 (t=0), the cathode potential increased. The cathode potential is determined by the ratio between the ferrocyanide and ferricynide in the catholyte (oxidized and reduced compound). Before the change no current is generated with cathode 2 which resulted in a higher ratio between the ferrocyanide and ferricynide and therefore higher cathode potential than in cathode 1. With cathode 1 current was already generated and thus the ratio between the ferrocyanide and ferricynide was lower and therefore the cathode potential was lower.

Part of the increase in cell potential (and hence power output) could be attributed to the difference in cathode potential. To see whether or not the increase of the cathode potential was the sole cause of the increase in cell potential, the cell potential after the change from cathode 1 to cathode 2 was subtracted with the increase in cathode potential (Figure 5.2). In this manner, the corrected power output was calculated with the corrected cell potential using Joules law. The corrected average power output increased by 130 % for the MFC at 50 Ω and 286 % for the PMFC. More specifically, the average corrected power output ($0 < t < 200$) was 0.4 W m^2_{mem} for the MFC, and 0.042 W m^2_{mem} for the PMFC.

The average anode potential slowly increased in both setups after the change from cathode 1 to cathode 2. The increase in average anode potential indicated that current generation in the electrochemically active biofilm increased (Hamelers et al., 2011). Due to the increase in current generation more protons and bicarbonate are produced in the electrochemically active biofilm while more substrate is consumed (Harnisch & Schröder, 2009). The increase in current generation therefore resulted in an enhancement of the proton, bicarbonate, and substrate concentration gradients in the electrochemically active biofilm, which resulted in the increase in average anode potential (and thus anode overpotential) (Torres et al., 2008).

5.3.2 Decrease of membrane resistance after change of transport direction

Internal resistance of microbial fuel cells consists of membrane resistance, anode resistance, and cathode resistance (Sleutels et al., 2009a). The change in transport direction in the (P)MFC resulted in a decrease of the internal resistance. The decrease of internal resistance was due to a decrease of membrane resistance and anode resistance, whereas the change in cathode resistance was negligible (Figure 5.3). Figure 5.3 shows the membrane resistance before and after the change from cathode 1 to cathode 2. The average membrane resistance decreased from 0.3 Ω m^2 to 0.2 Ω m^2 in the MFC and from 2.8 Ω m^2 to 1.1 Ω m^2 in the PMFC. The decrease in membrane resistance could likely be attributed to the reduced accumulation in cathode 2 compared to cathode 1. In the MFC the

conductivity in cathode 1 was 13.0 mS m^{-1}, and was 12.6 mS m^{-1} in cathode 2. In the PMFC the conductivity in cathode 1 was 13.8 mS m^{-1} and was 11.2 mS m^{-1} in cathode 2. In both setups the conductivity in cathode 2 was lower than in cathode 1 which indicated that cations indeed accumulated in cathode 1 during current generation with this cathode. Due to the lower conductivity in cathode 2 it was likely that the concentration gradient between cathode 2 and the anode was less steep than the concentration gradient between the cathode 1 and the anode. Consequently the potential gradient required to overcome the concentration gradient to drive cation transport to the cathode was smaller, and thus the membrane resistance decreased.

The decrease of membrane resistance was affected by the difference in accumulation of cations, however the conductivity gradient could also have contributed to the decrease in membrane resistance. Before the change in transport direction, the conductivity gradient was -4.5 S m^{-1} in the PMFC and -1.5 S m^{-1} in the MFC. The presence of a negative conductivity gradient indicated the presence of a concentration gradient in the anode opposite to the required direction of transport. After the change to cathode 2 the required transport direction changed into the direction of the concentration gradient which likely resulted in less resistance to cation transport in the anode.

The lower membrane resistance in the MFC compared to the PMFC could be attributed to the higher conductivity of the anolyte of the MFC, 5.3 mS m^{-1} versus 1.4 mS m^{-1} in the PMFC. The higher anolyte conductivity of the MFC resulted in smaller difference in conductivity between the anode and the cathode in the MFC compared to the PMFC. The smaller conductivity difference likely represented a smaller concentration gradient between the anode and the cathode and therefore the MFC required a smaller potential gradient to drive cation to the cathode and thus a smaller membrane resistance.

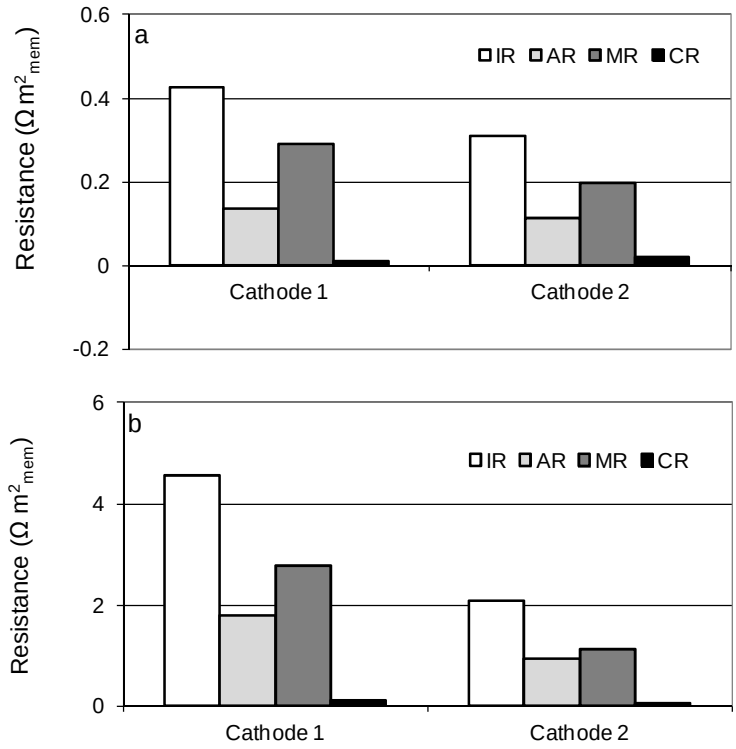

Figure 5.3: *Decrease of internal resistance after the change from cathode 1 to cathode 2.*

a) Average membrane resistance (MR), Average anode resistance (AR), Average cathode resistance (CR) and Average internal resistance (IR) before and after the change from cathode 1 to cathode 2 of the microbial fuel cell operated at an external resistance of 50 Ω. b) Membrane resistance (MR), Anode resistance (AR), Cathode resistance (CR) and Internal resistance (IR) before and after the change from cathode 1 to cathode 2 of the plant microbial fuel cell operated at an external resistance of 500 Ω. The average anode resistance and membrane resistance was defined as the average over the sample points of which the average was taken of 200 s before and 200 s after the change between cathode 1 and cathode 2.

5.3.3 Decrease of anode resistance after change of transport direction

Unexpectedly, the anode resistance also decreased after the change from cathode 1 to cathode 2. Figure 5.3 shows the anode resistance before and after the direction of cation transport was changed. The average anode resistance decreased from 0.13 Ω m^2 to 0.11 Ω m^2 in the MFC and from 2.94 Ω m^2 to 1.52 Ω m^2 in the PMFC. The anode resistance in the PMFC as well as

the MFC is attributed to resistance to proton transfer in the electrochemically active biofilm (Torres et al., 2008). The decrease of the anode resistance indicated that proton transfer in the electrochemically active biofilm was enhanced after the change of transport direction. It is not clear how the change in transport direction in the PMFC enhanced mass transport out of the electrochemically active biofilm. However it can be hypothesized that this was due to differences in current generation by the electrochemically active biofilm throughout the anode. During current generation with cathode 2 the electrochemically active biofilm in anode part in the vicinity of cathode 2 (i.e. around the sample point at 0.075 m) generated more current than the electrochemically active biofilm close to cathode 1 (i.e. around the sample point at 0.025 m). The differences in current generation by the electrochemically was supported by the difference in anode overpotential. The anode overpotential close to cathode 2 (0.075 m) increased while the overpotential close to cathode 1 (0.025 m) decreased (see Appendix 5.1). The pH gradient indicated that the anode at 0.075 m was less acidic than at 0.025 m. Due to the less acidic condition in this part of the anode there was less resistance to transport of protons out of the electrochemically active biofilm and thus the anode overpotential was lower. The anode resistance of the PMFC decreased more than the anode resistance than the anode resistance of the MFC. This was consistent with the pH gradient, the pH gradient of the MFC was smaller than the pH gradient in the PMFC i.e., 3.2 pH m^{-1} for the MFC versus 30.2 pH m^{-1} for the PMFC.

Again, like the membrane resistance, the anode resistance of the MFC was much lower than the anode resistance of the PMFC. The difference in anode resistance was probably due to difference in pH between the anode of the MFC (7.4 ± 0.1) and the PMFC (5.6 ± 0.8). Due to the lower anode pH of the PMFC, the resistance to proton transport out of the electrochemically active biofilm will be higher and therefore the anode resistance will be higher. However it is beyond the scope of this research to fully elaborate the origin of the decrease in anode resistance.

5.3.4 Repeated changes between cathode 1 and cathode 2 resulted in convergence power output of PMFC

The second cathode generated more power than the first cathode, however, both cathode 1 and cathode 2 produced a power density that was in the range of the average power densities reported in literature (De Schamphelaire et al., 2008; Kaku et al., 2008; Strik et al., 2008; Strik et al., 2011; Timmers et al., 2010). To see the effect of repeated changes between cathode 1 and 2 on the power output of the PMFC the cathode was changed three times for 200 seconds. These repeated changes between cathode 1 and cathode 2 resulted in an increased power output generated with cathode 1, in contrast the power output generated with cathode 2 which decreased i.e., the power output with cathode 1 and cathode 2 converged (Figure 5.4). However the average power output remained constant 0.036 ± 0.0005 W $m^{-2}_{membrane}$, this was 246 % higher than the initial power output of cathode 1.

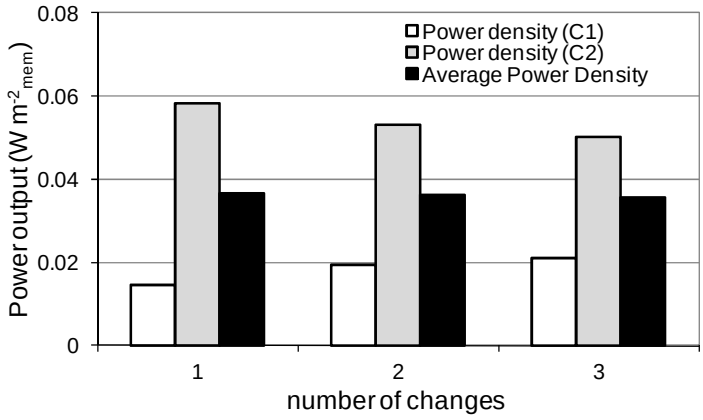

Figure 5.4: *Convergence of power density during repeated changes between cathode 1 and cathode 2. The initial situation is cathode 1 at the first change. The achieved power density with cathode 1 increased while the achieved power density with cathode 2 decreased. The average achieved power density remained constant (0.036 ± 0.0005 W* m^{-2}_{mem}*).*

This convergence was also observed for the internal resistance, membrane resistance, and anode resistance. The internal (IR), membrane (MR), and anode resistance (AR) during current generation with cathode 1 decreased while they decreased during current generation with cathode 2 increased

(Figure 5.5). Figure 5.5 shows that the contribution of the cathode resistance (CR) to the internal resistance was negligible.

The convergence of the membrane resistance was likely explained by reduction of accumulation of cations in cathode 1 in combination with an enhancement of accumulation of cations in cathode 1. The membrane resistance during current generation with cathode 1 decreased (Figure 5.5). This finding indicated a reduction of accumulation of cations in cathode 1 and thus that more cation were transported out of the cathode, when no current was generated, than were accumulated during current generation. The opposite hold for the increase in membrane resistance during current generation with cathode 2 decreased (Figure 5.5). This finding indicated an increase of accumulation of cations in cathode 2 and thus that more cation were transported into the cathode during current generation than were transported out of cathode 2 during the period when no current was generated.

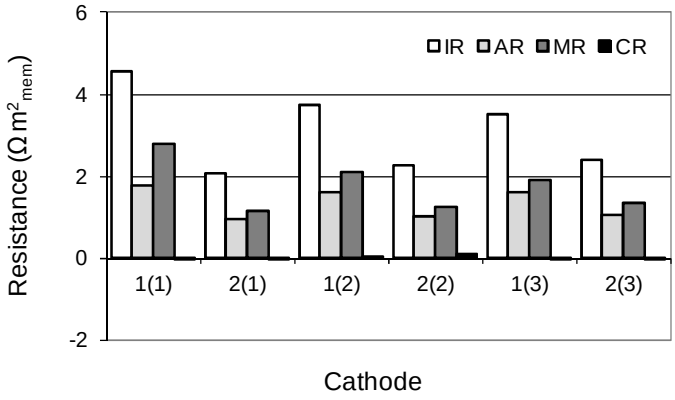

Figure 5.5: *Convergence of internal resistance during repeated changes between cathode 1 and cathode 1. And the average membrane resistance (MR), Average anode resistance (AR), Average cathode resistance (CR) and Average internal resistance (IR) of a plant microbial fuel cell during repeated changes between cathode 1 and 2.*

The convergence of the anode resistance was likely explained by reduction of resistance to proton transport out of the electrochemically active biofilm during current generation with cathode 1, and subsequently an increase of the resistance to proton transport out of the electrochemically active biofilm during current generation with cathode 2. Based on the hypothesis posed in paragraph 3.3 that the initial reduction of anode resistance was

due to an enhancement of current generation of the electrochemically where the anolyte was less acidic i.e. at 0.075 m. This convergence in anode resistance could be explained by a reduction of the pH gradient, because of a higher acidification rate of the less acidic part of the anode in combination with a lower acidification rate or even alkanization of the more acidic part of the anode (0.025 m). The likely acidification of the less acidic part of the anode resulted in an increase of the resistance to proton transport out of the electrochemically active biofilm and thus an increase in anode resistance. The lower acidification rate or even alkanization of the more acidic part of the anode (0.025 m) resulted in a decrease of the resistance to proton transport out of the electrochemically active biofilm and thus a decrease in anode resistance.

5.4 Conclusions

The change between cathode 1 and cathode 2 enhanced the power output of the MFC by 167 % and enhanced the power output of the PMFC by 398 %.

Part of the increase in power output was contributed to the increase in cathode potential after the change between cathode 1 and cathode 2. However after the correction for the increase of cathode potential the power output still enhanced with 130 % and 286 % for the MFC and PMFC respectively.

The increase in power output was due to the reduction of internal resistance from 0.37 Ω m^2 to 0.25 Ω m^2 in the MFC and from 4.3 Ω m^2 to 1.2 Ω m^2 in the PMFC after the change between cathode 1 and cathode 2.

The membrane resistance decreased after the change to cathode 2, likely due to reduction of accumulation of cations in the cathode compartments, likely because cation diffuse back to the anode when the cathode was not used for power generation.

The anode resistance decreased after the change to cathode 2. The effect of the change from cathode 1 to cathode 2 on the anode resistance is not fully understood and should be investigated in the future.

Repeated changes of between cathode 1 and cathode 2 resulted in an increase in the power generated with cathode 1 and a decrease of the power generated with cathode 2. However the average power output remained constant 0.036 ± 0.0005 W $m^{-2}_{membrane}$, this was 246 % higher than the initial power output of cathode 1.

Acknowledgements

This research was funded by Senternovem, the Dutch governmental agency for sustainability and innovation in the Ministry of Finance (grant no. EOSLT06020), and supported by Nuon. The authors would like to thank Marjolein Helder, Kirsten Steinbusch, and Wouter Bac for their useful comments.

References

De Schamphelaire, L., Cabezas, A., Marzorati, M., Friedrich, M.W., Boon, N., Verstraete, W. 2010. Microbial community analysis of anodes from sediment microbial fuel cells powered by rhizodeposits of living rice plants. *Applied and Environmental Microbiology*, **76**(6), 2002-2008.

De Schamphelaire, L., Van Den Bossche, L., Hai, S.D., Höfte, M., Boon, N., Rabaey, K., Verstraete, W. 2008. Microbial fuel cells generating electricity from rhizodeposits of rice plants. *Environmental Science and Technology*, **42**(8), 3053-3058.

Hamelers, H.V.M., ter Heijne, A., Stein, N., Rozendal, R.A., Buisman, C.J.N. 2011. Butler-Volmer-Monod model for describing bio-anode polarization curves. *Bioresource Technology*, **102**(1), 381-387.

Harnisch, F., Schröder, U. 2009. Selectivity versus mobility: Separation of anode and cathode in microbial bioelectrochemical systems. *ChemSusChem*, **2**(10), 921-926.

Harnisch, F., Warmbier, R., Schneider, R., Schröder, U. 2009. Modeling the ion transfer and polarization of ion exchange membranes in bioelectrochemical systems. *Bioelectrochemistry*, **75**(2), 136-141.

Helder, M., Strik, D.P.B.T.B., Hamelers, H.V.M., Kuhn, A.J., Blok, C., Buisman, C.J.N. 2010. Concurrent bio-electricity and biomass production in three Plant-Microbial Fuel Cells using *Spartina anglica*, *Arundinella anomala* and *Arundo donax*. *Bioresource Technology*, **101**(10), 3541-3547.

Jeremiasse, A.W., Hamelers, H.V.M., Kleijn, J.M., Buisman, C.J.N. 2009. Use of biocompatible buffers to reduce the concentration overpotential for hydrogen evolution. *Environmental Science and Technology*, **43**(17), 6882-6887.

Kaku, N., Yonezawa, N., Kodama, Y., Watanabe, K. 2008. Plant/microbe cooperation for electricity generation in a rice paddy field. *Applied Microbiology and Biotechnology*, **79**(1), 43-49.

Logan, B.E., Hamelers, B., Rozendal, R., Schröder, U., Keller, J., Freguia, S., Aelterman, P., Verstraete, W., Rabaey, K. 2006. Microbial fuel cells: Methodology and technology. *Environmental Science and Technology*, **40**(17), 5181-5192.

Rozendal, R.A., Hamelers, H.V.M., Rabaey, K., Keller, J., Buisman, C.J.N. 2008. Towards practical implementation of bioelectrochemical wastewater treatment. *Trends in Biotechnology,* **26**(8), 450-459.

Sleutels, T.H.J.A., Hamelers, H.V.M., Buisman, C.J.N. 2011. Effect of mass and charge transport speed and direction in porous anodes on microbial electrolysis cell performance. *Bioresource Technology,* **102**(1), 399-403.

Sleutels, T.H.J.A., Hamelers, H.V.M., Rozendal, R.A., Buisman, C.J.N. 2009a. Ion transport resistance in Microbial Electrolysis Cells with anion and cation exchange membranes. *International Journal of Hydrogen Energy,* **34**(9), 3612-3620.

Sleutels, T.H.J.A., Lodder, R., Hamelers, H.V.M., Buisman, C.J.N. 2009b. Improved performance of porous bio-anodes in microbial electrolysis cells by enhancing mass and charge transport. *International Journal of Hydrogen Energy*, **34**(24), 9655-9661.

Strik, D.P.B.T.B., Hamelers, H.V.M., Snel, J.F.H., Buisman, C.J.N. 2008. Green electricity production with living plants and bacteria in a fuel cell. *International Journal of Energy Research*, **32**(9), 870-876.

Strik, D.P.B.T.B., Timmers, R.A., Helder, M., Steinbusch, K.J.J., Hamelers, H.V.M., Buisman, C.J.N. 2011. Microbial solar cells: Applying photosynthetic and electrochemically active organisms. *Trends in Biotechnology*, **29**(1), 41-49.

Ter Heijne, A., Hamelers, H.V.M., De Wilde, V., Rozendal, R.A., Buisman, C.J.N. 2006. A bipolar membrane combined with ferric iron reduction as an efficient cathode system in microbial fuel cells. *Environmental Science and Technology*, **40**(17), 5200-5205.

Ter Heijne, A., Liu, F., Van Rijnsoever, L.S., Saakes, M., Hamelers, H.V.M., Buisman, C.J.N. 2011a. Performance of a scaled-up Microbial Fuel Cell with iron reduction as the cathode reaction. *Journal of Power Sources*, **196**(18), 7572-7577.

Ter Heijne, A., Schaetzle, O., Gimenez, S., Fabregat-Santiago, F., Bisquert, J., Strik, D.P.B.T.B., Barriere, F., Buisman, C.J.N., Hamelers, H.V.M. 2011b. Identifying charge and mass transfer resistances of an oxygen reducing biocathode. *Energy & Environmental Science*. **4(**12), 5034-5043

Timmers, R.A., Strik, D.P.B.T.B., Hamelers, H.V.M., Buisman, C.J.N. 2010. Long-term performance of a plant microbial fuel cell with *Spartina anglica*. *Applied Microbiology and Biotechnology*, **86**(3), 973-981.

Torres, C.I., Marcus, A.K., Rittmann, B.E. 2008. Proton transport inside the biofilm limits electrical current generation by anode-respiring bacteria. *Biotechnology and Bioengineering*, **100**(5), 872-881.

von Witzke, H. 2008. Agriculture, world food security, bio-energy and climate change: Some inconvenient facts. *Quarterly Journal of International Agriculture*, **47**(1), 1-4.

Appendix 5.1: Anode potentials at 0.025, 0.05, and 0.075m from membrane 1 before change in transport direction (t<0) and after the change in transport direction (t>0).

a) microbial fuel cell setup (MFC).

b) plant microbial fuel cell setup (PMFC)

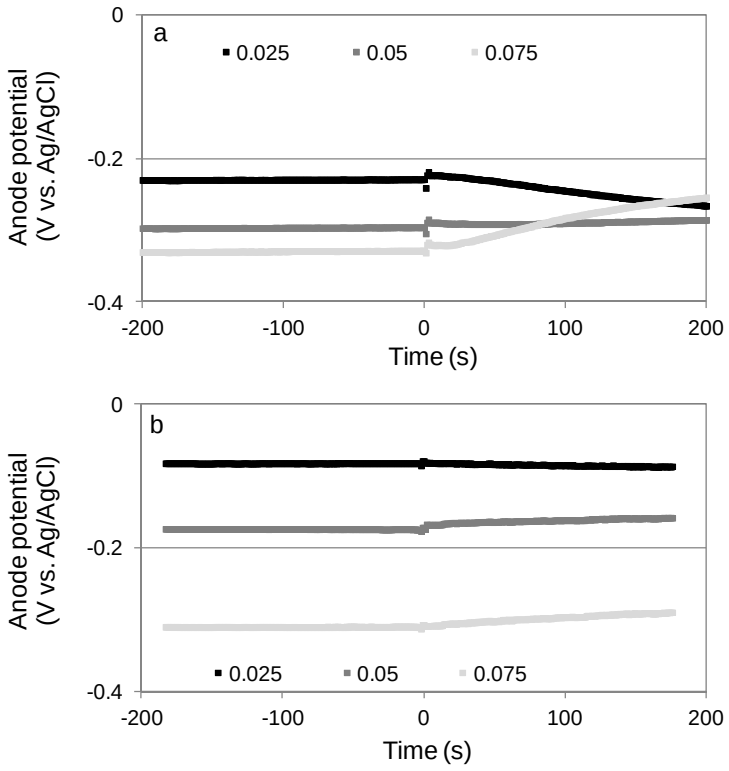

6 Electricity generation with a novel design tubular plant microbial fuel cell

Abstract

The tubular PMFC was designed to increase the feasibility of the PMFC. The average power output was 10 mW $m^{-2}_{membrane}$ and 12 mW $m^{-2}_{membrane}$, for the felt and graphite granules, respectively. Based on mass of electrode material the graphite felt exhibited a 15 times higher power output than the PMFC with the graphite granules. Based on volume the graphite felt performed even better and exhibited a 69 times higher power output. This showed reduction of anode electrode material is possible while achieving comparable power outputs per square meter of membrane. These findings make future applications of the PMFC technology more feasible. Because it showed that the amount of anode electrode material can be reduced while the power output per membrane surface remained in the same range. Furthermore it showed a PMFC design that likely can be applied into soils without the need to excavate the topsoil.

Keywords: Plant Microbial Fuel Cell, Rhizodeposition, Ultrafiltration membrane, Glyceria maxima, horizontal drilling

6 Electricity generation with a novel design tubular plant microbial fuel cell

6.1 Introduction

The Plant Microbial Fuel Cell (PMFC) is a technology for the production of renewable and clean bio-energy based on photosynthesis. The PMFC technology is based on two principles, loss of organic compounds by plant roots i.e. rhizodeposition, and electricity generation by electrochemically active bacteria in a microbial fuel cell (MFC) (De Schamphelaire et al., 2008; Kaku et al., 2008; Strik et al., 2008). In the PMFC, the plant roots are integrated in the anode compartment of a MFC. The plant roots provide the electrochemically active bacteria with substrate via rhizodeposition and via hydrolysis of dead plant material. The electrochemically active bacteria, present in the anode compartment of the PMFC, convert the low molecular weight compounds into carbon dioxide, protons and donate electrons to the graphite electrode present in the anode (De Schamphelaire et al., 2010). Subsequently, the electrons flow through an electrical circuit and power harvester to the cathode compartment where they are consumed. This process results in electrical power generation without the need to harvest the plant. The theoretical maximum electrical power generation of a PMFC, is 3.2 W m^{-2} which is 280 MWh ha^{-1} $year^{-1}$ (Strik et al., 2011).

The PMFC technology has the potential to avoid competition with food production whereas it can be integrated with agricultural food production (De Schamphelaire et al., 2008; Kaku et al., 2008). Furthermore the PMFC has the potential to be applied at locations unsuitable for food production such as wetlands and green roofs (Strik et al., 2011). Up to now there are three basic designs of PMFCs, namely the sediment type microbial fuel cell (Chen et al.; De Schamphelaire et al., 2008; Kaku et al., 2008), the plant microbial fuel cell (Strik et al., 2008; Timmers et al., 2010) and the flat-plate plant microbial fuel cell (Helder et al., 2011). One of major bottlenecks is the large amount of electrode material (Strik et al., 2011) and consequently integration of the anode electrode and cathode electrode into agricultural food production and wetlands. All these designs have the disadvantage that excavation of top soil is required to integrate the PMFC technology into agricultural food production and wetlands. Excavation of top soil has major drawbacks, such as ecosystem destruction, soil erosion, and high rates of fuel consumption (EPA, 2008). Furthermore the inability to preserve top soil without compromising its fertility will result in the destruction of valuable

agricultural soil (Ghose, 2004). Tubular shapes such as pipelines can be applied into the soil without the need to excavate the soil by horizontal drilling (McKim, 1997). Horizontal drilling reduces the negative effects of excavation such as ecosystem destruction, soil erosion, high rate of fuel consumption and loss fertility due to storage of top soil (Woodroffe & Ariaratnam, 2009).

The objective of this research was to design a PMFC in which the anode and cathode were integrated in one unit which can be applied without the need to excavate all the soil. And, furthermore to investigate if a reduction the amount of anode material is possible without the loss of power output. To achieve this, PMFC was designed with a tubular ultrafiltration membrane. The ultrafiltration membrane was chosen due to its permeability for anions as well as cations which could reduce the high transport resistance of the PMFC (Timmers et al., 2010). The anode consisted of a graphite felt covering the ultrafiltration membrane while the cathode consisted of a graphite felt placed inside the ultrafiltration membrane. Additionally, in order to test if a reduction the amount of anode material is possible without the loss of power output two different anode electrode materials were compared (graphite granules and graphite felt).

6.2 Material and Methods

6.2.1 PMFC setup

The setups consisted of a polyvinyl chloride reduced T-piece in which a polyvinyl chloride disk were fixed in both ends (110 mm) of the T-piece to create a water tight compartment (Figure 6.1). The tubular ultra-filtration membrane (Triqua, the Netherlands) had a diameter of 0.009 m and an effective length of 0.08 m (0.0023 m^2) and was fixed through the centre of both disks. Sample ports were located in both disks at 0.025, 0.035, and 0.045 m from the centre. The anode was located outside the ultra-filtration membrane while the cathode was located inside the membrane. Two setups were operated as blanks i.e. without a plant to determine if current generation was due to oxidation of organic compounds.

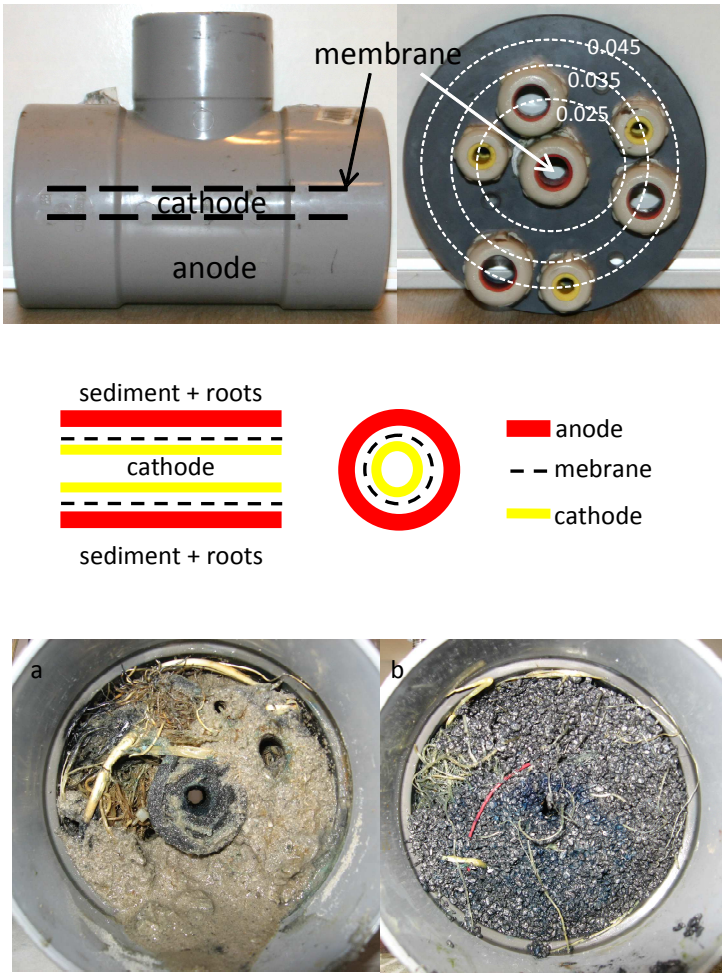

Figure 6.1: *Picture and schematic representation of the tubular plant microbial fuel cell. A) anode compartment with graphite felt, B) anode compartment with graphite granules*

Two anode electrodes were tested in the setups. One anode electrode consisted of a graphite felts of 2.8 mm thick graphite felt (Grade WDF, National Specialty Products Carbon and Graphite Felt, Taiwan) with a length of 0.19 m and a width of 0.1 m (weight 42.6 g, volume $5.3 \cdot 10^{-6}$ m^3) wrapped around the membrane. The remaining part of the anode compartment was filled with play sand (van der Meulen, 2003) (Gamma, Wageningen, the Netherlands) The other anode electrode consisted of graphite granules (weight of 750 g, volume 0.00094 m^3) with a diameter between 1 and 2 mm (le Carbone, Wemmel, Belgium). The current collector

was a 40 mm golden wire glued to a teflon-coated copper wire. To measure the anode potential, Haber-Luggin capillaries were placed in the anode at a distance of 0.025 m, 0.035 m, and 0.045 m from the centre of the membrane. To measure the anode potential, the capillaries were connected via a 3 M potassium chloride solution to an Ag/AgCl reference electrode (+205 mV versus NHE; Prosense Qis, Oosterhout, the Netherlands).

The cathode electrode consisted of 2.8 mm thick graphite felt (Grade WDF, National Specialty Products Carbon and Graphite Felt, Taiwan) with a length of 0.1 m and a width of 0.005 m placed inside the membrane. The current collector used was similar to the one used in the anode (described above). To measure the cathode potential, one Haber-Luggin capillary was placed in the tubing just after the membrane cathode used to recirculate the catholyte. A vessel containing 5 L of catholyte solution was used to recirculate the catholyte. The catholyte was 0.005 M ferric cyanide ($K_3[Fe(CN)]_6$) solution buffered with 0.01 M potassium phosphate buffer (pH 6.8). The capillary was connected via a 3 M potassium chloride solution to an Ag/AgCl reference electrode (+205 mV versus NHE; Prosense Qis, Oosterhout, the Netherlands). The current collectors of the cathode compartments were connected to the anode current collector over an external resistance of 900 Ω.

6.2.2 Operation

The PMFC setup was fed with the adapted ammonium rich ½ Hoagland solution (Taiz & Zeiger, 2006) in which nitrate was omitted and ammonium was added to replace the nitrogen in the form of nitrate. The nitrate sources KNO_3 (0.003 M) and $Ca(NO_3)\cdot 4H_2O$ (0.004 M) was replaced by NH_4HCO_3 (0.007 M). The MFC setup was inoculated with 5 mL of an acetate operated MFC (Ter Heijne et al., 2011). Before the plant Glyceria maxima was planted in the PMFC, the setup was operated as a MFC (blank) fed with 0.02 mole L^{-1} acetate to ensure the presence of electrochemically active bacteria. Before graphite granules and electrochemically active biofilm were used for the PMFC, they were mixed and rinsed with tap water to remove any residual substrate. In the PMFC, several stems of G. maxima (D'n Bart Waterplanten, Handel, the Netherlands) with a total mass of 83 g were planted. The medium used to feed the PMFC was the same adapted ½

Hoagland (pH 6.8, conductivity between 1.5 through 1.7 mS m^{-1}) without the acetate. The medium was fed from the top with a flow rate of 0.17 mL s^{-1}. The feeding frequency of the PMFC with the adapted ½ Hoagland medium was 5 minutes every 6 hours.

Both, MFC and PMFC setups were placed in a climate control cabinet (Microclima 1750 Snijders, Tilburg the Netherlands). Applied plant growth conditions were: illumination period of 14 h d^{-1}, average light density in the photo active region of 596 ± 161 µmole m^{-2} s^{-1}, temperature of 25 ^{o}C, and humidity of 75%.

6.2.3 Measurements

Cell potential, anode potential, and temperature were measured online with a data acquisition instrument (Fieldpoint module FP-AI-112) connected to a personal computer with Labview software via the Fieldpoint Ethernet Controller Module FP-2000 (National Instruments, Austin, Texas, USA). As mentioned previously, anode potentials were measured at 0.025 m, 0.035 m, and 0.045 m from the ultrafiltration membrane.

Chronoamperometry performed with an IviumStat potentiostat and IviumSoft software (IVIUM technologies B.V., Eindhoven, the Netherlands) was used to acquire polarization curves. To determine the maximum power output a polarization curve were applied at day 86 of the experiment after 20 hours of open circuit. To acquire polarization curves, cell potential was decreased stepwise from 0.5 V to 0.005 V (via 0.4 V, 0.3 V, 0.2 V, 0.1 V, and 0.05 V). Immediately after the last step (0.005 V) the cell potential was increased to 0.5 V and the procedure was repeated, i.e. the cell potential was decreased stepwise from 0.5 V to 0.005 V (via 0.4 V, 0.3 V, 0.2 V, 0.1 V, and 0.05 V). The controlled potential was applied for 5 minutes.

To investigate the long term effect of applying a certain cell potential on the power output the cell potential of the PMFCs were controlled at 0.1 V for 20 hours at day 87, after 20 hours of open circuit.

6.3 Calculations

6.3.1 Power density

The current density was calculated via Ohm´s Law and divided by the membrane area of one membrane (0.0023 m^2).

$$i = \frac{E_{cell}}{A_{mem} R_{ext}} \quad (1)$$

In the above equation i is the current density (A m^2_{mem}), E_{cell} is the cell potential (V), and R_{ext} is the external resistance (Ω).

Subsequently the current density was used to calculate the power density via Joule´s Law

$$P = E_{cell} i \quad (2)$$

In the above equation P is the power density (W m^{-2}). To be able to make a distinction between the graphite felt and the graphite granules based on the amount of anode electrode material used. The power output was calculated per kilogram of anode electrode material and volume of the reactor.

$$P_{mass} = \frac{E_{cell}^2}{R_{ext} m_{elect}} \quad (3)$$

$$P_{volume} = \frac{E_{cell}^2}{R_{ext} V_{volume}} \quad (4)$$

In the above equation P_{mass} is the power density (W kg_{elect}), m is the amount of electrode material used in (kg), P_{volume} is the volumetric power density (W $m^{-3}_{reactor}$) and $V_{reactor}$ is the volume of the reactor (m^3), that is the volume of electrode material added with the volume of the ultrafiltration membrane.

6.3.2 Internal resistance

In microbial fuel cells, the cell potential is a linear function of the maximum theoretical cell potential, current density and, internal resistance in which the maximum cell potential can be approximated by open cell potential (Logan et al., 2006).

$$E_{cell} = E_{OCP} - iR_{\text{int}} \quad 5$$

Thus the internal resistance can be calculated as:

$$R_{\text{int}} = \frac{E_{OCP} - E_{cell}}{i} \quad 6$$

In the above equations R_{int} is the internal resistance in Ω m^2, E_{OCP} is the open cell potential in V, E_{cell} is the measured cell potential in V, and i is the current density in A m^{-2}.

The internal resistance consists of resistances due to the cathode overpotential, anode overpotential, and current dependent potential losses. Those losses include ionic and transport losses (Logan et al., 2006) and they are measured as membrane potential (Harnisch et al., 2009).

$$E_{cell} = E_{OCP} - \eta_{cath} - \eta_{an} - i(R_M) \quad 7$$

In the above equation, E_{cell} is the measured cell potential (V), η_{cath} is the cathode overpotential (V), η_{an} is the anode overpotential (V), and R_M is membrane resistance (Ω m^2).

The cathode overpotential is defined as the cathode potential at open cell potential subtracted from the measured cathode potential while the anode overpotential is the measured anode potential subtracted from the anode potential at open cell potential (Sleutels et al., 2009).

$$\eta_{cath} = E_{cath} - E_{OCP,cath} \quad 8$$

$$\eta_{an} = E_{OCP,an} - E_{an} \quad 9$$

In the above equations, E_{cath} is the measured cathode potential (V), $E_{OCP,cath}$ is the cathode potential at open cell potential (V), $E_{OCP,an}$ is the anode potential at open cell potential (V), and E_{an} is the measured anode potential (V).

The membrane potential loss is defined as the difference between reference electrodes in the anode and the reference electrode in the cathode (Ter Heijne et al., 2006). More specifically, membrane potential loss was calculated according to Sleutels (2009):

$$E_M = E_{cath} - E_{an} - E_{cell} \qquad 10$$

where E_M is the membrane potential loss (V), E_{cath} is the measured cathode potential (V), E_{an} is the measured anode potential (V), and E_{cell} is the measured cell potential (V). In this setup, the anode potential was measured at 0.025 m, 0.05 m, and 0.075 from the cation exchange membranes. Consequently, there were three different anode overpotential losses and membrane potential losses.

The partial internal resistances were calculated by Ohm's law, i.e. by dividing the partial potential losses by the current density. The average partial resistances were defined as the average partial resistance of the three different sample points.

6.4 Results and discussion

6.4.1 Power generation by tubular membrane PMFC

The results showed that the Glyceria maxima tubular membrane PMFC was as suitable as cation exchange membrane for generating power (Strik et al., 2008). Figure 6.2 depicts the power generated from day 50 until day 85 of a PMFC with a felt and granules as anode electrode and the blanks. No electrical power was generated before 60 days, this startup was in the same order of the startup times reported in literature for a G. maxima PMFC (Strik et al., 2008).

The average power generation was 10 ± 2 mW m^{-2} (from day 70 through 85) and 12 ± 4 mW m^{-2} (from day 64 through 85) for the PMFC with the graphite felt and graphite granules, respectively. Both blanks did not generate any power for the first 73 days. At that day, acetate was injected to provide substrate to the electrochemically active bacteria and power was generated. This indicated that no power was generated due to the absence of substrate and that it was likely that the power output in the PMFC was due to the presence of plant roots in the anode. The plant roots provided substrate for the electrochemically active bacteria by either excretion of low molecular weight organic compounds or hydrolysis of dead plant material. The average power generation was in the same range as reported in literature (De Schamphelaire et al., 2008) (Helder et al., 2010) (Kaku et al., 2008) (Strik et al., 2008) (Timmers et al., 2010).

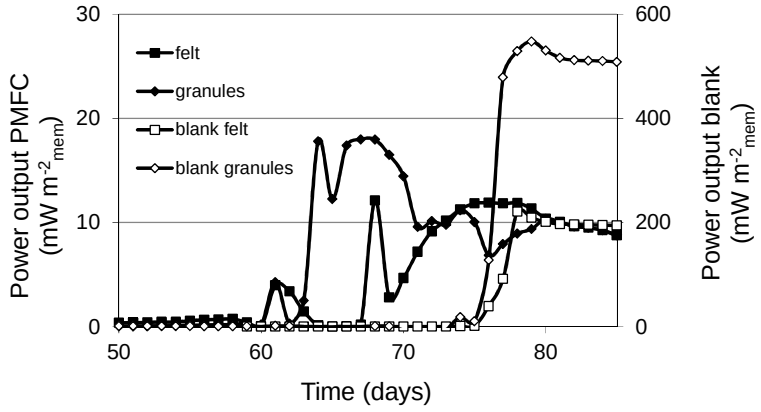

Figure 6.2: *Average daily power density of the tubular PMFC, the setup with the graphite felt as anode, the blank setup, the graphite granule setup, and the blank with granules. The black arrow indicated the day that acetate was injected in the blank setups. The figure shows a higher power density for the graphite granule set up compared to the graphite felt setup.*

The maximum power generation during operation with an external resistance of 900 Ω was 12 mW m^{-2} for the PMFC with the graphite felt setup and 18 mW m^{-2} for the graphite granules setup. Both maxima were reached at day 67 and day 74, i.e., 7 and 14 days after the start of power generation. After the maximum was achieved, the power generation decreased. The same development of power generation was observed by Strik et al. (2008).

The observed difference in maximum power output between both setups was consistent with differences in internal resistance during operation with an external resistance of 900 Ω. The internal resistance of the graphite felt setup was 5.8 Ω m^2 which was higher than 4.6 Ω m^2 which was the internal resistance of the graphite granules setup. The internal resistance was below the reported internal resistance for the sediment type plant microbial fuel cell 21 Ω m^2 (Kaku et al., 2008).

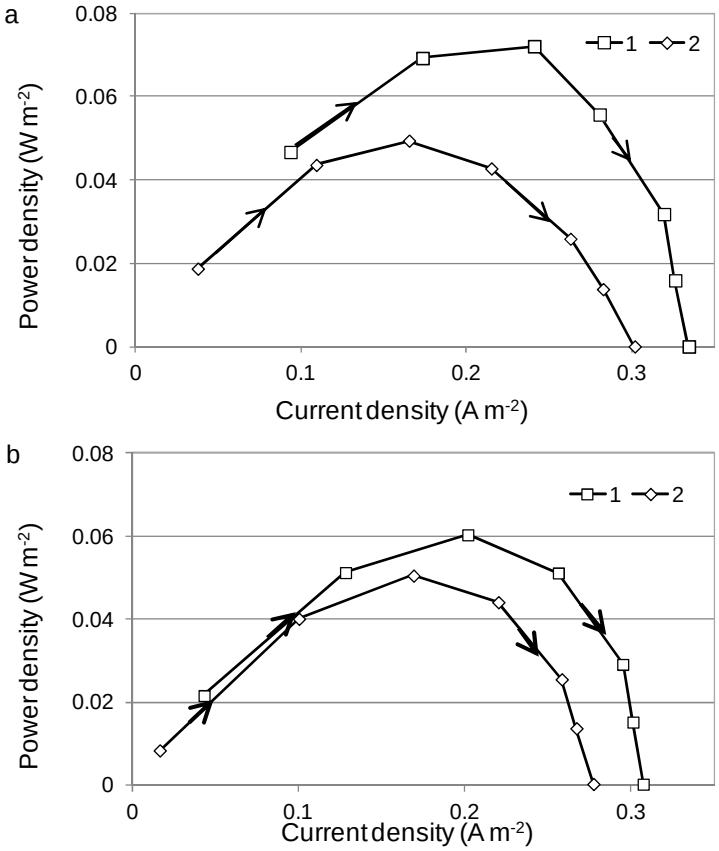

Figure 6.3: a) *The power curves of the graphite granules PMFC showed that the power output of the first polarization was higher than with the second polarization, this indicated that the high power output could not be sustained.* ***b****) The power curves of the graphite felt PMFC showed that the power output of the first polarization was higher than with the second polarization, this indicated that the high power output could not be sustained.*

During polarization, the cell potential was decreased stepwise. The maximum power output during the first polarization was 60 mW m^{-2} and 72

mW m^{-2} for the graphite felt and graphite granules (Figure 6.3). This difference was consistent with the difference in internal resistance which was 1.3 Ω m^2 and 1.2 Ω m^2 for the graphite felt and graphite granules respectively at the maximum power point of the first polarization. This higher internal resistance explained the differences in power output.

The maximum power output during the second polarization was lower, 51 mW m^{-2} and 49 mW m^{-2} for the graphite felt and graphite granules, respectively. This difference was consistent with the difference in internal resistance which was 1.6 Ω m^2 and 1.8 Ω m^2 for the graphite felt and graphite granules respectively at the maximum power point of the second polarization. The increase in internal resistance between the consecutive polarization curves implied that the maximum power output could not be maintained. The increase of the internal resistance can attributed to substrate depletion in combination with an in increase of the resistance to mass transfer in the electrochemically active biofilm and between the anode and cathode due to current generation.

6.4.2 Internal resistance of PMFC with tubular membrane

Figure 6.4 shows the power output at the controlled potential of 0.1V. This controlled potential was selected because it is lower than the average cell potential at 900 Ω. Because the controlled potential was lower than the average cell potential the electrochemically active bacteria in the tubular PMFC should be able to maintain the controlled potential at an external resistance lower than 900 Ω. For the graphite felt as well as the graphite granules the external resistance, at which the controlled potential was maintained, was indeed lower than 900 Ω (Figure 6.4 a and c).

The graph depicted higher power output of the graphite granules setup (Figure 6.4 a) than the graphite felt setup (Figure 6.4 c), which was consistent with the previous findings during polarization and operation at an external resistance of 900 Ω. In both setups, the power output decreased with time and did not reach a steady state. The continuous

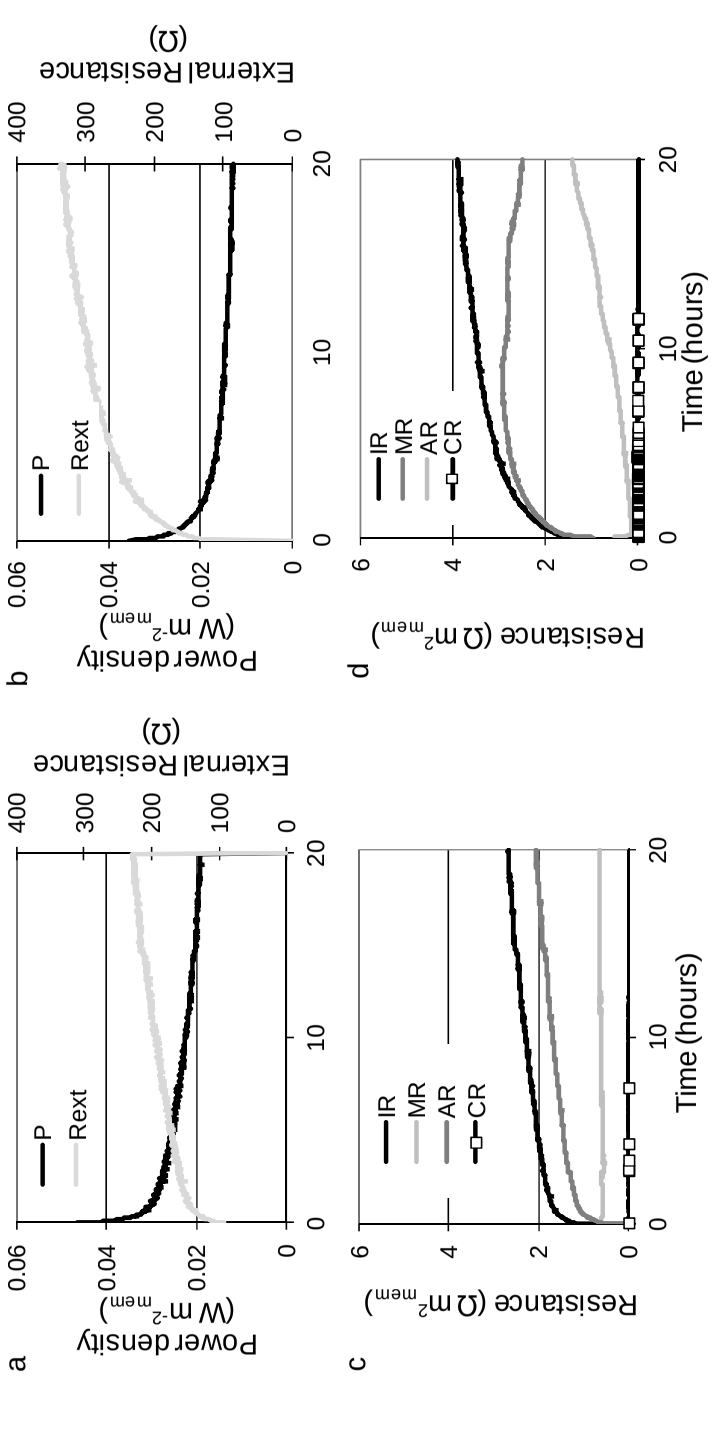

Figure 6.4: *Continuous decrease of power density and increase of internal resistance at a controlled potential of 0.1 V. Power density of the graphite granule setup (a) and the graphite felt setup (b) at an applied potential of 0.1 V. Internal resistance (IR), Membrane resistance (MR), Anode resistance (AR) and Cathode resistance (CR) of the graphite granule setup (c) and the graphite felt setup (d).*

decrease of the power output was due to the continuous increase in the internal resistance. Initially the internal resistance was 1.1 Ω m^2 for the graphite granules and 1.7 Ω m^2 for the graphite felt. After 20 hours the internal resistance increased to 2.7 Ω m^2 for the graphite granules and 4.9 Ω m^2 for the graphite felt (Figure 6.4 b and 4 d). The average power output during the period of controlled potential was considerably higher than the average power output during operation with the external resistance of 900 Ω which was consistent with the lower internal resistance in both setups. The internal resistance at the constant controlled potential was lower compared to the internal resistance at an external resistance of 900 Ω. After 20 hours of open circuit, reduction of the proton concentration gradient in the electrochemically active biofilm likely caused a lower initial internal resistance at the start of current generation.

6.4.3 Anode resistance major part of internal resistance with graphite granules

The increase in internal resistance in the graphite granule setup was due to the increase of the anode resistance (Figure 6.4 c). After 20 hours of open circuit, the anode resistance increased from 0.5 Ω m^2 to 2.1 Ω m^2 after 20 hours of closed circuit. It was likely that, during current generation in the PMFC, the anode resistance increase was due to an increase of the resistance to proton transfer out of the electrochemically active biofilm, like it is in MFCs (Torres et al., 2008). In this manner, a decrease of anolyte bulk pH was observed in the graphite granules set-up. At open circuit, pH registered was approximately 5.7 while after 20 hours of current generation, pH was approximately 4.2.

The membrane resistance in the graphite granule set up was constant during the 20 hours of current generation (Figure 6.4 c). The membrane resistance was 0.6 ± 0.03 Ω m^2 which is low compared to the membrane resistances reported in literature (Timmers et al., 2010). The reason for this low membrane resistance was attributed to negligible accumulation of cations in the cathode in this setup during current generation. The maximum amount of monovalent cations accumulated in the cathode is equal to the total amount of electrons generated during current generation. The amount of electrons generated during current generation

was $6.6 \cdot 10^{-6}$ mol (the total amount of coulombs produced divided by Faraday's constant) and thus maximally $6.6 \cdot 10^{-6}$ mol of monovalent cations were transported to the cathode. This amount of monovalent cations was negligible compared to the total monovalent cations present in the catholyte (0.15 mol). Besides cations also anions can also be transported through the ultrafiltration membrane which also contributed to transport required to maintain electroneutrality. Since anions transport contributed as well to this transport, less cations had to be transported, therefore it was likely that the accumulation of cations was less than estimated here.

6.4.4 Membrane resistance major part of internal resistance with graphite felt

The increase in the internal resistance in the graphite felt setup was due to a combination of an increase in anode resistance and membrane resistance (Figure 6.4 d). The anode resistance initially decreased after which it continuously increased from 0.16 to 1.8 Ω m^2. The anode resistance of the graphite felt setup was lower than the anode resistance of the graphite granules and did not follow the continuous decrease of power output. The lower anode resistance was likely due to the higher pH in the soil surrounding the graphite felt. The average pH in the anode before current generation was 5.8 ± 0.30 and slightly increased to 5.9 ± 0.2 after 20 hours of current generation. Even though the pH increased, the anode resistance increased. This indicated that the increase in anode potential was not due to proton transport out of the electrochemically active biofilm. Consequently, the increase in anode resistance was likely due to a decrease of substrate concentration or an increase in bicarbonate concentration in the electrochemically active biofilm on the graphite felt. The decrease substrate concentration in the graphite felt could be due to the limited penetration of the graphite felt with roots (Figure 6.5).

Opposite to membrane resistance behaviour observed in the graphite granule set-up, membrane resistance in the graphite felt was not constant. The initial increase of the internal resistance was due to increase of the membrane resistance. The membrane resistance initially increased from 1.3 to 3.7 Ω m^2 and decreased onwards to 3.1 Ω m^2. Later on the increase of the anode resistance resulted in the increase of the internal resistance

(Figure 6.4 d). The slow response of the anode resistance was likely attributed to the play sand surrounding the reference electrodes. The anode resistance is a combination of energy losses due activation of the anode electrode, and energy losses due to mass transfer to the anode electrode surface. The energy loss due to mass transfer is due to a built up of concentration gradients. In the case of graphite felt, the reference electrodes in the anode were surrounded by soil surrounding the graphite felt electrode. The spatial separation between the current generation and the reference electrodes in the graphite felt setup likely resulted initially in smaller concentration gradients between the electrode surface and the reference electrodes. Initially this resulted in a smaller measured anode resistance. During current generation concentration gradients likely developed which resulted in the increase of the anode resistance. The fact that the pH in the graphite felt setup was constant during current generation indicated that likely substrate transport to the anode electrode surface was causing the increase in anode resistance.

Figure 6.5: *Picture of the graphite felt of the setup after dismantling of the PMFC 2. The picture shows that the graphite felt was not well penetrated by plant roots.*

6.4.5 Graphite granules higher power output based on membrane surface

Based on membrane surface the power output of the graphite granules was consistently higher than the power output of the graphite felt. The average power output with the graphite granules was 12 ± 3.6 mW m^{-2}; while for the graphite felt the average power output was 10 ± 3 mW m^{-2}. This was the result of the higher internal resistance of the graphite felt compared to

the internal resistance of graphite granules setup. It is beyond the scope of this research to fully elaborate the nature of the difference in internal resistance. However it was observed that one major difference between the graphite felt and the graphite granules was the pore size of the material. The major advantage of graphite granules was the higher pore size rendering this material more accessible for plant roots and hence reducing the possibility of substrate limitation. Furthermore, pore size can also have an effect on anode and membrane resistance by reduction of mass transfer limitations. More specifically, it can be hypothesised that graphite granules can facilitated a higher mass transfer through the bulk anolyte due to a higher permeability. Additionally, differences in the internal resistance of the graphite felt and graphite granules and differences in plant growth between both PMFC could have played a role.

6.4.6 Graphite felt higher power output based on amount of anode electrode material

Based on the mass of electrode material used, the power output of the graphite felt was about 15 times higher than the power output of the graphite granules. The average power output was 0.53 ± 0.1 mW kg^{-1}_{anode}, and 0.035 ± 0.01 mW kg^{-1}_{anode} for the graphite felt, and graphite granules, respectively. Based on the volume of the total reactor volume, the power output of the graphite felt was about 69 times higher than the power output of the graphite granules. The average power output was 0.192 ± 0.04 W $m^{-3}_{reactor}$, and 0.003 ± 0.0009 W $m^{-3}_{reactor}$ for the graphite felt, and graphite granules, respectively. The average power output per square meter of membrane of the graphite felt was only 0.83 times lower than the power output of the graphite granules. This showed reduction of anode electrode material is possible while achieving comparable power outputs per square meter of membrane.

6.5 Conclusions

A new tubular PMFC set up where anode and cathode were integrated in the same unit generated current which makes it possible to apply the PMFC technology with horizontal drilling and thus without excavation of the topsoil.

The PMFC with graphite felt exhibited a 15 times higher power output than the PMFC with the graphite granules based on mass of electrode material while based. And exhibited a 69 times higher power output based on the volume of the reactor. This showed reduction of anode electrode material is possible while achieving comparable power outputs per square meter of membrane.

Acknowlegement

This research was funded by Senternovem, the Dutch governmental agency for sustainability and innovation in the Ministry of Finance (grant no. EOSLT06020), and supported by Alliander.

References

Chen, Z., Huang, Y.C., Liang, J.-h., Zhao, F., Zhu, Y.-g. A novel sediment microbial fuel cell with a biocathode in the rice rhizosphere. *Bioresource Technology,* doi10.1016/j.biortech.2011.10.040.

De Schamphelaire, L., Cabezas, A., Marzorati, M., Friedrich, M.W., Boon, N., Verstraete, W. 2010. Microbial community analysis of anodes from sediment microbial fuel cells powered by rhizodeposits of living rice plants. *Applied and Environmental Microbiology,* **76**(6), 2002-2008.

De Schamphelaire, L., Van Den Bossche, L., Hai, S.D., Höfte, M., Boon, N., Rabaey, K., Verstraete, W. 2008. Microbial fuel cells generating electricity from rhizodeposits of rice plants. *Environmental Science and Technology,* **42**(8), 3053-3058.

EPA. 2008. Green Remediation: Best Management Practices for Excavation and Surface Restoration.

Ghose, M.K. 2004. Effect of opencast mining on soil fertility. *Journal of Scientific and Industrial Research,* **63**(12), 1006-1009.

Harnisch, F., Warmbier, R., Schneider, R., Schröder, U. 2009. Modeling the ion transfer and polarization of ion exchange membranes in bioelectrochemical systems. *Bioelectrochemistry,* **75**(2), 136-141.

Helder, M., Strik, D.P., Hamelers, H.V., Buisman, C.J. 2011. Year round performance of the flat-plate plant-microbial fuel cell. *Communications in agricultural and applied biological sciences,* **76**(2), 55-57.

Helder, M., Strik, D.P.B.T.B., Hamelers, H.V.M., Kuhn, A.J., Blok, C., Buisman, C.J.N. 2010. Concurrent bio-electricity and biomass production in three Plant-Microbial Fuel Cells using *Spartina anglica*, *Arundinella anomala* and *Arundo donax*. *Bioresource Technology,* **101**(10), 3541-3547.

Kaku, N., Yonezawa, N., Kodama, Y., Watanabe, K. 2008. Plant/microbe cooperation for electricity generation in a rice paddy field. *Applied Microbiology and Biotechnology,* **79**(1), 43-49.

Logan, B.E., Hamelers, B., Rozendal, R., Schröder, U., Keller, J., Freguia, S., Aelterman, P., Verstraete, W., Rabaey, K. 2006. Microbial fuel cells: Methodology and technology. *Environmental Science and Technology,* **40**(17), 5181-5192.

McKim, R.A. 1997. Selection method for trenchless technologies. *Journal of Infrastructure Systems*, **3**(3), 119-124.

Sleutels, T.H.J.A., Hamelers, H.V.M., Rozendal, R.A., Buisman, C.J.N. 2009. Ion transport resistance in Microbial Electrolysis Cells with anion and cation exchange membranes. *International Journal of Hydrogen Energy*, **34**(9), 3612-3620.

Strik, D.P.B.T.B., Hamelers, H.V.M., Snel, J.F.H., Buisman, C.J.N. 2008. Green electricity production with living plants and bacteria in a fuel cell. *International Journal of Energy Research,* **32**(9), 870-876.

Strik, D.P.B.T.B., Timmers, R.A., Helder, M., Steinbusch, K.J.J., Hamelers, H.V.M., Buisman, C.J.N. 2011. Microbial solar cells: Applying photosynthetic and electrochemically active organisms. *Trends in Biotechnology,* **29**(1), 41-49.

Taiz, L., Zeiger, E. 2006. *Plant physiology.* Sinauer Associates, Sunderland, Mass.

Ter Heijne, A., Hamelers, H.V.M., De Wilde, V., Rozendal, R.A., Buisman, C.J.N. 2006. A bipolar membrane combined with ferric iron reduction as an efficient cathode system in microbial fuel cells. *Environmental Science and Technology,* **40**(17), 5200-5205.

Ter Heijne, A., Liu, F., Van Rijnsoever, L.S., Saakes, M., Hamelers, H.V.M., Buisman, C.J.N. 2011. Performance of a scaled-up Microbial Fuel Cell with iron reduction as the cathode reaction. *Journal of Power Sources,* **196**(18), 7572-7577.

Timmers, R.A., Strik, D.P.B.T.B., Hamelers, H.V.M., Buisman, C.J.N. 2010. Long-term performance of a plant microbial fuel cell with Spartina anglica. *Applied Microbiology and Biotechnology,* **86**(3), 973-981.

Torres, C.I., Marcus, A.K., Rittmann, B.E. 2008. Proton transport inside the biofilm limits electrical current generation by anode-respiring bacteria. *Biotechnology and Bioengineering,* **100**(5), 872-881.

van der Meulen, M.J. 2003. *Grondstoffen en delfstoffen bij naam. Dienst Weg- en Waterbouwkunde*, Delft.

Woodroffe, N.J.A., Ariaratnam, S.T. 2009. Contractor perspective on factors for evaluating installation options for small-diameter utilities. *Journal of Construction Engineering and Management,* **135**(2), 75-87.

7 Long term performance of a plant microbial fuel cell with *Spartina anglica*

This chapter has been published as:
Timmers, R.A., Strik, D.P.B.T.B., Hamelers, H.V.M., Buisman, C.J.N. Long-term performance of a plant microbial fuel cell with *Spartina anglica*. *Applied Microbiology and Biotechnology*

Abstract

The plant microbial fuel cell is a sustainable and renewable way of electricity production. The plant is integrated in the anode of the microbial fuel cell consisting of a bed of graphite granules. In the anode organic compounds deposited by plant roots are oxidized by electrochemically active bacteria. In this research salt marsh species *Spartina anglica* generated current for up to 119 days in a plant microbial fuel cell. Maximum power production was 100 mW m^{-2} geometric anode area, highest reported power output for a plant microbial fuel cell. Cathode overpotential was the main potential loss in the period of oxygen reduction due to slow oxygen reduction kinetics at the cathode. Ferricyanide reduction improved the kinetics at the cathode and increased current generation with a maximum of 254%. In the period of ferricyanide reduction the main potential loss was transport loss. This research shows potential application of microbial fuel cell technology in salt marshes for bio-energy production with the plant microbial fuel cell.

Keywords: Plant Microbial Fuel Cell, Rhizodeposition, Bioenergy, Spartina anglica, Potential losses, Green electricity

7 Long term performance of a plant microbial fuel cell with *Spartina anglica*

7.1 Introduction

Nowadays the need for sustainable renewable energy is urgent due to depletion of fossil fuels, increasing energy consumption, climate change and environmental pollution. Current production processes for bio-energy such as bio-ethanol or biodiesel often compete with food production. Competition with food production not only increases food prices and malnourishment (Pimentel et al., 2009), but also increases incentives for deforestation by claiming land for food production or bio-energy crops. Deforestation is the second most important source of greenhouse gas emissions in the world (von Witzke, 2008). Therefore to have sustainable renewable energy there should be no competition with food production. In search for renewable and sustainable bio-energy production Strik et al. (2008) presented the plant microbial fuel cell (P-MFC). The P-MFC harvests solar energy as electricity by combination of: electricity generation by bacteria through oxidation of organic compounds, and deposition of organic compounds by plants into the rhizosphere. Aim of the P-MFC is to transform solar energy into electrical energy through oxidation of rhizodeposits by electrochemically active bacteria. Potential electrical output without crop harvesting is 5800 kWh ha^{-1} $year^{-1}$ (Strik et al. 2008), comparable to conventional renewable bio energy sources with crop harvesting.

De Schamphelaire et al. (2008) presented the sediment type P-MFC which consisted of an anode and cathode without membrane separation. The P-MFC as described by Strik et al. (2008) consisted of an anode and cathode separated by a membrane. In the anode electrochemically active bacteria oxidize rhizodeposits whereby electrons, protons and CO_2 are produced. Electrons and protons are transferred to the cathode compartment; CO_2 escapes to the atmosphere where it can be used again by plants for photosynthesis. At the cathode electrons, protons, and oxygen are consumed by reduction of oxygen to water. Production and consumption of electrons results in a potential difference between anode and cathode which makes electrons flow through the electrical circuit.

To avoid competition with agricultural food production salt marsh species should be tested in the P-MFC, because there is no competition for arable

land (Galvani, 2007). Until now no salt marsh species was tested in the P-MFC. Furthermore there is no literature describing biochemical conditions and potential losses in the P-MFC.

First objective is to prove long term electricity generation by *Spartina anglica* (*S. anglica)* in the P-MFC. Second objective is to gain insight in potential losses of the P-MFC as well as biochemical conditions in the anode compartment. To meet both objectives the *S. anglica* P-MFC was monitored for a period equal to the length of one growth season. One growth season is defined as the period *S. anglica* is able to photosynthesize which is at temperatures above 7 ^{o}C (Gray et al., 1991), in the Netherlands in 2008 from mid March to mid November (around 240 days). In this period cell potential, cathode potential, anode potential, membrane potential, pH, and conductivity of the P-MFC were monitored.

7.2 Material and Methods

7.2.1 Experimental set-up

The P-MFC consisted of a cathode and an anode separated by a membrane. The cathode consisted of graphite felt in a beaker. The anode consisted of graphite granules in a glass cylinder in which *S. anglica* was planted, and a membrane at the bottom of the glass cylinder. The anode was placed with the membrane on the graphite felt in the cathode and the P-MFC was formed. Strik et al. (Strik et al., 2008) described the P-MFC in detail. The current collector was different, here the current collector was a golden wire glued to a Teflon coated copper wire placed in the anode as well as the cathode. To close the electrical circuit current collectors were connected over an external resistance of 1000 Ω.

The P-MFCs were placed in a cabinet of which both front and back were open. In the cabinet temperature fluctuated between 23-27 ^{o}C, humidity was uncontrolled, light intensity in the photosynthetic active region was 261 ± 56 µmole $m^{-2}s^{-1}$, and illumination period was 14 h d^{-1}. To provide illumination metal-halogen lamps (2 of 250 W and 2 of 400 W Spacesaver) were used. On day 154 P-MFCs were moved into a climate control cabinet (Microclima 1750 Snijders). In the climate control cabinet temperature was 25 ^{o}C, humidity was 75%, light intensity in the photosynthetic active region

was 248 ± 44 µmole $m^{-2}s^{-1}$, and illumination period was 14 h d^{-1}. On day 168 light intensity in the photosynthetic active region was increased to 596 ± 161 µmole $m^{-2}s^{-1}$.

7.2.2 Preparation of graphite granules

Graphite granules with a diameter of 1 mm to 2 mm (le Carbone, Wemmel Belgium) were used as electrode material in the anode. An acetate fed P-MFC was used to grow electrochemical active biofilm on graphite granules. To grow electrochemical active biofilm the plant was left out and the top of the P-MFC was closed with a screw cap. Anolyte solution was Modified Hoagland solution buffered with 8 mM phosphate buffer (pH 7.0). Substrate was 20 mL L^{-1} of 2 M potassium acetate added after the anolyte solution was flushed with nitrogen gas for 15 minutes. Catholyte was a 50 mM potassium ferricyanide (K_3FeCN_6) solution buffered with 8 mM phosphate buffer (pH 7.0). To both anolyte and catolyte 20 g L^{-1} sodium chloride and 5 g L^{-1} magnesium chloride was added to reach the conductivity of the pore water solution of the soil on which *S. anglica* was grown (47 mS m^{-1}). Each acetate fed P-MFC was inoculated with 20 mL of anolyte of a potassium acetate fed flat plate microbial fuel cell (conductivity 4.98 mS m^{-1}), which was inoculated with sediment harvested in July 2007 at GPS coordinates N58.04.00 G011.33.50, containing 27 g L^{-1} NaCl. The electrochemical active biofilm was grown for 39 days in the acetate fed P-MFC of which the anolyte was refreshed at day 18.

7.2.3 P-MFC operation

Four P-MFCs, two blanks (P-MFCs without plant) and two duplicates: P-MFC1 and P-MFC2, were used. In P-MFC1 and P-MFC2 one clump with two or three stems (fresh weight 8.0 to 15.0 g) of *S. anglica* was planted in 165 g of prepared graphite granules in the anode. *S. anglica* was harvested in July 2007 at GPS coordinates N51.67.654 G004.13.656 where soil pore water conductivity was 47 mS cm^{-1}. Until October 2007 *S. anglica* was grown indoors under artificial illumination.

Anolyte was ½ Modified Hoagland solution, buffered at pH 6.5 with 8 mM phosphate buffer and a conductivity between 1.5-1.6 mS m^{-1} (no extra salts were added). Iron complex in ½ Modified Hoagland solution was

diethylenetraiminepentaacetic acid ferric sodium complex (Dissolvine D-Fe-11, AKZO NOBEL Functional Chemicals bv, Herkenbosch, the Netherlands). From day 1 through day 216 the catholyte was demineralized water buffered with 8 mM phosphate buffer (pH 6.5). From day 217 through day 250 the catholyte solution was 50 mM potassium ferricyanide (K_3FeCN_6) solution, buffered with 8 mM phosphate buffer (pH 6.5).

To prevent osmotic shock for *S. anglica* and electrochemical active biofilm at the construction of the P-MFC 20 g L^{-1} sodium chloride and 5 g L^{-1} magnesium chloride was added to both anolyte and catholyte (anolyte 37.6 mS m^{-1}, and catholyte 37.1 mS m^{-1})

All P-MFCs (including blanks) were daily watered from top of anode with the anolyte at a flow rate 0.9 mL $min^{-1}$for 15 minutes in the period from day 0 through day 89 and for 30 minutes in the period from day 90 through day 250. In the open cabinet catholyte was replenished weekly with demineralized water. In the climate control cabinet catholyte was refreshed on day 189. The anode was sampled weekly (4 mL) of the cathode the pH was measured weekly

7.2.4 Analytical techniques

Of anode samples pH, conductivity and of a selection of samples volatile fatty acids (VFA, C2 to C5) and chemical oxygen demand (COD) were measured.

Conductivity of anode samples was measured after diluting 50 times with demineralized water which had a conductivity of 0.8 µScm^{-1}.

Anode samples were centrifuged 10 minutes at 10000 rpm before analysis of VFA concentration and COD concentration. VFA concentration was measured by a gas chromatography (Hewlett Packard model 5890 series 2, Agilent Technologies, Amstelveen, the Netherlands) accommodated with an AT –Aquawax-DA column (Altech) and a flame ionization detector. COD concentration was measured by a COD cuvette test (LCK314; Dr Lange, GmbH, Düsseldorf, Germany).

7.2.5 Electrochemical characterization

Cell potential was measured online with a data acquisition instrument (Fieldpoint modules and a personal computer with Labview software, National Instruments). Cell potential, anode potential, cathode potential and membrane potential were measured offline with a precision multimeter (True RMS multimeter, fluke 189). Anode potential and cathode potential were measured as potential difference between current collector and a silver/silverchloride (Ag/AgCl) reference electrode (3M KCl electrode, ProSense QiS, Oosterhout, the Netherlands, +205 mV vs. NHE). Membrane potential (Ter Heijne et al., 2006) was measured as difference between the Ag/AgCl reference electrodes in anode and cathode.

The incubation period is defined as the period from start of the experiment until a current density of 100 mA m^{-2} is generated.

7.2.6 General vitality of *S. anglica*

To monitor general plant vitality, shoot density and number of living shoots per square meter was determined weekly (Haines, 1979; Linthurst & Seneca, 1980). . There is no significant effect of salinity, ranging from 30 g NaCl L^{-1} (seawater) to 0.6 g NaCl L^{-1} (freshwater) on above and below ground biomass production (vitality) of *S. anglica* (Huckle et al., 2000).

7.2.7 Calculations

To interpret anode potential, acetate degradation was used as model reaction whereas for cathode potential oxygen reduction and ferricyanide reduction were used. Relation between theoretical potential, reactants and products is given by the Nernst equation. For the anode potential:

$$E_{Th,an} = E^0 - \frac{RT}{nF}\ln\frac{\left[CH_3COO^-\right]}{\left[HCO_3^-\right]^2\left[H^+\right]^9} \qquad 1$$

for the cathode potential:

$$E_{Th,cath} = E^0 - \frac{RT}{nF}\ln\frac{1}{pO_2\left[H^+\right]^4} \quad (2)$$

$$E_{Th,cath} = E^0 - \frac{RT}{nF}\ln\frac{\left[Fe(CN)_6^{4-}\right]}{\left[Fe(CN)_6^{3-}\right]} \quad (3)$$

where $E_{Th,x}$ is the theoretical potential (V), E^0 is the standard electrode potential of the reaction (V), R is the universal gas constant (J K^{-1} mol^{-1}), T is the temperature (K), n is the number of electrons transferred in the reaction (-), F is Faraday's constant (96485 C mol^{-1}), [x] is the concentration of reactants or products (mol L^{-1}), pO_2 is the partial pressure of oxygen (Pascal). The electromotive force (E_{emf}) was calculated by subtracting theoretical anode potential ($E_{Th,\,an}$) from theoretical cathode potential ($E_{Th,cath}$) (Logan et al., 2006a).

$$E_{emf} = E_{Th,cath} - E_{Th,an} \quad (4)$$

Measured cell potential (E_{cell}) is equal to electromotive force (E_{emf}) minus total potential loss which is sum of: anode overpotential (η_{an}), cathode overpotential (η_{cath}), and membrane potential ($E_{a\text{-}c}$) (Sleutels et al., 2009a).

$$E_{cell} = E_{emf} - \eta_{an} - \eta_{cath} - E_{a-c} \quad (5)$$

Anode overpotential was defined as measured anode potential (E_{an}) minus theoretical anode potential ($E_{an,calc}$). Cathode overpotential was defined as theoretical cathode potential ($E_{cath,calc}$) minus measured cathode potential (E_{cath}) (Logan et al., 2006b).

$$\eta_{an} = E_{an} - E_{an,calc} \quad (6)$$

$$\eta_{cath} = E_{cath,calc} - E_{cath} \quad (7)$$

It is not possible to determine the theoretical anode potential ($E_{an,calc}$) because of diversity of rhizodeposits. Diversity in rhizodeposits will result in a mixed potential in the anode compartment. Because of the large specific surface area of graphite granules in the anode current density was low. From Ter Heine et al. (2008) can be deduced that low current densities

result in an anode potential close to theoretical anode potential, hence a low anode overpotential.

Membrane potential (E_{a-c}) consists of: i) pH gradient loss ($E_{\Delta pH}$) , ii) ionic loss (E_{ionic}), and iii) transport loss (E_T) (Sleutels et al., 2009a). pH gradient loss is potential loss due to pH difference between anode and cathode ($E_{\Delta pH}$) and was calculated according to (Ter Heijne et al., 2006).

$$E_{\Delta pH} = \frac{RT}{F}\ln\left(10^{(pH_{cath}-pH_{an})}\right) \quad 8$$

Where $E_{\Delta pH}$ is pH gradient loss (V), pH_{cath} is pH in the cathode and pH_{an} is pH in the anode.

Ionic loss is potential loss due to ohmic resistance in the anolyte (E_{ionic}) and was calculated according to (Ter Heijne et al., 2006).

$$E_{ionic} = i\left(\frac{d_{an}}{\sigma_{an}}\right) \quad 9$$

Where E_{ionic} is ionic loss in anolyte (V), i is current density (A m^{-2}), d_{an} is distance between membrane and reference electrode (m) and σ_{an} is conductivity of the anode compartment (S m^{-1}). Ionic loss in the catholyte was assumed zero due to relative small distance between membrane and reference electrode in the cathode compartment compared to the anode compartment.

Transport loss is potential loss due to ion transport in the anolyte and through the membrane was calculated by subtracting pH gradient loss ($E_{\Delta pH}$) and ionic loss (E_{ionic}) from membrane potential (E_{a-c}) (Sleutels et al., 2009a).

$$E_T = E_{a-c} - E_{\Delta pH} - E_{ionic} \quad 10$$

To compare partial potential losses at different current densities partial resistances were calculated by dividing the different potential loss by current density at that given time.

7.3 Results

7.3.1 Long term electricity generation

Results showed that long term electricity generation by *S. anglica* in a P-MFC is achievable without being lethal to the plant. The incubation period lasted 92 days for P-MFC1 and 126 for P-MFC2. After incubation P-MFC1 generated electricity 119 out of 167 days and P-MFC2 107 out of 125 days. Figure 7.1 shows generated current density from day 50 until day 251 (end of the experiment) of P-MFC1, P-MFC2, and a blank.

In the period of oxygen reduction (day 0 through day 217), P-MFC1 generated current for 86 days with an average current density of 84 ± 70 mA m^{-2} (load of 1000 Ω), resulting in an average power density of 10 ± 12 mW m^{-2} and a total energy production of 79 J. P-MFC2 generated current for 78 days with an average current density of 141 ± 52 mA m^{-2} (load of 1000 Ω), resulting in an average power density 22 ± 14 mW m^{-2} and a total energy production of 119 J.

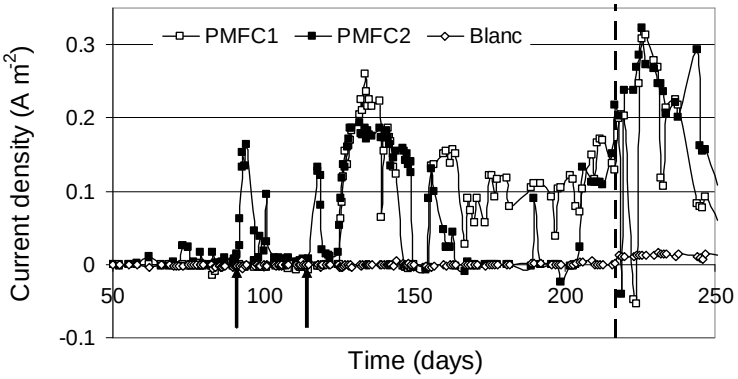

Figure 7.1: *Current density vs. time of P-MFC1, P-MFC2 and 1 blank from day 50 through day 250. Arrows indicate incubation period of P-MFC1 and P-MFC2. The dotted line shows change of oxygen reduction at the cathode into ferricyanide reduction at the cathode.*

In the period of ferricyanide reduction (day 217 through day 250), P-MFC1 generated current for 33 days with an average current density of 214 ± 78 mA m^{-2} (load of 1000 Ω), resulting in an average power density of 50 ± 25

mW/m^2 and a total energy production of 139 J. P-MFC2 generated current for 29 days with an average current density of 195 ± 84 mA m^{-2} (load of 1000 Ω), resulting in an average power density 42 ± 31 mW m^{-2} and a total energy production of 89 J. Blanks generated no significant current and averaged -0.3 ± 3.8 mA m^{-2} for oxygen reduction and 12 ± 2 mA m^{-2} for ferricyanide reduction.

In the period of oxygen reduction maximum power output was 79 mWm^{-2} at day 133 determined by polarization (data not shown). In the period of ferricyanide reduction maximum power output was 100 mW m^{-2} determined by the maximum cell potential. To our knowledge this is the highest reported power output for a P-MFC.

7.3.2 COD and VFA concentration in the anode

COD concentration increased from of 66 mg L^{-1} in the anode of both the P-MFCs at start of the experiment to an average COD concentration of 203 ± 83 mg L^{-1} in the anode of P-MFC1 and 163 ± 83 mg L^{-1} in the anode of P-MFC2. In the blanks average COD concentration was 50 ± 20 mg L^{-1}, which originated from the non biodegradable iron complex in the ½ Hoagland solution. Difference between COD concentration in blanks and P-MFCs indicated rhizodeposition of COD by plant roots.

VFA concentration in the anode of both P-MFCs was around detection limit (2 mg L^{-1}). When current was generated 50% of VFA samples were below detection limit, average concentration was 1.3 ± 1.2 mg L^{-1} (this included samples below detection limit). When no current was generated 46% of samples were below detection limit, average concentration was 2.9 ± 3.1 mg L^{-1} (this included samples below detection limit).

7.3.3 pH in the bio-anode and cathode

The pH in the anode of P-MFC1 and P-MFC2 varied from 5.2 and 7.3. The pH in the cathode varied from 6.4-9.1 for P-MFC1, and from 6.5-9.0 for P-MFC2. When current was generated during oxygen reduction, the pH in the anode decreased from 6.9 to 6.5 for P-MFC 1 and from 6.9 to 5.3 for P-MFC2. When current was generated during cathodic ferricyanide reduction,

the pH in the anode decreased from 6.5 to 5.2. for P-MFC 1 and from 5.3 to 5.2 for P-MFC2.

7.3.4 Conductivity of the anolyte

Conductivity of the anolyte decreased gradually with time from 46.7 to 4.9 mS cm^{-1} for P-MFC1 and from 56.8 to 3.1 mS m^{-1} for P-MFC2, due to watering with ½ Hoagland solution which had a conductivity of 1.5 to 1.6 mS m^{-1}.

7.3.5 General vitality of *S. anglica*

General vitality of P-MFC1 increased until day 210, the number of stems increased from 2 to 10 for P-MFC1. General vitality of P-MFC2 increased until day 222, the number of stems increased from 2 to 7.

At the end of the experiment the vitality of both P-MFC1 and P-MFC2 decreased. The number of living stems of P-MFC1 decreased from 10 to 8 from day 210 through 245. The number of living stems of P-MFC2 decreased from 7 to 6 from day 222 through 245

7.3.6 Cell, anode, and cathode potential versus time

Both P-MFCs showed fluctuations in cell potential, anode potential, cathode potential, and membrane potential. Figure 7.2 shows cell potential (E_{cell}), anode potential (E_{an}), cathode potential (E_{cath}), and potential across the membrane (E_{a-c}) from day 50 through day 250 (P-MFC1 is not shown because the same trend was observed). In the incubation period of P-MFC2, anode potential and cathode potential were relatively stable with anode potential between 300 mV to 400 mV (vs.Ag/AgCl) and cathode potential between 200 to 300 mV (vs.Ag/AgCl). The potential across the membrane was negative and appeared to follow fluctuations in cathode potential. After incubation period of P-MFC2, 125 days, anode potential and cathode potential were variable over long periods of time, resulting in a variable cell potential. The anode potential of P-MFC2 varied between 465 mV and -447 mV (vs. Ag/AgCl). When current was generated anode potential was below cathode potential and the potential across the membrane became positive.

The change to ferricyanide reduction at day 217 increased cathode potential of P-MFC2 to 325 mV after which it gradually decreased to 250 mV. Cell potential and anode potential of P-MFC2 showed large fluctuations from day 217 through day 225. After day 225, anode potential gradually increased from -402 mV to121 mV (day 247) with a large fluctuation at day 232. From day 225 through day 227 cell potential increased, to 302 mV after day 227 cell potential gradually decreased to 57 mV.

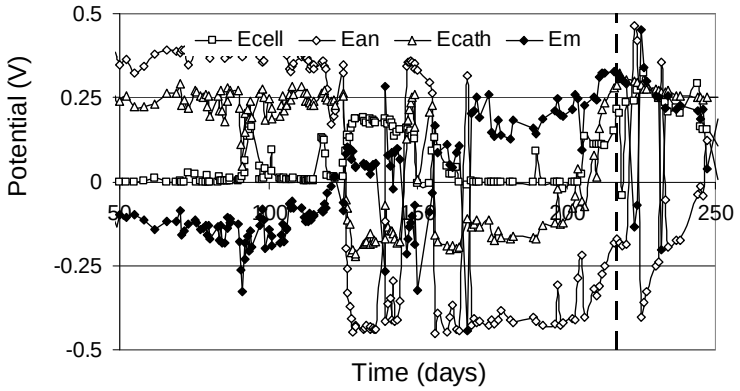

Figure 7.2: *Cell potential (E_{cell}), anode potential (E_{an}), cathode potential (E_{cath}), and membrane potential (E_{a-c}) vs. time of P-MFC2, from day 50 through day 250. The dotted line shows change of oxygen reduction at the cathode into ferricyanide reduction at the cathode.*

7.3.7 Potential losses and partial resistances

Figure 7.3 a and b show partial internal resistances and external resistance of P-MFC1 (a) and P-MFC2 (b). Figure 7.3 c and d show partial potential losses and cell potential of P-MFC1 (c) and P-MFC2 (d).In the period of oxygen reduction the major potential loss was: cathode overpotential, followed by transport potential loss. In the period of ferricyanide reduction cathode overpotential decreased as expected, major potential loss was: transport loss, followed by ionic loss.

7.4 Discussion

7.4.1 Long term electricity generation

S. anglica was able to live in a P-MFC for up to 167 days after incubation period and generate current up to119 days (P-MFC1). The 119 days of

current generation was an increase of 175 % compared to the current generation period of Strik et al. (Strik et al., 2008). Sediment P-MFCs with rice plants of De Schamphelaire et al. ((De Schamphelaire et al., 2008)and Kaku et al. (Kaku et al., 2008) produced electricity for comparable time periods. However, sediment P-MFC had lower power densities 33 mW m^{-2} (De Schamphelaire et al., 2008)and 6 mW m^{-2} (Kaku et al., 2008), compared to 79 mW m^{-2} for cathodic oxygen reduction in this study.

7.4.2 No Michaelis Menten relation between rhizodeposits measured as COD and current

The average COD concentration in the anode of both P-MFCs was 3 to 4 times higher than COD concentration in blanks, this indicated that there was rhizodeposition of COD. In sediment P-MFC of De Schamphelaire et al. (2008) the relation between COD and current generation was Michaelis-Menten like. In this research there was no clear relation between COD concentration and current generation. This could be caused by: i) the COD concentration did not represent substrate for electrochemically active bacteria, ii) saturation of electrochemically active bacteria with substrate, or iii) limitation by external resistance. Saturation of electrochemically active bacteria with substrate was improbable because therefore the half saturation constant has to be small compared to substrate concentration. Half saturation constants of electrochemically active bacteria for different substrates vary from 111 mg L^{-1} to 725 mg L^{-1} (Catal et al., 2008) which is in same order as even lower limits of COD concentration in the anode, hence there was probably no substrate saturation. Limitation of current generation by external resistance was improbable because of high anode potential (-221 ± 275 mV) compared to open cell potential (-369 ± 97 mV). Furthermore the ratio between the external resistance and internal resistance was 1.5 which indicated that the external resistance was relatively small.

7.4.3 Electricity generation limited by VFA in the anode

It is improbable that COD concentration in the anode limited current generation as the average COD concentration is in the same range of the half saturation constants (see previous paragraph). However current

generation may be limited by formation of VFA from biodegradable COD. In anoxic environments - such as the anode compartment of the P-MFC - biodegradable organic compounds are degraded via formation of VFAs (Stams, 1994). Low concentrations of VFAs in the anode in combination with relatively high COD concentration in the anode indicated that VFA consumption was faster than VFA formation by degradation of biodegradable COD. In other words current generation could be limited by conversion of biodegradable COD into VFAs. However, it is not possible to validate the assumption that COD in the anode was biodegradable, therefore rhizodeposition of biodegradable COD could also have limited current generation. However this is improbable because biodegradable organic compounds make up a large part of rhizodeposits (Farrar et al. 2003).

7.4.4 Acidification of anode compartment as a result of electricity generation

The production of protons by electricity generation can only result in a decrease of pH when proton production exceeds acid buffer capacity of the anode. The ½ Hoagland solution was able to buffer 4 mM of acid. Assumed that 20% (27 mL) of anolyte was refreshed every day there was an acid buffer capacity in the anode of 0.108 mmol protons per day. Therefore to saturate the acid buffer capacity 0.108 mmol of protons had to be produced per day. When electricity was generated there was an average proton production 0.13 ± 0.08 mmol per day, based on stoichiometric ratio of acetate degradation. The average proton production exceeded acid buffer capacity, hence acidification of the anode was the result of electricity generation. Acidification of the anode was expected because in conventional microbial fuel cells the anode acidifies as well due to electricity generation (Rozendal et al., 2006).

7.4.5 Fluctuations in anode potential induced by dynamics of root development

Rhizodeposits consist of a large range of organic compounds (Farrar et al. 2003), therefore there was probably a mixed potential in the anode. Mixed potential is the average potential of simultaneous reactions of different

redox couples or simultaneous oxidation of different organic compounds. Amount and speciation of rhizodeposits is related to the physiological state of individual root and changes with the life cycle of the root (Pinton & Varanini, 2007). Without doubt there were changes in life cycle of the root which resulted in fluctuation in amount and speciation of rhizodeposits. Fluctuations in amount and speciation of rhizodeposits probably resulted in changes in flux of rhizodeposition and/or rhizodeposition of different organic compounds and therefore fluctuations in anode potential and as a consequence cell potential. Furthermore *S. anglica* is able to transport a substantial amount of oxygen to their roots via the aerenchyma (Maricle & Lee, 2002) which results in oxic microzone of up to 2.5 mm around roots due to an oxygen flux from roots into the rhizosphere (Holmer et al., 2002). Change in life cycle of the root results in change of metabolic consumption of oxygen by the root cells. Change of metabolic consumption result in a change of oxygen concentration in root cells and could therefore result in fluctuations in oxygen flux from the roots into the rhizosphere. Fluctuations in oxygen flux into the rhizosphere could result in fluctuations in the anode potential and as a consequence cell potential.

Furthermore activity of electrochemically active bacteria which influenced the anode potential is also be affected by: fluctuations in speciation of substrate (Rabaey & Verstraete, 2005) , fluctuation in the anode potential (Aelterman et al., 2008), and oxygen in the anode compartment (Harnisch & Schroder, 2009) However it is beyond the scope of this research to fully determine the mechanisms which caused the anode potential to fluctuate.

7.4.6 Increase in current generation after decrease of cathode overpotential

In the period of oxygen reduction the current was limited by the VFA concentration. It is therefore surprising that the period of ferric cyanide reduction resulted not only in higher potential but also in a higher current. This higher current can be explained by the increase of the anode potential that occurred after change to ferric cyanide reduction at the cathode. Anode potential increase can lead to i) higher activity of electrochemically active bacteria (Aelterman et al., 2008) or ii) higher coulombic efficiency (Sleutels et al., 2009b).

The activity of electrochemical active bacteria is affected by anode potential Aelterman et al. (2008) found an optimal anode potential of -200 mV (vs. Ag/AgCl). Therefore increase of anode potential from -425 mV to 125 mV (vs. Ag/AgCl) could increase current generation (Figure 7.2 day 227 through day 250). Furthermore the activity of electrochemically active bacteria could be limited by flux of biodegradable and bioavailable rhizodeposits. The flux of biodegradable and bioavailable rhizodeposits could have increased because of a decrease in vitality of *S. anglica*. A decrease in vitality of *S. anglica* could have resulted in an increase of cell membrane permeability of roots and therefore an increase flux of biodegradable and bioavailable rhizodeposits hence an increased activity of electrochemically active bacteria and thus higher current.

Sleutels et al. (2009a) found that an increase in current density results in an increase of coulombic efficiency because of improvement of competitive advantage of electrochemically active bacteria over methanogens. However, our data did not allow to point out the exact cause of increase of current generation after the decrease in cathode overpotential.

7.4.7 Transport loss is main component of membrane potential loss

To fulfill the requirement of electroneutrality, negative charge transfer due to current generation is balanced by cation transport through the membrane. Anion transport could be neglected because a cation exchange membrane was used. Because there was no forced convection through the membrane transport of a specific cation through the membrane was sum of diffusion and migration. Diffusion is driven by concentration gradient over the membrane; migration is driven by electrostatic force over the membrane which results in transport potential loss. Transport of cations other than protons result in a concentration gradient opposite to the electrostatic force (Harnisch & Schröder 2009). Therefore to fulfill electroneutrality a large electrostatic force is needed because it needs to overcome the membrane resistance as well as the concentration gradients. The large electrostatic force results in a large membrane potential loss and therefore a large transport loss.

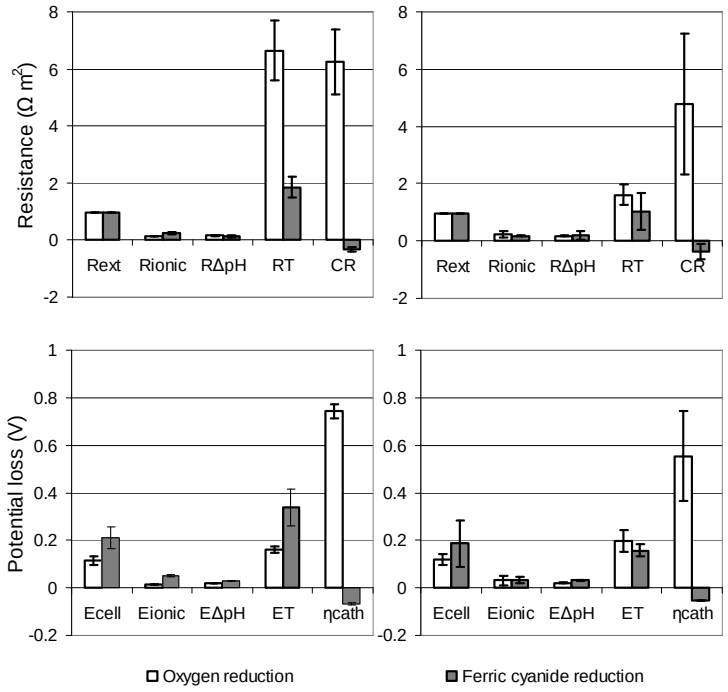

Figure 7.3 a, b: *Average partial resistances (Ω m^2) of day 196, 202, 209 and 216 for oxygen reduction, and day 230, 237 and 245 for ferric cyanide reduction of P-MFC1 (a) and P-MFC2 (b). Partial resistances are: external resistance (Rext) ionic resistance (Rionic), pH gradient resistance (RΔpH), transport resistance (RT) and cathode overpotential resistance (Rcath), calculated by dividing potential losses with produced current density. Current density defined as current per geometric surface area of the anode.* ***Fig 3 c, d*** *) Average partial potentials (V) of day 196, 202, 209 and 216 for oxygen reduction, and day 230, 237 and 245 for ferric cyanide reduction of P-MFC1 (c) and P-MFC2 (d). Partial potential are: cell potential (Ecell), ionic loss (Eionic), pH gradient loss (EΔpH) and transport loss (ET) and cathode overpotential (ηcath) of P-MFC1 (c) and P-MFC1 (d).*

Contribution of proton transport to charge transfer was probably negligible due to low proton concentration (about 10^{-5} M in the anolyte) compared to potassium and calcium concentration. (K 0.015 M and Ca^{2+} 0.002 M in medium). Proton transport could also be facilitated by phosphate buffer because of a concentration gradient of $H_2PO_4^-$ to the membrane (Fan et al., 2007). However, facilitated proton transfer was improbable because diffusion of $H_2PO_4^-$ to the membrane was small due to the graphite bed in the anode compartment which made diffusion distance large. Furthermore

the negative charge on the membrane surface repelled $H_2PO_4^-$. It is important to realize that even when protons were transported a large electrostatic force is needed fulfill electroneutrality because diffusion will be small due to the small concentration gradient of protons. Furthermore a larger proton concentration gradient would not result in a lower membrane potential loss. A large proton gradient would give a high diffusion flux which eliminates the need of an additional electrostatic force for migration. This large proton gradient however leads to a an additional pH gradient loss, counteracting the decrease in electrostatic force needed for migration. Overall this would not lead to a substantial decrease of membrane potential loss.

Acknowledgements

This research was funded by Senternovem, the Dutch governmental agency for sustainability and innovation from the Ministery of Economic Affairs (grant no. EOSLT06020) and supported by Nuon. The authors like to thank Kanjana Tuantet for executing part of the experimental work and Jan Snel for his expertise regarding plants.

References

Aelterman, P., Freguia, S., Keller, J., Verstraete, W., Rabaey, K. 2008. The anode potential regulates bacterial activity in microbial fuel cells. *Applied Microbiology and Biotechnology*, **78**(3), 409-418.

Catal, T., Li, K., Bermek, H., Liu, H. 2008. Electricity production from twelve monosaccharides using microbial fuel cells. *Journal of Power Sources*, 175(1), 196-200.

De Schamphelaire, L., Van Den Bossche, L., Hai, S.D., Hofte, M., Boon, N., Rabaey, K., Verstraete, W. 2008. Microbial fuel cells generating electricity from rhizodeposits of rice plants. *Environmental Science and Technology*, **42**(8), 3053-3058.

Fan, Y., Hu, H., Liu, H. 2007. Sustainable power generation in microbial fuel cells using bicarbonate buffer and proton transfer mechanisms. *Environmental Science and Technology*, **41**(23), 8154-8158.

Galvani, A. 2007. The challenge of the food sufficiency through salt tolerant crops. *Re-views in Environmental Science and Biotechnology*, **6**(1-3), 3-16.

Gray, A.J., Marshall, D.F., Raybould, A.F., M. Begon, A.H.F.a.A.M. 1991. A Century of Evolution in *Spartina anglica*. in: *Advances in Ecological Research*, Vol. Volume 21, Academic Press, pp. 1-62.

Haines, E.B. 1979. Growth dynamics of cordgrass, *Spartina alterniflora*, on control and sewage sludge fertilized plots in a Georgia salt marsh. *Estuaries and Coasts*, **2**(1), 50-53.

Harnisch, F., Schröder, U. 2009. Selectivity versus Mobility: Separation of Anode and Cathode in Microbial Bioelectrochemical Systems. *ChemSusChem*, **2**(10), 921-926.

Holmer, M., Gribsholt, B., Kristensen, E. 2002. Effects of sea level rise on growth of *Spartina anglica* and oxygen dynamics in rhizosphere and salt marsh sediments. *Marine Ecology Progress Series*, **225**, 197-204.

Huckle, J.M., Potter, J.A., Marrs, R.H. 2000. Influence of environmental factors on the growth and interactions between salt marsh plants: effects of salinity, sediment and waterlogging. *Journal of Ecology*, **88**(3), 492-505.

Kaku, N., Yonezawa, N., Kodama, Y., Watanabe, K. 2008. Plant/microbe cooperation for electricity generation in a rice paddy field. *Applied Microbiology and Biotechnology*, **79**(1), 43-49.

Linthurst, R.A., Seneca, E.D. 1980. The effects of standing water and drainage potential on the *Spartina Alterniflora*-substrate complex in a North Carolina salt marsh. *Estuarine and Coastal Marine Science*, **11**(1), 41-52.

Logan, B.E., Hamelers, B., Rozendal, R., Schröder, U., Keller, J., Freguia, S., Aelterman, P., Verstraete, W., Rabaey, K. 2006a. Microbial fuel cells: Methodology and technology. *Environmental Science and Technology*, **40**(17), 5181-5192.

Maricle, B.R., Lee, R.W. 2002. Aerenchyma development and oxygen transport in the estuarine cordgrasses *Spartina alterniflora* and *S. anglica*. *Aquatic Botany*, **74**(2), 109-120.

Pimentel, D., Marklein, A., Toth, M.A., Karpoff, M.N., Paul, G.S., McCormack, R., Kyriazis, J., Krueger, T. 2009. Food versus biofuels: Environmental and economic costs. *Human Ecology*, **37**(1), 1-12.

Pinton, R., Varanini, Z. 2007. The rhizosphere : biochemistry and organic substances at the soil-plant interface. CRC, Boca Raton, Fl.

Rabaey, K., Verstraete, W. 2005. Microbial fuel cells: novel biotechnology for energy generation. *Trends in Biotechnology*, **23**(6), 291-298.

Rozendal, R.A., Hamelers, H.V.M., Buisman, C.J.N. 2006. Effects of membrane cation transport on pH and microbial fuel cell performance. *Environmental Science & Technology*, **40**(17), 5206-5211.

Sleutels, T.H.J.A., Hamelers, H.V.M., Rozendal, R.A., Buisman, C.J.N. 2009a. Ion transport resistance in Microbial Electrolysis Cells with anion and cation exchange membranes. *International Journal of Hydrogen Energy*, **34**(9), 3612-3620.

Sleutels, T.H.J.A., Lodder, R., Hamelers, H.V.M., Buisman, C.J.N. 2009b. Improved performance of porous bio-anodes in microbial electrolysis cells by enhancing mass and charge transport. *International Journal of Hydrogen Energy*, **34**(24), 9655-9661.

Stams, A.J.M. 1994. Metabolic interactions between anaerobic bacteria in methanogenic environments. *Antonie van Leeuwenhoek, International Journal of General and Molecular Microbiology*, **66**(1-3), 271-294.

Strik, D.P.B.T.B., Hamelers, H.V.M., Snel, J.F.H., Buisman, C.J.N. 2008. Green electricity production with living plants and bacteria in a fuel cell. *International Journal of Energy Research*, **32**(9), 870-876.

Ter Heijne, A., Hamelers, H.V.M., De Wilde, V., Rozendal, R.A., Buisman, C.J.N. 2006. A bipolar membrane combined with ferric iron reduction as an efficient cathode system in microbial fuel cells. *Environmental Science and Technology*, **40**(17), 5200-5205.

von Witzke, H. 2008. Agriculture, world food security, bio-energy and climate change: Some inconvenient facts. *Quarterly Journal of International Agriculture*, **47**(1), 1-4.

8 Concluding remarks

8.1 Introduction

Due to depletion of fossil fuels, mankind is facing the challenge to secure world energy demand. Ideally, energy should be produced from a renewable source via an efficient and clean conversion process. The PMFC is a technology that integrates photosynthetic, i.e. higher plants, and electrochemically active organisms to generate *in situ* "green" electricity. The strong point of the PMFC is that it generates its own organic matter (in the form of organic rhizodeposits) and converts this organic matter *in situ* into electricity. As a matter of fact the PMFC makes it possible to harvest organic rhizodeposition as electricity. Without the PMFC technology organic rhizodeposits will be lost for bioenergy production because they are degraded by micro-organisms in the rhizosphere (Pinton and Varanini, 2007). The advantage of *in situ* generation is that there is no need to harvest the biomass and thus that no infrastructure is required to transport the biomass to the location of the biomass conversion technology (like microbial electrolysis cell, anaerobic digester, furnace). The energy demand of the harvest and transport of biomass reduces the net energy production of the biomass conversion technologies. Because the PMFC generates electricity or chemicals *in situ* there is no energy input required to harvest and transport the biomass. This fact makes energy input of the PMFC, in principle, to be very low. Furthermore, there is no need to construct this infrastructure needed for transport of the energy source in case it is not readily available. The lack of a need for an infrastructure for transport of the energy source together with capability of self-repair (Strik et al., 2010) makes the PMFC technology highly suitable for remote areas.

At September 2007, the start of this thesis there was no literature available on the PMFC technology. This thesis describes the first steps in the development of the PMFC technology. The first step (Chapters two to four) was dedicated to unravel the PMFC technology to identify and address the main limitation of the technology. Final part of the thesis, Chapter 5, 6 and 7, introduce two new designs and a salt marsh species (*Spartina anglica*) to counteract some of those main limitations. In this final chapter, the main limitations found during the thesis development are discussed as well as the perspective of the PMFC technology with regard to electrical power generation.

8.2 Efficiency of substrate conversion in the PMFC

The electrical power generated by the PMFC is determined by the efficiency of the substrate conversion and the voltage efficiency. The efficiency of substrate conversion in PMFC is defined as the amount of electrons measured as current divided by the amount of electrons present on the rhizodeposits. The major difficulty in determining the exact efficiency of substrate conversion is that is experimentally impossible to directly determine the exact flux and composition of rhizodeposits. Furthermore, rhizodeposits vary in both flux and composition due to variation in the roots environment (Jones et al., 2009) (Whipps and Lynch, 1985) . In this manner, rhizosphere is an highly dynamic environment. To get an indication of the substrate conversion efficiency it is necessary to understand the microbial competition and substrate conversion pathways. The next paragraph gives an overview on this topic.

8.2.1 Substrate conversion pathway

Current generation is a clear indication that low molecular weight organic compounds are oxidized in the anode of the PMFC (chapter 2). This raises the question about the origin of the low molecular weight organic compounds: are they directly excreted by the plant roots (exudates) or are they formed via hydrolysis of dead plant material? The availability of exudates for electrochemically active bacteria depends on the flux of low molecular weight organic compounds and oxygen flux into the rhizosphere, and the availability of nitrate in the rhizosphere. The rhizosphere anode model predicted that low molecular weight exudates are unavailable for current generation at commonly reported exudation rates (in the range of 10^{-9} mol m^{-2} s^{-1}) (Delhaize et al., 1993; Hoffland et al., 1989; Lu et al., 1999; Van Bodegom et al., 2001). This indicates that the low molecular weight organic compounds available for current generation originated from the hydrolysis of dead plant biomass (plant biomass consist for 35 to 50% of cellulose (Lynd et al., 1999)). Taking into consideration that electrochemically active bacteria are not able to generate electricity directly from cellulose (Ren et al., 2008), the inherent low substrate conversion efficiency calculated for PMFC, based on measured current densities and literature values of rhizodeposition, is not surprising (chapter 2). Therefore,

it is likely that the hydrolysis of cellulose originating from root debris, sloughed-off border cells, and the aerobic biofilm is the source of low molecular weight organic compounds supporting current generation. In anaerobic conditions, the production of low molecular weight organic compounds is limited by the hydrolysis rate of cellulose (Pavlostathis and Giraldo-Gomez, 1991), which indicates that current generation in the PMFC is limited by hydrolysis of cellulose and other complex organic compounds.

8.2.2 Microbial competition negatively affects substrate conversion efficiency

Besides the graphite electrode, four electron acceptors (oxygen, nitrate, sulphate and carbon dioxide) are present in the anode of PMFCs. The sources of these electron acceptors are nutrients required for plant growth (nitrate and sulphate), plant roots (oxygen and carbon dioxide) and ambient air (oxygen and carbon dioxide). Due to all these alternative electron acceptors, microbial competition between electrochemically active bacteria and the other microorganisms such as aerobic, denitrifying, sulphate reducing and methanogenic micro-organisms can potentially decrease current generation. Chapter two provided a theoretical framework to gain insight in the microbial competition in the PMFC. It was hypothesised that aerobic bacteria and denitrifying bacteria outcompete electrochemically active bacteria at the measured anode potentials (chapter 2). Likewise, electrochemically active bacteria outcompete sulphate reducing and methanogenic bacteria. In chapter three, this hypothesis was confirmed by the analysis of the microbial population present in the anode of the PMFC. The microbial population mainly consisted of facultative denitrifying bacteria which could use acetate as substrate and could hydrolyze cellulose as substrate. As expected, based on the theoretical framework, no sulphate reducing bacteria were detected. Methanogens were detected, however Archaeal DNA found was far less abundant than bacterial DNA. The identified methanogens mainly consisted of *Methanobacteriaceae* which are unable to use acetate as substrate and thus likely do not compete for acetate with electrochemically active bacteria such as *G*. *sulfurreducens* and *G. metallireducens*.

To increase the substrate conversion efficiency, the competitive position of the electrochemically active bacteria must be optimized. Two strategies may be followed for such a goal, namely increase of the anode overpotential to increase the yield of the electrochemically active bacteria, or limitation of oxygen and nitrate availability to limit growth of aerobic and denitrifying bacteria. The first option exhibits a major disadvantage, more specifically, increase in anode overpotential can only be achieved by an increase in the anode potential. Consequently the cell potential and thus the energy conversion efficiency would decrease. The second strategy involves the limitation of substrate consumption of aerobic and denitrifying bacteria by limitation of their growth through limited availability of the electron acceptor. By limiting availability of the electron acceptors (oxygen and nitrate), less substrate will be consumed by aerobic and denitrifying bacteria and thus more substrate will be available for electrochemically active bacteria. Helder et al. (2011), proved this concept by increasing power output of the PMFC after removal of nitrate from the nutrient solution.

The reasons for such low substrate conversion efficiency were highlighted in this thesis. Overall, it was concluded that low substrate conversion efficiency was due to the presence of alternative electron acceptors and the high internal resistance of the PMFC.

8.3 Internal resistance in the PMFC

The internal resistance of the PMFC was for the first time analyzed in chapter four of this thesis. The internal resistance in PMFC mainly consist of anode resistance and membrane resistance (chapter 4). Both, anode and membrane resistance, are predominantly due to mass transfer resistance. Important facts elucidating behaviour of both resistances as well as their effect on current generation was discussed in the present thesis.

8.3.1 Anode resistance

In MFCs, anode resistance is mainly due to an increase of proton concentration in the electrochemically active biofilm due to the resistance to proton transport out of the electrochemically active biofilm and the

adjacent stagnant diffusion layer (Torres et al., 2008). In PMFC, the anode resistance decreased during open circuit conditions, thus when no current was generated by the electrochemically active biofilm. Consequently, no protons were generated in the electrochemically active biofilm and the proton concentration in the electrochemically active biofilm decreased, and therefore the anode resistance decreased. Opposite tendency was observed during current generation, the anode resistance increased. This increase was likely due to proton production in the electrochemically active biofilm during current generation. In this manner, increasing proton production concomitantly increases proton concentration in the electrochemically active biofilm and thus anode resistance increased. The continuous increase of the anode resistance indicated that the proton concentration in the electrochemically active biofilm continuously increased. This was likely due to the limited buffer capacity of the anolyte and limited proton transfer from the anode to the cathode.

8.3.2 Membrane resistance

In MFCs, the membrane resistance is due to ohmic resistance and transport resistance. The ohmic resistance represents the resistance to ion transfer in the bulk electrolyte. The transport resistance represents the resistance to ion transfer through the membrane and the adjacent film layer. In the particular case of PMFC, ohmic resistance was negligible by the current interrupt method (Chapter 4). Thus, membrane resistance mainly consisted of the resistance to ion transfer in the membrane and the adjacent film layer. During open circuit, decreasing membrane resistance was explained by transport processes in the anode compartment. No current was generated during open circuit, thus there was no need for charge transfer to maintain electroneutrality. Since no charge transfer was required to maintain electro neutrality during open circuit, accumulation of cations in the cathode stopped. Moreover, the accumulation of cations decreased due to diffusion from the cathode to the anode and hence, membrane resistance decreased. Furthermore, as discussed in Chapter 4, in agreement with estimated time constants for diffusion in the biofilm and the anode compartment, the decrease observed for membrane resistance was less than the decrease of the anode resistance.

During current generation, the second tested scenario, the membrane resistance increased. This increase was attributed to the continuous increase of cations accumulated in the cathode compartment. This accumulation resulted in a continuous increase of concentration gradient opposing the required direction of transport. Consequently a larger potential gradient, and thus membrane potential, was required to drive cations against the concentration gradient into the cathode.

8.4 Perspectives for the PMFC

8.4.1 Decrease of internal resistance needed to reach estimated power output

The major challenge of the PMFC technology is to decrease the high internal resistance in an energy efficient way. This requires that the energy input, to reduce the internal resistance, must be lower than the energy output gained by the decrease in internal resistance. In the PMFC the anode compartment is a sediment-like structure (De Schamphelaire et al., 2008; Kaku et al., 2008; Strik et al., 2008). Therefore it is unlikely that increasing the flow rate in the anode to enhance mass transfer will be an energy efficient option. Because increasing flow rates in sediments requires a high energy input. This will diminish power generation by the PMFC. Increase of the buffer capacity in the anode of the PMFC requires addition of large amounts of buffer. The addition of large amount of buffer is not sustainable (Rozendal et al., 2008), furthermore it negatively affects plant growth and thus electrical power output [13].

The internal resistance of the PMFC has major impact on the power output of the PMFC, whereas the power output is determined by internal resistance (R_{int} (Ω m^2)), open circuit cell potential (E_{cell}^{oc} (V)), and current density (i (A m^{-2})):

$$P = iE_{cell}^{oc} - i^2 R_{\text{int}} \qquad 1$$

Assuming that PMFC cell potential at open circuit is approximately 0.7 V, maximum internal resistance required to achieve the theoretical average power output of the PMFC (1.6 W m^{-2}) can be calculated. In this manner,

maximum internal resistance would be 0.075 Ω m^2 which would generate this power at a current density of 4.7 A m^{-2}. The internal resistance determined as the slope of the polarization curve ranged 0.5- 21 Ωm^2 (Kaku et al., 2008) (Strik et al., 2008). The lowest reported internal resistance after open circuit was 0.1 Ω m^2 (chapter 4) (Helder et al., 2011). Nevertheless, this low internal resistance can not be maintained during current generation due to increase in anode resistance and membrane resistance during current generation.

The bi-cathode setup presented in chapter 5 decreased the internal resistance from 4.3 Ω m^2 to a minimum of 1.2 Ω m^2 in the PMFC without the need of an extra energy input. This showed that a decrease of the internal resistance is possible without extra energy input. However there is still a long way to go to reach the internal resistance required (0.075 Ω m^2) to reach the theoretical estimated average power output of 14 kWh m^{-2} $year^{-1}$ (Introduction).

8.4.2 Feasibility of the PMFC as a renewable electricity source

The revenue of a renewable electricity source is highly dependent on the technology by which it is produced and the local tariffs that are paid by the utilities company. Here the focus is on the European market. In most European Union member states the price that the utilities company pay for renewable energy is regulated by Feed-in tariffs. These Feed-in tariffs a highly dependent on the technology and country, therefore, besides the location the feasibility of the PMFC is determined by the classification of the technology. The PMFC converts biomass into electricity and can therefore be classified as renewable electricity based on biomass. In Europe the Feed-in tariff that a company, or individual is paid for electricity production with biomass conversion technology is in between 0.038 through 0.3 € kWh^{-1} (http://www.energy.eu/#Feedin accessed 14/12/2011).

In current state of the development of the PMFC it is difficult to calculate the exact costs of a full scale application of the PMFC technology. However the full scale application that is envisioned has low operational costs because no chemicals and or pumping are required. Therefore it is possible

to make a cost estimation based on based on the material use and an estimation of the implementation costs. Table 8.1 gives an overview of the material and implementation costs. With a lifetime of 5 years for the spacer, electrode, and current collectors the costs per square meter of planted area per year are in between 26 through 182 € m^{-2} $year^{-1}$ (Pant et al., 2011; Rozendal et al., 2008). Based on these costs the price of electricity generation was calculated and expressed versus the energy output of the PMFC (8. 1). However because no catalysts other than electrochemically active bacteria are used the expected life time is longer than five years and may be in the order of 30 years. Furthermore, because no catalysts other than electrochemically active bacteria are used the costs of the PMFC are probably in the lower range of the price range (127 € m^{-2}, thus 26 € m^{-2} $year^{-1}$). The costs of electricity generation by renewable technologies are in the range of 0.064 through 0.23 € kWh^{-1} (http://www.eia.gov/oiaf /aeo/ electricity_generation.html, accessed 28/12/2011). Assumed the maximum theoretical power output is achieved the cost of electricity generation by the PMFC is 0.15 € kWh^{-1} which is in the range of the competing renewable technologies.

Table 8.1: Overview of the costs of the PMFC technology based on the materials used and the implementation of the PMFC technology in agricultural food production, wetlands, or green roofs.

Material	Costs (€m^{-2} or €kg^{-1})	Usage m^2 planted area	Costs m^2 planted area	%	Reference
Electrode material	700-7000	0.1 m^3	70-700 €	55	Le Carbonne
Current collector	5	2 m^{-2}	10 €	8	Coidan Graphite Products
Spacer	0.6	0.5 kg	0.3 €	0.2	Alibaba.com
Wiring	0.5	1 m	0.5 €	0.4	
Control hardware	1	1	1 €	0.8	Workshop WUR
Implementation	45-185	1	45-185 €	36	a
Total			127-897 €		

a) http://huis-en-tuin.infonu.nl/diversen/56178-aanleg-groen-dak-kosten-en-subsidie.html/ http://www.frtr.gov/matrix2/section4/4-36.html accessed 28/12/2011

Nevertheless, nowadays even at the maximum power output (126 GJ ha^{-1} $year^{-1}$ (chapter 4)), the PMFC technology does not seem to be economically feasible as a technology to produce renewable electricity. Most of the costs are in the electrode material therefore the logical way to reduce the costs per kWh is to reduce the amount of electrode material used. Another critical point in for the PMFC is successful integration of this technology in agricultural production is unlikely. This is because the PMFC technology requires anaerobic environment (waterlogged conditions) to generate electricity. In contrast to the anaerobic conditions required for the PMFC technology most agricultural crops require an aerobic root environment to achieve a high production. In general anaerobic conditions are imposing stress to a plant and will therefore likely have a negative effect on the yield of most agricultural production crops. It is good to realize that of the significant agricultural crops only rice is resistant to extended periods of anaerobic conditions.

8.4.3 Added value of the PMFC

It is vital for the future of the PMFC to create an added value to be able to compete in the energy market. The main opportunity for the PMFC technology is to create an added value by providing a self sustaining energy source in remote areas. In remote areas there is a need for stand alone renewable electricity generation, which usually consists of solar panels and / or wind turbines in combination with a power storage system. The costs electricity generations of these stand alone systems vary from 1.1 to 1.5 € kWh^{-1} (1.44 to 1.95 $ kWh^{-1}) (Diaf et al., 2007). The inset in figure 8.1 shows that that the PMFC could be a competitive alternative to these stand alone systems for electricity generation in remote areas. The cost estimation of the PMFC does not include a power storage system, however as the PMFC generates electricity day and night a power storage system is not required (provided the PMFC generates electricity in every season).

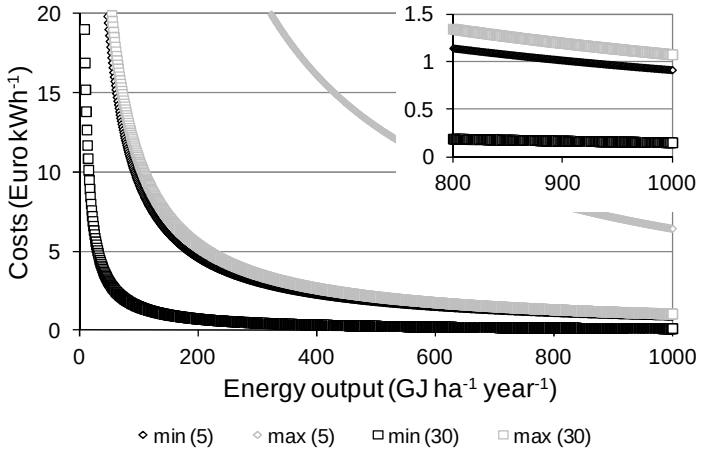

Figure 8.1: *The costs of electricity generation by the PMFC based on the investment costs (127-897 € m^{-2}) and an estimated lifetime of 5 and 30 years for the spacer, electrode material, and current collectors. The theoretical maximum output is 1000 GJ ha^{-1} $year^{-1}$ (introduction). Until now the maximum measured output is 126 GJ ha^{-1} $year^{-1}$ (chapter 4), and the maximum average output is 16 GJ ha^{-1} $year^{-1}$ (chapter 7)*

In remote areas low power input applications such as sensors and led light are generally powered by batteries. Batteries have two disadvantages; they contain toxic compounds and only provide electrical power for a limited time. The electrical power price generated by batteries is in the range of 6.5 through 660 € kWh^{-1}, depending on the type of battery (http://batteryuniversity.com/learn/article/cost_of_power, accessed 28/12/2011). The cost of electrical power generated by the PMFC is equivalent to 9.5 € kWh^{-1} (Figure 8.1), based on the highest reported average power output per square meter of membrane (0.05 W m^{-2} 16 GJ ha^{-1} $year^{-1}$ chapter 4) and the lowest costs. This shows that the PMFC is already competitive with batteries regarding the price of a kWh. Besides offering a good price the additional added value of the PMFC technology would be the indefinite generation of electrical power and the absence of toxic compounds. Taking into consideration all mentioned drawbacks of batteries, it can be suggested that application of the PMFC technology as a power source for low power input application in remote areas is just around the corner.

References

De Schamphelaire, L., Van Den Bossche, L., Hai, S.D., Höfte, M., Boon, N., Rabaey, K., Verstraete, W. 2008. Microbial fuel cells generating electricity from rhizodeposits of rice plants. Environmental Science and Technology, 42(8), 3053-3058.

Delhaize, E., Craig, S., Beaton, C.D., Bennet, R.J., Jagadish, V.C., Randall, P.J. 1993. Aluminum tolerance in wheat (*Triticum aestivum L.*). I.Uptake and distribution of aluminum in root apices. Plant Physiology, 103(3), 685-693.

Diaf, S., Diaf, D., Belhamel, M., Haddadi, M., Louche, A. 2007. A methodology or optimal sizing of autonomous hybrid PV/wind system. Energy Policy, 35(11), 5708-5718.

Helder, M., Strik, D.P., Hamelers, H.V., Buisman, C.J. 2011. Year round performance of the flat-plate plant-microbial fuel cell. Communications in agricultural and applied biological sciences, 76(2), 55-57.

Hoffland, E., Findenegg, G.R., Nelemans, J.A. 1989. Solubilization of rock phosphate by rape - II. Local root exudation of organic acids as a response to P-starvation. Plant and Soil, 113(2), 161-165.

Jones, D.L., Nguyen, C., Finlay, R.D. 2009. Carbon flow in the rhizosphere: Carbon trading at the soil-root interface. Plant and Soil, 321(1-2), 5-33.

Kaku, N., Yonezawa, N., Kodama, Y., Watanabe, K. 2008. Plant/microbe cooperation for electricity generation in a rice paddy field. Applied Microbiology and Biotechnology, 79(1), 43-49.

Lu, Y., Wassmann, R., Neue, H.U., Huang, C. 1999. Impact of phosphorus supply on root exudation, aerenchyma formation and methane emission of rice plants. Biogeochemistry, 47(2), 203-218.

Lynd, L.R., Wyman, C.E., Gerngross, T.U. 1999. Biocommodity engineering. Biotechnology Progress, 15(5), 777-793.

Pant, D., Singh, A., Van Bogaert, G., Gallego, Y.A., Diels, L., Vanbroekhoven, K. 2011. An introduction to the life cycle assessment (LCA) of bioelectrochemical systems (BES) for sustainable energy and product generation: Relevance and key aspects. Renewable and Sustainable Energy Reviews, 15(2), 1305-1313.

Pavlostathis, S.G., Giraldo-Gomez, E. 1991. Kinetics of anaerobic treatment. Water Science and Technology, 24(8), 35-59.

Pinton, R., Varanini, Z. 2007. The rhizosphere : biochemistry and organic substances at the soil-plant interface. CRC, Boca Raton, Fl.

Ren, Z., Steinberg, L.M., Regan, J.M. 2008. Vol. 58, pp. 617-622.

Rozendal, R.A., Hamelers, H.V.M., Rabaey, K., Keller, J., Buisman, C.J.N. 2008. Towards practical implementation of bioelectrochemical wastewater treatment. Trends in Biotechnology, 26(8), 450-459.

Strik, D.P.B.T.B., Hamelers, H.V.M., Buisman, C.J.N. 2010. Solar energy powered microbial fuel cell with a reversible bioelectrode. Environmental Science and Technology, 44(1), 532-537.

Strik, D.P.B.T.B., Hamelers, H.V.M., Snel, J.F.H., Buisman, C.J.N. 2008. Green electricity production with living plants and bacteria in a fuel cell. International Journal of Energy Research, 32(9), 870-876.

Torres, C.I., Marcus, A.K., Rittmann, B.E. 2008. Proton transport inside the biofilm limits electrical current generation by anode-respiring bacteria. Biotechnology and Bioengineering, 100(5), 872-881.

Van Bodegom, P., Goudriaan, J., Leffelaar, P. 2001. A mechanistic model on methane oxidation in a rice rhizosphere. Biogeochemistry, 55(2), 145-177.

Whipps, J.M., Lynch, J.M. 1985. Energy losses by the plant in rhizodeposition. Ann. Proc. Phytochem. Soc. Eur., 26, 59-71.

About the author

Ruud was born on 20 March 1978 in Eersel, the Netherlands. He finished high school in 1996 and 6 months of chemical engineering he started working in tree and flower cultivation at Wil Maas boomkwekerijen BV. He did this until September 2000 when he started his bachelor degree in environmental engineering at the HAS in Den Bosch. In 2004 he graduated and decided to pursue a Master degree at the University of Wageningen. After his graduation in 2007 he heard about electricity production by living plants and decided it would be nice to return to work with plants and applied for the PhD position. Based on his experience on working with plants he got the position. In 2008 he met his Spanish girlfriend and after travelling to Spain for 3.5 years he moved there in September 2011. Since January 2012 he works at Universidad Rey Juan Carlos at Departamento de Tecnología Química y Ambiental as a researcher on photocatalytic wastewater treatment.

Publications

Characterization of the internal resistance of the plant microbial fuel cell. Ruud A. Timmers, David P.B.T.B. Strik, Hubertus V.M. Hamelers, Cees J.N. Buisman. *Electrochimica Acta*, 2012 accepted

Microbial community structure elucidates performance of Glyceria maxima plant microbial fuel cell. Ruud A. Timmers, Michael Rothballer, David P.B.T.B. Strik, Marion Engel, Stephan Schulz, Michael Schloter, Anton Hartmann, Bert Hamelers, Cees Buisman *Applied Microbiology and Biotechnology,*2012

Rhizosphere anode model explains high oxygen levels during operation of a Glyceria maxima PMFC. Ruud A. Timmers, David P.B.T.B. Strik, Cristina Arampatzoglou, Cees J.N. Buisman, Hubertus V.M. Hamelers. *Bioresource Technology,* 2012

Microbial solar cells: applying photosynthetic and electrochemically active organisms. Strik DP, Timmers RA, Helder M, Steinbusch KJ, Hamelers HV, Buisman CJ. *Trends Biotechnology.* 2010 29(1), 41-49

Zn-Ni sulfide selective precipitation: The role of supersaturation. Sampaio R.M.M., Timmers R.A., Kocks N., Andre V., Duarte M.T., Van Hullebusch E.D., Farges F., Lens P.N.L. *Separation and purification technology,* 2010 74(1) pp 108-118

Long term electricity generation of *Spartina anglica* in a plant microbial fuel cell. Timmers R.A., Strik D.P.B.T.B., Hamelers H.V.M., Buisman C.J.N. *Applied Microbiology and Technology*, 2010 86(3), 973-981

Selective precipitation of Cu from Zn in a pS controlled continuously stirred tank reactor. Sampaio RM, Timmers RA, Xu Y, Keesman KJ, Lens PN. *Journal of Hazardous Materials.* 2009 15(165), 256-65.

Conference contributions

Increase of power output by change of ion transport direction in a (P)MFC. Timmers, R.A., Strik, D.P., Hamelers, H.V., Buisman, C.J. 3rd International Microbial Fuel Cell Conference 2011, 6-8 June 2011. Leeuwarden , the Netherlands.

Radial oxygen loss decreases available substrate for electrochemically active bacteria in a PMFC. Timmers, R.A., Strik, D.P., Arampatzoglou, C., Hamelers, H.V., Buisman, C.J. 1st international PlantPower symposium, 10th February 2011. Ghent, Belgium

Modelling the plant microbial fuel cell. Hamelers, H.V., Timmers, R.A., Steinbusch, K.J., Strik, D.P. Communications in agricultural and applied biological sciences. 2011 vol 76, 2, pp 93-95

Energetic performance of microbial solar cells. Strik, D.P., Timmers, R.A., Helder, M., Steinbusch, K.J., Hamelers, H.V., Buisman, C.J. Communications in agricultural and applied biological sciences. 2011 vol 76, 2, pp 97-99

Comparison of bacterial rhizosphere communities from plant microbial fuel cells with different current production by 454 amplicon sequencing. Rothballer, M., Engel, M., Strik, D.P., Timmers, R., Schloter, M., Hartmann, A. Communications in agricultural and applied biological sciences. 2011 vol 76, 2, pp 31-32

Radial oxygen loss decreases available substrate for electrochemically active bacteria in a PMFC. Timmers, R.A., Strik, D.P., Arampatzoglou, C., Hamelers, H.V., Buisman, C.J. Communications in agricultural and applied biological sciences. 2011 vol 76, 2, pp 79-82

Ion transport determines maximum current during polarization of the plant microbial fuel cell. Timmers, R.A., Strik, D.P., Hamelers, H.V., Buisman, C.J.
61st Annual Meeting of the International Society of Electrochemistry. 26 September – 1 October. Nice France

Long term electricity generation from rhizodeposits of salt marsh species *Spartina anglica* in a plant microbial fuel cell. Timmers R.A., Strik D.P.B.T.B., Hamelers H.V.M., Buisman C.J.N. Conference proceeding "Waste To Energy" 2nd Microbial Fuel Cell Conference. Gwangju Institute of Science and Technology, Gwangju South-Korea 10th-12th June 2009

Green electricity production by living plants in a microbial fuel cell. Timmers R.A., Strik D.P.B.T.B., Hamelers H.V.M., Buisman C.J.N. "Novel Cost Effective Technologies for Wastewaters Treatment and Bioenergy Production" Sense Symposium. 4-5 September 2008. Wageningen the Netherlands

Awards

Best poster award at: 1st international PlantPower symposium, 10th February 2011. Ghent, Belgium, with: Radial oxygen loss decreases available substrate for electrochemically active bacteria in a PMFC. Timmers, R.A., Strik, D.P., Arampatzoglou, C., Hamelers, H.V., Buisman, C.J.

Acknowledgements

Finally, the last part of the doctoral thesis has arrived: the acknowledgements.

First of all, I would like to thank the students that I supervised: Kanjana, Christina and Wouter, for their contribution to this thesis. It was a pleasure working with you all. The main thing I remember of those days is that we had lots of fun in the lab. Another moment I treasure is the pleasure of teaching Nico my very straight forward technique to fill capillaries.

Secondly, I would like to thank my supervisors David, Bert and Cees for giving me the opportunity to carry out this research. Especially to David, I would like to thank for his perseverance, which was clearly required for being able to read all the concept manuscripts I produced in “bringlish”.

Of my other colleagues, I especially want to thank Mieke and Christel for the good times we had in our office… it is probably not easy to share the office with a guy who always has a very clean desk! I would also like to thank Tania, indirectly you probably helped me the most to finish this thesis… The rest of my former colleagues at ETE and the bioenergy group of Wetsus are also thanked. In most thesis acknowledgements, I see that now it follows a long list of names. I choose not to do this because I will probably forget to mention one or more former colleagues.

After thanking the former colleagues, it is customary to thank the family and friends. To honor this custom, I would like to say: thank you family!! I guess it had to be quite funny to hear the same monologue of cynical complaints every other week.

After the family, it is mostly the partner´s turn to be acknowledged. Therefore, Cristina muchas gracias for kicking my ass.

Netherlands Research School for the
Socio-Economic and Natural Sciences of the Environment

C E R T I F I C A T E

The Netherlands Research School for the
Socio-Economic and Natural Sciences of the Environment
(SENSE), declares that

Rudolphus Antonius Timmers

born on 20 March 1978 in Eersel, The Netherlands

has successfully fulfilled all requirements of the
Educational Programme of SENSE.

Wageningen, 15 May 2012

the Chairman of the SENSE board
Prof. dr. Rik Leemans

the SENSE Director of Education
Dr. Ad van Dommelen

The SENSE Research School has been accredited by the Royal Netherlands Academy of Arts and Sciences (KNAW)

KONINKLIJKE NEDERLANDSE
AKADEMIE VAN WETENSCHAPPEN

The SENSE Research School declares that Mr. Rudolphus Antonius Timmers has successfully fulfilled all requirements of the Educational PhD Programme of SENSE with a work load of 49 ECTS, including the following activities:

SENSE PhD courses

- Environmental Research in Context
- Research Context Activity: Organizing Colloquia on environmental technology and Conference on: Novel Cost Effective Technologies for Waste Water Treatment and Bio-energy Production (4-5 September 2008, Wageningen)
- Speciation and Bioavailability
- The Art of Modelling
- PhD Scientific Writing

Other PhD courses

- Bath Electrochemistry Summer School
- Modeling of plant uptake and application in environmental science and engineering
- Advanced Course Environmental Biotechnology

Oral Presentations

- Living plant produce electricity, Novel Cost Effective Technologies for Waste Water Treatment and Bio-energy Production, 5 September 2008, Wageningen, The Netherlands
- Long term electricity generation from rhizodeposits of salt marsh species Spartina anglica in a plant microbial fuel cell, Second International Microbial Fuel Cell Conference,12 June 2009, Gwagnju, South-Korea
- Radial oxygen loss decreases available substrate for electrochemically active, First International PlantPower Symposium, 10 February 2011, Ghent, Belgium

SENSE Coordinator PhD Education and Research

Mr. Johan Feenstra